AD-A140 620 MULTIPLE-ELEMENT THRESHOLD SIGNAL DETECTION OF UNDERWATER ACOUSTIC SIGNAL..(U) MIDDLETON (DAVID) NEW YORK D MIDDLETON 18 MAY 83 NOSC-CR-231 1/2

UNCLASSIFIED N66001-82-C-0322 F/G 20/1 NL

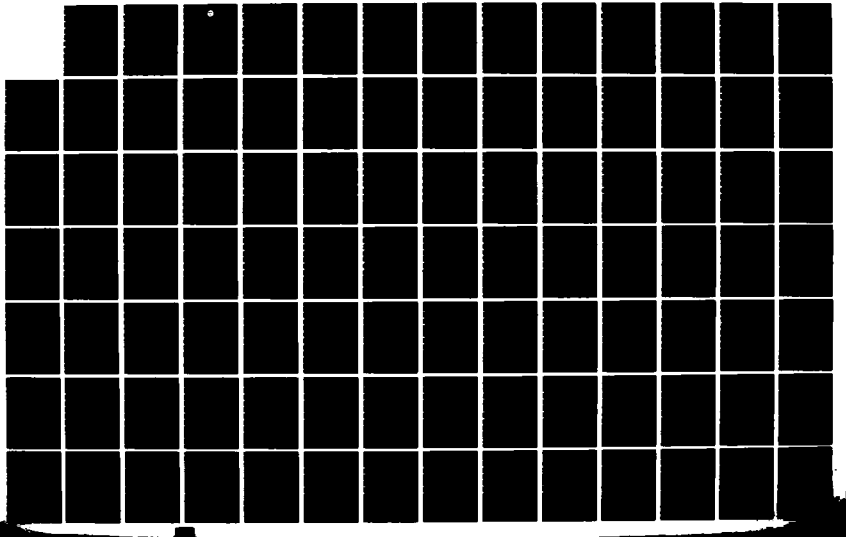

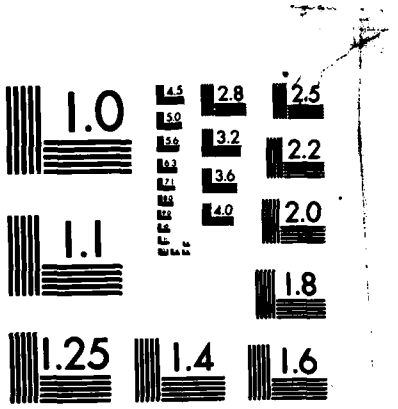

MICROCOPY RESOLUTION TEST CHART
NATIONAL BUREAU OF STANDARDS-1963-A

(12)

NOSC CR 231

NOSC CR 231

Contractor Report 231

MULTIPLE-ELEMENT THRESHOLD SIGNAL DETECTION OF UNDERWATER ACOUSTIC SIGNALS IN NONGAUSSIAN INTERFERENCE ENVIRONMENTS

David Middleton

18 May 1984

Prepared for
NOSC Independent Research/
Independent Exploratory Development Program
(Code 013)

Approved for public release; distribution unlimited.

NOSC

NAVAL OCEAN SYSTEMS CENTER
San Diego, California 92152

NAVAL OCEAN SYSTEMS CENTER SAN DIEGO, CA 92152

AN ACTIVITY OF THE NAVAL MATERIAL COMMAND

J.M. PATTON, CAPT, USN
Commander

R.M. HILLYER
Technical Director

ADMINISTRATIVE INFORMATION

The work reported here was performed by the author during the period 18 June 1982 - 18 May 1983, under NOSC contract N66001-82-C-0322.

Released under the authority of
E. P. Cooper, Head
NOSC Independent Research/Independent
Exploratory Development Program (IR/IED)

ACKNOWLEDGEMENTS

The author would like to thank J. M. Speiser, H. J. Whitehouse, E. D. Maynard, and Dr. John Northrup for their frequent discussions and detailed interest in this work. In particular, the author is indebted to Dr. Charles Persons for his interest in and evaluation of the manuscript. The author also acknowledges with appreciation both the sustaining interest of (then) NOSC Technical Director, Dr. Howard L. Blood, in the technical possibilities of the concepts and methods developed here, and the continued support of Dr. Eugene Cooper, Head, NOSC IR/IED Program.

RH

UNCLASSIFIED

SECURITY CLASSIFICATION OF THIS PAGE (When Data Entered)

REPORT DOCUMENTATION PAGE

READ INSTRUCTIONS BEFORE COMPLETING FORM

1. REPORT NUMBER: NOSC CR 231	2. GOVT ACCESSION NO.: AH96620
3. RECIPIENT'S CATALOG NUMBER:	
4. TITLE (and Subtitle): MULTIPLE-ELEMENT THRESHOLD SIGNAL DETECTION OF UNDERWATER ACOUSTIC SIGNALS IN NONGAUSSIAN INTERFERENCE ENVIRONMENTS	5. TYPE OF REPORT & PERIOD COVERED: 18 June 1982–18 May 1983
	6. PERFORMING ORG. REPORT NUMBER:
7. AUTHOR(s): David Middleton	8. CONTRACT OR GRANT NUMBER(s): N66001-82-C-0322
9. PERFORMING ORGANIZATION NAME AND ADDRESS: Dr. David Middleton, 127 E. 91 St., New York, NY 10028	10. PROGRAM ELEMENT, PROJECT, TASK AREA & WORK UNIT NUMBERS: Funding provided by NOSC Independent Research/Independent Exploratory Development (IR/IED) Program
11. CONTROLLING OFFICE NAME AND ADDRESS: Naval Ocean Systems Center, San Diego, CA 92152	12. REPORT DATE: 18 May 1983
	13. NUMBER OF PAGES: 170
14. MONITORING AGENCY NAME & ADDRESS (if different from Controlling Office):	15. SECURITY CLASS. (of this report): Unclassified
	15a. DECLASSIFICATION/DOWNGRADING SCHEDULE:

16. DISTRIBUTION STATEMENT (of this Report)

Approved for public release; distribution unlimited.

17. DISTRIBUTION STATEMENT (of the abstract entered in Block 20, if different from Report)

18. SUPPLEMENTARY NOTES

19. KEY WORDS (Continue on reverse side if necessary and identify by block number)

Optimum threshold detection; multiple sensor detectors; threshold detection algorithms; underwater acoustic interference; noise and signal fields; space-time processing, nongaussian noise; coherent, incoherent, composite signal detection; beam forming, adaptive beams; noise scenarios, space-time bandwidths, and processing gains; minimum detectable signals; detection probability.

20. ABSTRACT (Continue on reverse side if necessary and identify by block number)

In addition to the general development of a weak-signal M-sensor detection theory, optimum (binary) space-time threshold signal detection algorithms are obtained for specific (Class A) nongaussian underwater acoustic noise environments, as well as for the fully canonical cases of general interference and general signal waveforms. These include algorithms for coherent, incoherent, and composite (coherent + incoherent) reception. It is shown that spatial and temporal processing are interchangeable as long as sampling (of the noise data) is statistically independent, in time and in space (i.e., "sparse sampling"). It is also estimated that "dense sampling" –

(Continued on reverse side)

DD FORM 1 JAN 73 1473 EDITION OF 1 NOV 65 IS OBSOLETE

S/N 0102-LF-014-6601

UNCLASSIFIED

SECURITY CLASSIFICATION OF THIS PAGE (When Data Entered)

20. Continued

continuous or analog sampling – can give only O(2-3 db) improvement over sparse-sampling in the highly non-gaussian (Class A) cases, and O(∅ db) in gauss noise, as long as large space-time-bandwidth products ($J \gg 1$) are employed. ($J >> 1$)

Generally, with coherent signal waveforms (in space and time) and beam-forming the minimum detectable signal, $\langle a_0^2 \rangle^*_{min}$, varies as J^{-1}, whereas with incoherent signal waveforms, $\langle a_0^2 \rangle^*_{min} \sim J^{-1/2}$, similar to the purely temporal processors of single element or single beam conditions. Fading and "doppler-smear" of the desired signal are always destructive, although the composite detector is robust (insensitive) to slow-fading and partially so to rapid fading. Spatial statistics (covariances) of the noise and signal fields are obtained for use in spatial sampling (i.e., array configuration).

Comparisons in structure and performance with suboptimum detectors (matched-filter detectors and clipper-correlators) are provided, with an extensive set of numerical examples illustrating performance for typical noise and signal conditions. While clipper correlators give noticeable improvement O(20-30 dB) over the conventional matched-filter receivers (optimum in gauss noise) in these threshold cases, they also can be significantly less effective O(6-10 dB) than the optimum algorithm, even when composite detectors are employed. In all cases, increasing the number of independent spatial samples (array processing gain, M>1) over the single-element, or single-beam configurations (M=1), when possible, can give significant improvement in performance. Many other special results and general observations are also included, cf. Sec. 12.

SUMMARY

OBJECTIVES

The principal general purpose of this study is to extend the recently developed canonical theory of optimum binary (i.e., two-alternative) threshold signal detection in the time domain to include the important cases of spatial sampling (i.e., array processing), when the noise or interference is highly nongaussian, when general (narrow- or broad-band) signals are employed, and where arbitrary arrays of sensors (elements) are permitted. Such a canonical theory includes: (1), optimum threshold detection algorithms; (2), measures of performance, usually minimum detectable signals under various probability controls and sample size (space-time-bandwidth products) $J(>>1)$; and (3), comparisons with other (simpler) suboptimum algorithms.

The principal specific purposes of the study are: (1), to apply the general extensions above to various classes of specific underwater acoustic detection situations; and (2), to obtain typical spatio-temporal threshold algorithms, and their associated performances, with quantitative numerical results. These include the detection of signals subject to fading and "doppler-smear," and the construction of space-time noise scenarios from which the needed (first-order) probability distributions of the noise can be analytically derived. In addition, spatio-temporal statistics of the noise and signal fields are required, in order to assist suitable spatial (as well as temporal) sampling procedures. Comparisons with conventional (temporal) processors (e.g., matched-filter detectors and clipper-correlators) are sought in order to provide a quantitative measure of the improvement (dB) to be expected if the theoretically optimum processor is used, as well as the amounts by which suboptimum detectors are degraded.

RESULTS

In addition to the general development of the M-sensor detection theory specified above in the Objectives, optimum (binary) space-time threshold signal detection algorithms are obtained for specific (Class A) nongaussian underwater acoustic noise environments, as well as for the fully canonical cases of general interference and general signal waveforms. These include

algorithms for coherent, incoherent, and composite (coherent + incoherent) reception. It is shown that spatial and temporal processing are interchangeable as long as sampling (of the noise data) is statistically independent, in time and in space (i.e., "sparse sampling"). It is also estimated that "dense sampling"--continuous or analog sampling--can give only O(2-3 db) improvement over sparse-sampling in the highly nongaussian (Class A) cases, and O(0 db) in gauss noise, as long as large space-time-bandwidth products ($J \gg 1$) are employed.

Generally, with coherent signal waveforms (in space and time) and beam-forming, the minimum detectable signal, $\langle a_o^2 \rangle^*_{min}$, varies as J^{-1}, whereas with incoherent signal waveforms, $\langle a_o^2 \rangle^*_{min} \sim J^{-\frac{1}{2}}$, similar to the purely temporal processors of single element or single beam conditions. Fading and "doppler-smear" of the desired signal are always destructive, although the composite detector is robust (insensitive) to slow-fading and partially so to rapid fading. Spatial statistics (covariances) of the noise and signal fields are obtained for use in spatial sampling (i.e., array configuration).

Comparisons in structure and performance with suboptimum detectors (matched-filter detectors and clipper-correlators) are provided, with an extensive set of numerical examples illustrating performance for typical noise and signal conditions. While clipper correlators give noticeable improvement O(20-30 db) over the conventional matched-filter receivers (optimum in gauss noise) in these threshold cases, they also can be significantly less effective O(6-10 db) than the optimum algorithm, even when composite detectors are employed. In all cases, increasing the number of independent spatial samples (array processing gain, $M > 1$) over the single-element, or single-beam configurations ($M = 1$), when possible, can give significant improvement in performance. Many other special results and general observations are also included, cf. Sec. 12.

CONTENTS

Section 1. Introduction

The problem of detecting weak signals in noise is a well-known, fundamental task in all areas of signal processing. In this paper we are concerned with the general problem of obtaining and comparing optimum and suboptimum procedures for detecting weak signals in nongaussian acoustic noise or interference environments (although the methods and analytic results derived here are equally applicable to electromagnetic and other types of signal detection and extraction). Thus, a canonical theory is desired, the form of whose results is independent of any particular signal waveform and specific noise statistics. Closely associated with such signal processing tasks is the development of tractable analytic, statistical-physical models of the nongaussian interference against which our optimum and suboptimum processing "algorithms" (i.e., procedures) must operate, and by which they are themselves specified. [For relevant earlier work on nongaussian noise models, see [1]-[6], [31], [32], and see also [7]-[12], [22]-[34] for threshold signal detection, as well as references therein.]

Most earlier work has also been based on single-sensor (element) or single-beam systems (which is appropriate when the interference or noise field is strongly correlated over the sensor or array). In our treatment here, however, we extend these efforts (including the M-sensor analysis of [13]-[15]) and various foreign studies [35]) in one or more of the following respects: (1), to include arbitrary spatial configurations of M elements ($M \gg 1$) in noise environments dominated by highly nongaussian interfering sources, whose spatial correlations in turn are usually highly nonuniform; (2), whose spatial statistics are explicitly derived from a general interference scenario; and (3), where, in particular, the threshold detection algorithms are properly designed (i.e., have the correct "bias" terms) to achieve the necessary optimality for the large space-time bandwidth products which are required for an effectively large probability of correct detection decisions.

In our present effort the principal general new results are: (1), a canonical theory, whereby are obtained optimum threshold detection algorithms for any type of noise or interference (combined with the usual gaussian noise backgrounds) and general signals, which now include adaptive, data processing steerable beams, for arbitrary M-sensor arrays; (2), performance

measures, namely, minimum detectable signals, space-time processing gains, probabilities of correct signal detection, etc., associated with the algorithms of (1) above; and (3), quantitative comparisons with typical suboptimum detectors such as "matched-filter" (i.e., correlation) receivers, and receivers using hard-limiters (i.e., "clipper-correlators"). (These latter are respectively threshold optimum in gauss and Laplace noise [cf. Sec. 10 ff.].) Included, also, are explicit signal classes, whose waveform structures are typical of many of the underwater acoustic environments encountered in practice. Generally, for best performance we should attempt to:

I. Adapt the detector to the interference environment (i.e., estimate the noise parameters, and apply these to the canonical detection algorithm);

II. Match the receiver first to the interference and then match this result (linearly) to the desired signal;

III. Obtain the largest space-time bandwidth products ($J=MN>>1$), consistent with our ability to achieve "independent" space- and time-sampling in the space-time data domain available;

IV. Employ a composite threshold detection algorithm (i.e., a linear combination of the (optimum) algorithms for coherent and incoherent detection;

V. Form and steer the beam associated with the M-sensor distribution, whenever the wavefront of the desired received signal permits.

In addition to these general results (Part I) are many specific relations (Part II), for important particular cases, as well. A detailed account of the major general and particular results is given in Section 12 of the Report.

This Report is organized as follows: In Part I we present a general canonical theory of optimum M-sensor threshold signal detection in non-gaussian space-time noise or interference. Section 2 includes the threshold algorithms for general correlated sampling, sufficient conditions for asymptotic optimality of detector structure and performance, and conditions under which spatial and temporal processing may be interchanged. Sections 3 and 4 give the explicit forms of optimum threshold algorithms and their

interpretation as adaptive systems employing various "matched filters" for the dominant noise and weak signals, under independent sampling régimes Section 5 completes Part I with the explicit algorithms for stationary and homogeneous field environments.

In Part II we make applications specifically to underwater acoustic interference environments. Thus, in Secs. 6, 7 we develop statistical-physical models of typical received signal and various noise environments, with particular attention to their space-time covariance functions, in addition to the needed first-order probability density function (pdf) of the noise itself. Section 8 presents various optimum threshold detection algorithms, specifically for the fading, sinusoidal signals of interest here. The associated optimum weak-signal performance is determined in Sec. 9, expressed as a minimum detectable signal, itself an explicit function of sample-size, signal waveform moments, and appropriate first-order interference statistics. Suboptimum detectors--simple correlators and "clipper"-correlators--are obtained in Section 9, along with measures of the degradation of their performance caused by their nonoptimality. These results are illustrated numerically by a series of typical examples in Section 11: significant improvement o(6 db or more, sometimes much more) can be expected by employing a composite detector which is close to optimum. General and particular results are summarized in Section 12, which includes an extensive list of further analytical and experimental topics for investigation. Several, more immediate next-steps suggested by the results of the present study are indicated.

We emphasize that our general approach here is "global" or "top-down," in that we aim initially to create as broad a conceptual structure as possible (and still remain quantitatively manageable and explicit). From this we proceed with as few approximations and limiting assumptions as possible, to reach specific subclasses of the general (detection) problem whose "anatomy" can then be fully expressed analytically, i.e., by explicit algorithms and performance measures, from which detailed numerical results can also be obtained. [It is perhaps instructive to note that this global approach, incidentally, is similar to that employed by a number of foreign investigators [35], who, however, have confined their analyses to date largely to the gaussian environment.]

Finally, to assist the nonspecialist reader who wishes to understand the concepts involved, the broad outlines of the technical approach, and the quantitative results obtained, we suggest that Sections 1 and 2 be surveyed, along with the introductory material to Sections 3-11. Particular attention should be given to Sections 4, 5.4, 5.5 in Part I, and to Sections 6.1, 8, 9.3, and all of Sections 11 and 12. (A survey of the Table of Contents may indicate other areas of immediate interest.)

Part I. Optimum Canonical Binary M-Element Threshold Detection Theory

Section 2. Optimum Threshold Detection: Canonical M-Sensor Algorithms

In keeping with our "top-down" philosophy (as stated in Sec. 1, penultimate ¶), we begin with a concise summary of the principal results of recent studies of canonical threshold detection theory for binary, i.e., two-alternative situations [10]-[12], [16], extended here specifically to the general M-element (or M sensor) receiving array. For the present we leave open the specific geometry of the array, as well as the particular class of desired signal and applicable interference fields. These will be discussed in some detail in Part II following, where examples of specific applications of the theory are presented. We emphasize that we are still dealing with the possible presence or absence of a single signal, unlike the "L-ary" or L-alternative (L>2) cases, where more than one signal can be present [18].

As mentioned earlier [cf. Sec. 1.], a fundamental problem in developing effective threshold algorithms (for both detection and estimation) is to obtain expressions which are bounded in complexity. Thus, only a few terms of an appropriate series expansion of the (always optimum) likelihood ratio algorithm, $\Lambda_J(\underset{\sim}{x}|\theta)$, [17], about the null-signal ($\theta=0$) can be practically retained. These, in turn, must likewise maintain their threshold optimum character as the sample-size (~J) of the received data $\underset{\sim}{x}(=x_1,\ldots,x_J)$ becomes increasingly large. This is critically important when the signal is weak, which is the situation of primary interest here, since these large effective data samples are required for the practically useful small probabilities of error (or large correct detection probabilities).

Detectors based on an appropriate expansion of Λ_J about $\theta=0$, which likewise minimize these error probabilities, are usually called Locally Optimum Bayes Detectors (LOBD's), [8]-[12]; esp. [12], Sec. 2.2. For these LOBD's to retain their optimal properties as $J\to\infty$, i.e., to become asymptotically optimum (AO), so that no additional terms in the expansion are needed, it is necessary to employ the <u>correct bias</u>, $B_J^{(*)}(\theta)$, as has been recently shown ([11], [12] Appendix 3, [16]). A major difficulty of most earlier work [14], [15] has been the lack of correct bias [dependent on sample size and input signal-to-noise ratio (θ)], which in turn has vitiated the optimal character of these processing algorithms [16].

Accordingly, using the results of the single-element or single beam (M=1) aperture obtained principally in [10]-[12], we shall develop here binary threshold detection algorithms which have the correct bias component, and thus are both LOBD and AO, as $J \to \infty$, for M (≥ 1) array elements. Three principal modes of reception are examined: (1) coherent detection; (2) incoherent detection; and (3) composite detection, which employs an additive combination of (1) and (2). Our basic initial* problem is to determine the presence or absence of a desired signal in a broad class of underwater acoustic environments. Thus, the decision process requires typically distinguishing between the "on-off" hypothesis states H_1: $S \oplus N_0 \oplus I$ vs. H_0: $N_0 \oplus I$, where N_0 is background noise and I represents the often-stronger ambient acoustic interference (AAI), whose specific structure we will develop in Part II following. Reception is passive, in the sense that the receiver has no direct control over the transmitted signals, both desired and undesired. However, it is reasonably assumed that the signal and various noise and interference fields are additive (so that $\oplus \equiv$"combined with" can be replaced by + in $H_{1,0}$, etc.). Although the background noise (N_0) may safely be regarded as gaussian, the AAI is highly nongaussian, a factor which significantly alters the processing algorithms, as we have noted in Sec. 1. , and which we shall address in Part II.

2.1 Remarks on Binary Detection Theory

Optimum reception, and particularly, optimum detection here, is well-known to require the minimization of the probabilities of decision error, in the more general context of minimizing the average risk, or cost, of decisions (cf. Chapter 18, [17]). For the binary, i.e., two-alternative situations discussed in this report, this is achieved by constructing the "test statistic" or reception algorithm, $\Lambda_J(\underset{\sim}{x}|\theta)$. Here Λ_J is the generalized likelihood ratio, defined in the standard way by

---

* We reserve to a subsequent study the important extensions to "signal extraction," where having determined the presence of the desired signal, we wish to estimate its space-time structure. Similarly deferred is the extension to (optimum) L-ary signal detection, cf. [18], where L (>2) signals may be present.

$$\Lambda_J(\underset{\sim}{x}|\theta) \equiv p\langle F_J(\underset{\sim}{x}|\underset{\sim}{S}(\theta))\rangle_S / qF_J(\underset{\sim}{x}|0) \ , \qquad \mu \equiv p/q \ , \tag{2.1}$$

where now (the column vector) $\underset{\sim}{x} = [X_1/\sqrt{\psi_1}, X_2/\sqrt{\psi_2}, \ldots, X_J/\sqrt{\psi_J}]$ is the set of J samples of the (here) normalized received data, $\underset{\sim}{X}$, in which $\psi_k=(N_o+I)_k=\langle n_o^2\rangle_k$ is the total accompanying (noise and interference) intensity. Both $\underset{\sim}{X}$ and the $[\psi_k]$ are measured at the same point: at the outputs (to the rest of the receiver) from each of the M-sensor elements, or at any other similar location before any subsequent nonlinear operations, for example, at the outputs of the ARI (≡ sensor-element × RF × IF) stages of a narrow band receiver, particularly as employed in electromagnetic interference (EMI) situations [10]-[12]. Here, also, $\underset{\sim}{S}$ (=$[S_1(\theta), \ldots, S_J(\theta)]$) represents the sampled desired signal, with $\langle\ \rangle_S$ denoting averages over the signal and/or its random parameters, while p (=1-q), ($0 \leqslant p,q \leqslant 1$) are respectively the a priori probabilities of H_1 and H_0, i.e., that the received data set $\underset{\sim}{x}$ does or does not contain the desired signal. Finally, the quantity $F_J(\underset{\sim}{x}|\underset{\sim}{S})$ is the probability density function (pdf) for the data set $\underset{\sim}{x}$, under the condition of the presence of a signal ($\underset{\sim}{S}$), in the usual way.

The optimum (here "on-off," or simple binary) detection process, then, consists of comparing Λ_J (or any monotonic function of Λ_J, say $\log \Lambda_J$) with a suitably chosen threshold, $\mathcal{K}$, e.g.,

$$\left.\begin{array}{lll} \underline{\text{decide } H_0}\text{: "no signal is present" if} & \log \Lambda_J < \log \mathcal{K} & \\ \underline{\text{decide } H_1}\text{: "signal as well as interference* is present if}} & \log \Lambda_J \geqslant \log \mathcal{K} & \end{array}\right\} \tag{2.2}$$

Thus, $\log \Lambda_J$ is the optimum detection algorithm, or rule, for processing the received data, while (2.2) embodies the detection process.

Similarly, for suboptimum (≡ nonoptimum) systems, the detection algorithm is represented by some (predetermined) function, $g_J(\underset{\sim}{x})$. The decision process, like (2.2), has the form

---

* We shall use the term "interference" henceforth to include background noise, as well as the ambient acoustic interference (AAI).

$$\left.\begin{array}{ll} \underline{\text{decide } H_0}\text{: "no signal is present," if} & g_J(\underline{x}) < \log K; \\ \underline{\text{decide } H_1}\text{: "signal is present," if} & g_J(\underline{x}) \geq \log K \end{array}\right\} \qquad (2.3)$$

where now the threshold K is $\mathcal{K}(K)$, and usually $K = a\mathcal{K}$, with $\underline{a}$ some (positive) constant.

Performance is expressed generally as some linear function of the type I and II error probabilities (α,β), e.g.,

$$\alpha = \alpha(S|N) = \int_{\log\mathcal{K}}^{\infty} w_1(g_J|0)dg; \quad \beta = \beta(N|S) = \int_{-\infty}^{\log\mathcal{K}} w_1(g_J|S)dg \qquad (2.4)$$

which for optimal systems (which minimize average cost or risk), become

$$\alpha^* = \int_{\log\mathcal{K}}^{\infty} w_1(\ell_J^*|0)d\ell_J^*; \quad \beta^* = \int_{-\infty}^{\log\mathcal{K}} w_1(\ell_J^*|S)d\ell_J^* \qquad (2.5)$$

Here the $w_1(\ell_J^*|0)$ etc. are the (first order) pdf's of the optimum or sub-optimum test statistic [or processing algorithm in conjunction with (2.2), (2.3)], $\ell_J^* = \log \Lambda_J$ or $g(\underline{x})^*$, respectively under H_0, H_1. [For the associated average costs or risks, see Sec. 19.1 of [17].] For our purposes here we shall employ a Neyman-Pearson Observer (Sec. 19.2-1, [17]), where the (conditional) false-alarm or Type I error probability $[\alpha=\alpha_F^{(*)}]$ is fixed and the probability $P_D^* = p(1-\beta^*)$ of correctly detecting the presence of the desired signal is maximized.†

2.2 Canonical Threshold (Binary ≡ "On-off") Detection: An M-Element Formalism

In the detection phase of reception, which is the topic of interest in the present report, it is not usually possible to obtain either explicit forms of the optimum algorithm $\ell_J^* = \log \Lambda_J$, (2.1), or its associated pdf's $w_1(\ell_J^*|0 \text{ or } S)$. These quantities can only be approximated. Ingenious efforts are required and even these are often insufficient, if results for all input signal levels are desired. The "literal"--i.e., purely computational attack on ℓ_J^*--is economically prohibitive and analytically unrevealing.

Since for the important purposes of predicting performance analytical

---

† More completely, the average risk is minimized under this constraint.

methods are not generally realizable, we must seek other approaches. Fortunately, as we have mentioned in Sec. 1 above, it is possible to obtain canonical results analytically, in the critical limiting cases of weak signals, which is necessarily of great interest, as it is the situation which establishes limiting performance, i.e., the best that can be done under this constraint.

Specifically, the limiting optimal algorithm for the "on-off" detection of any signal and interference, in the original case of a single receiving element or aperture (beam), M=1, cf. Eq. (2.9), [12], is readily extended to the M-element case (M≥1), by the same basic procedure of expanding ℓ_J^* about the null signal (θ=0), as described above. We obtain, for the usual situation of additive signal and interference,

$$\ell_J^* = \log \Lambda_J(\underline{x}|\theta) \equiv g_J^*(\underline{x};\theta_{MN}) + t_J(\underline{x},\theta_{MN}) \tag{2.6a}$$

where now

$$\boxed{g_J^*(\underline{x};\theta_M) = \log \mu - \theta_{MN}\tilde{\underline{y}}\bar{\underline{s}}' + \frac{\theta_{MN}^2}{2}[\tilde{\underline{y}}(\rho_s' - \bar{\underline{s}}'\tilde{\underline{s}}')y + \text{trace } \rho_{\underline{s}}'\tilde{\underline{z}}] + \hat{B}_J^*(\theta_{MN})} \tag{2.6b}$$

and t_J is a remainder term which [from recent work, cf. [11],[12]] can be made to vanish, prob. 1, under H_0 and H_1, as overall sample size J→∞, by proper choice of the bias term, $\hat{B}_J^*$, with θ_{MN} suitably small. Thus, g_J^* is asymptotically optimum (AO), as well as being locally optimum (LOB), cf. remarks in Sec. (2.3)ff.

The explicit meaning of the elements of (2.6b) is derived here under the general initial assumption that both the background noise and interference fields are not only non-stationary but are inhomogeneous, as well. Thus, we write in detail (where n refers to time, and m to space):

$$\boxed{\theta_{MN}^2 \equiv \sum_{m,n}^{M,N} \frac{\langle a_{on}^{(m)2}\rangle}{MN}} \; ; \quad a_{on}^{(m)} = A_{on}^{(m)}/\sqrt{2\psi_n^{(m)}} ; \quad S_n^{(m)} = a_{on}^{(m)} s_J^{(m)} \sqrt{\psi_n^{(m)}} \; ; \tag{2.7a}$$

$$\psi_n^{(m)} = \langle n_{on}^{(m)2}\rangle \; ; \quad \langle n_{on}^{(m)}\rangle = 0 \; ; \tag{2.7b}$$

$$\underline{s}^{(m)'} = [a_{on}^{(m)} s_n^{(m)} / \theta_M] \; ; \quad \theta_n^{(m)} \equiv a_{on}^{(m)} s_n^{(m)} \; ; \quad \langle a_{on}^{(m)2} \rangle = \langle s_n^{(m)2} \rangle / \psi_n^{(m)} ; \tag{2.7c}$$

$$\underline{s}^{(m)} = [s^{(m)}(t_n - \varepsilon)] = [s_1^{(m)}, s_2^{(m)}, \ldots, s_n^{(m)}, \ldots, s_N^{(m)}] \tag{2.7d}$$

where the $\underline{s}^{(m)}$ are normalized signal waveforms, such that $\langle s^{(m)2} \rangle = 1$. The $\langle a_{on}^{(m)2} \rangle$ are input signal-to-noise power ratio at each (m-)element, while the $\psi_n^{(m)}$ are the mean-intensities of the corresponding interference (plus background noise) (at times n=1, ..., N) which have no d.c. (i.e., means) components.

The various vectors and matrices in (2.6a,b) are specifically here

$$\underline{y} = [y_i] = [\frac{\partial}{\partial x_i} \log w_{J,o}] \; ; \quad \underline{z} = [z_{ij}] = [\frac{\partial^2}{\partial x_i \partial x_j} \log w_{J,o}] = \tilde{\underline{z}} ; \tag{2.8a}$$

$$\langle F_J | \underline{x} | S(\theta) \rangle_S = \langle w_J(\underline{x} - \theta_{MN} \underline{s}') \rangle_S \; ; \quad w_{J,o} = w_J(\underline{x}) = F_J(\underline{x} | 0) ; \tag{2.8b}$$

where $w_J(\underline{x})$ is the Jth-order pdf of the noise (and interference) alone (H_0), with

$$\underline{s}' = [\underline{s}^{(m)'}] = [\underline{s}^{(1)'}, \ldots, \underline{s}^{(m)'}, \ldots, \underline{s}^{(M)'}] \equiv [[a_{on}^{(m)} s_n^{(m)} / \theta_{MN}]] = [s_i'] \tag{2.9a}$$

$$\therefore \underline{\rho}_s' = [\langle s_i' s_j' \rangle] = [\langle \underline{s}^{(m)'} \tilde{\underline{s}}^{(m)'} \rangle_{ij}] = [\langle [a_{on}^{(m)} s_n^{(m)}][a_{on'}^{(m')} s_{n'}^{(m')}] / \theta_{MN}^2 \rangle_{ij}]$$
$$= \tilde{\underline{\rho}}_s' \; ; \tag{2.9b}$$

(the symbol "~" denotes the transposed vector or matrix). Notationally, we have [i,j=1,...,J] for the i^{th} (or j^{th}) sample of $\underline{x}=[x_i]=[\underline{x}_m]=[x_{m,n}]$, viz. $x_i = x_{(m,n)=i}$, where $\underline{x}$ is always a (column) vector. Since it is usually critical in practice to distinguish spatial sampling from time sampling, we have adopted the following notational conventions:

$$\begin{cases} (m,m') = 1, \ldots, M: & \text{spatial sample indexes} \equiv \text{the m- or m'-array or aperture element;} \\ (n,n') = 1, \ldots, N: & \text{temporal sample indexes} \equiv \text{the } n^{th} \text{ or } n'^{th} \text{ time sample.} \end{cases} \tag{2.10}$$

These interpretations are also to be regarded as independent of index-position in the notation: thus $y_{m,n}$ = the n^{th} time sample of y at the m^{th} element = $y_{n,m}$. Accordingly, we have

$$\underset{\sim}{y} = [\underset{\sim}{y}_m] = [\underset{\sim}{y}_1, \ldots, \underset{\sim}{y}_M] = [y_{m,n}] = [\underset{\sim}{y}_n] = [\underset{\sim}{y}_1, \ldots, \underset{\sim}{y}_N] = [y_{n,m}] \quad (2.11)$$

where $\underset{\sim}{y}_m$ represents the n=1,...,N time samples of y taken at the m^{th}-element, as distinct from $\underset{\sim}{y}_n$, which represents the m=1,...,M spatial samples taken at time n. Of course, $\underset{\sim}{y}_m \neq \underset{\sim}{y}_n$ (unless M and N=1), although $y_{m,n} = y_{n,m}$, from the interpretation of m and n, cf. (2.10), as independent of the index-position, i.e., n always refers to time-sampling, while m always refers to spatial sampling.

I. The Matrix Elements of the Desired Signal

Accordingly, we can write for the various desired signal samples the following first- and second-order moments:

$$\bar{\underset{\sim}{s}}' = [\langle \underset{\sim}{s}^{(m)'} \rangle] = [[\langle a_{on}^{(m)} s_n^{(m)} / \theta_{MN} \rangle]] = [\langle \underset{\sim}{s}_n' \rangle], \quad (2.12a)$$

$$(\underset{\sim}{\rho}_s')_{ij \equiv mm';nn'} = \left[\left[\frac{\langle a_{on}^{(m)} a_{on'}^{(m')} \rangle}{\theta_{MN}^2} \langle s_n^{(m)} s_{n'}^{(m')} \rangle\right]_{mm'}\right] = [\underset{\sim}{\rho}_{mm'}] \quad (2.12b)$$

$$= \left[\left[\frac{\langle a_{on}^{(m)} a_{on'}^{(m')} \rangle}{\theta_{MN}^2} \langle s_n^{(m)} s_{n'}^{(m')} \rangle\right]_{nn'}\right] = [\underset{\sim}{\rho}_{nn'}] . \quad (2.12c)$$

In more detail, we have for $\bar{\underset{\sim}{s}}'$:

$$\bar{\underset{\sim}{s}}' = \begin{bmatrix} [\bar{s}_1^{(1)'}, \bar{s}_2^{(1)'}, \ldots, \bar{s}_n^{(1)'}, \ldots, \bar{s}_N^{(1)'}] \\ \vdots \\ [\bar{s}_1^{(m)'}, \bar{s}_2^{(m)'}, \ldots, \bar{s}_n^{(m)'}, \ldots, \bar{s}_N^{(m)'}] \\ \vdots \\ [\bar{s}_1^{(M)'}, \bar{s}_2^{(M)'}, \ldots, \bar{s}_n^{(M)'}, \ldots, \bar{s}_N^{(M)'}] \end{bmatrix} \text{ (= column vector) =}$$

N×M rows = J elements

$$= \begin{bmatrix} [\underline{s}_1^{(1)\prime}, \ldots, \underline{s}_1^{(m)\prime}, \ldots, \underline{s}_1^{(M)\prime}] \\ \vdots \\ [\underline{s}_n^{(1)\prime}, \ldots, \underline{s}_n^{(m)\prime}, \ldots, \underline{s}_n^{(M)\prime}] \\ \vdots \\ [\underline{s}_N^{(1)\prime}, \ldots, \underline{s}_N^{(m)\prime}, \ldots, \underline{s}_N^{(M)\prime}] \end{bmatrix}_{M\times N \text{ rows} = J \text{ elements}} \tag{2.13}$$

where $\underline{s}_n^{(m)\prime} = \overline{a_{on}^{(m)}}\,\underline{s}_n^{(m)}/\theta_M$, and where there is negligible loss of generality in regarding waveform amplitude ($\sim a_{on}$) and the normalized waveform ($s_n^{(m)}$) as statistically independent, cf. (2.12b, c) also.

Similarly, we find that the signal covariances matrices $\underline{\rho}_s'$ (2.12b, c) can be expressed in more expanded form by

$$\underline{\rho}_s' = [\underline{\rho}_{mm'}^{(N)}] = \begin{bmatrix} \underline{\rho}_{11}^{(N)} & \underline{\rho}_{12}^{(N)} & \cdots & \underline{\rho}_{1M}^{(N)} \\ \underline{\rho}_{21}^{(N)} & \underline{\rho}_{22}^{(N)} & \boxed{\underline{\rho}_{mm'}^{(N)}} & \vdots \\ \underline{\rho}_{M1}^{(N)} & \cdots & \cdots & \underline{\rho}_{MM} \end{bmatrix}_{(M\times M) \text{ of } (N\times N)} \qquad \underline{\rho}_{mm'}^{(N)} \equiv [\hat{\mu}_{nn'}^{(mm')}\rho_{nn'}^{(mm')}]_{(N\times N)} \tag{2.14}$$

where the elements of $\underline{\rho}_{mm'}^{(N)}$ are

$$\hat{\mu}_{nn'}^{(mm')} \equiv \langle a_{on}^{(m)} a_{on'}^{(m')} \rangle / \theta_{MN}^2 \; ; \qquad \rho_{nn'}^{(mm')} \equiv \langle s_n^{(m)} s_{n'}^{(m')} \rangle \; . \tag{2.14a}$$

The averages $\langle\ \rangle$ here are over both time (n,n') and space (m,m'), e.g., $\langle\ \rangle = \langle\langle\ \rangle_{time}\rangle_{space} = \langle\langle\ \rangle_{space}\rangle_{time}$. Alternatively, we can write

$$\underline{\rho}_s' = [\underline{\rho}_{nn'}^{(M)}] = \begin{bmatrix} \underline{\rho}_{11}^{(M)} & \underline{\rho}_{12}^{(M)} & \cdots & \underline{\rho}_{1N}^{(M)} \\ \underline{\rho}_{21}^{(M)} & \underline{\rho}_{22}^{(M)} & \boxed{\underline{\rho}_{nn'}^{(M)}} & \vdots \\ \underline{\rho}_{N1}^{(M)} & \cdots & \cdots & \underline{\rho}_{NN} \end{bmatrix}_{(N\times N) \text{ of } (M\times M)} \qquad \underline{\rho}_{nn'}^{(M)} \equiv [\hat{\mu}_{nn'}^{(mm')}\rho_{nn'}^{(mm')}]_{(M\times M)} \tag{2.15}$$

where now the elements of $\underline{\rho}_{nn'}^{(M)}$ are again given by (2.14a). The basic difference between the matrix element covariances of (2.14) and (2.15) is

that the former are covariances over time (n,n') for a covariance between given spatial elements (m,m'), whereas the latter are covariances over spatial elements (m,m'), for covariance structures over specified time intervals (n,n'). In general, unless there is rapid fading of the amplitudes and/or large doppler smearing of the desired signal, the elements $\hat{\mu}_{nn'}^{(mm')}$ and $\rho_{nn'}^{(mm')}$ do not vanish significantly off the diagonal. In any case, we have from (2.7)

$$\rho_{nn}^{(mm)} = 1 \; ; \quad \hat{\mu}_{nn}^{(mm)} = \langle a_o^{(m)2} \rangle / \theta_{MN}^2 . \tag{2.16}$$

Of course, for the single element or single beam (M=1), $\underset{\sim}{\rho}_s' = [\rho_{nn'}^{(1)}] = [\hat{\mu}_{nn'}, \rho_{nn'}]$, which is the earlier, simpler result [10] - [12], as expected.

II. The Noise† Matrix Elements

The principal noise components of the general canonical LOBD, (2.6b), are described by (2.8a, b) and depend on the explicit nature of the "noise alone" multivariate pdf $w_J(\underset{\sim}{x})$. In many cases (such as the ones examined here) independent temporal and spatial sampling can be used, with very considerable analytic simplifications. Thus, we have

(i) Independent time samples: $$\therefore w_J(\underset{\sim}{x}) = \prod_{n=1}^{N} w_M(\underset{\sim}{x}_n); \quad \underset{\sim}{x}_n = [x_{1n}, x_{2n}, \ldots, x_{Mn}] \tag{2.17a}$$

and

(ii) Independent space samples: $$w_J(\underset{\sim}{x}) = \prod_{m=1}^{M} w_N(\underset{\sim}{x}_m); \quad \underset{\sim}{x}_m = [x_{m1}, x_{m2}, \ldots, x_{mN}] \tag{2.17b}$$

For totally independent sampling, we have

(iii) Independent time and space samples: $$w_J(\underset{\sim}{x}) = \prod_{m=1}^{M} \prod_{n=1}^{N} w_1(x_{mn}) = \prod_{n=1}^{N} \prod_{m=1}^{M} w_1(x_{m} \tag{2.17c}$$

---

† Henceforth, for compactness, we shall use the term "noise" to include both background noise (which is usually gaussian), and the interference, which is usually highly nongaussian.

Other possibilities are:

$$\left.\begin{aligned} &\underline{\text{(iv) Deterministic spatial samples}}: \quad w_J(\underset{\sim}{x}) = w_N(\underset{\sim}{x}_M) = w_N(\underset{\sim}{x}); \\ &\underset{\sim}{x} = [x_1, \ldots, x_N] \end{aligned}\right\} \tag{2.18}$$

Here there is no statistical dependence of the noise field on space, only on time, with analogous behaviour for deterministic temporal samples.

In addition to the great analytic simplifications of independent sampling, there is the important result that performance measures based on independent samples are conservative: if besides these sample values, one were able to use the further statistical information contained in the various correlation structures of the joint distribution, performance would, in principle, be improved. [We suspect that this improvement is relatively small, however, judging from the gaussian examples: most of the improvement comes, in any case, from increasing the sample size. See VIII, Sec. 12.3 ff.]

III. Canonical Threshold Detection Algorithms: The General Case

From (2.6b) we may describe the three principal types of optimum threshold algorithms, accoding to the mode of observation. The correct bias is obtained by taking the H_0-average (over $\underset{\sim}{x}$) of the next (non-vanishing) term in the expansion (2.6a) [cf. [11]; [12], Appendix A.1]. Thus, we find (cf. Appendix A.1, [12]) that, generally,

(1) Coherent Detection ($\langle\theta\rangle \neq 0$)

$$\left.\begin{aligned} &\boxed{g_c^* = B_c^* - \langle\tilde{\underset{\sim}{\theta}}\rangle \underset{\sim}{y}}\,; \qquad \underset{\sim}{\theta} = [\underline{\theta}_m] = [\theta_{m,n}] = [a_{on}^{(m)} s_n^{(m)}] \\ &\qquad\qquad\qquad\qquad\quad \underset{\sim}{y} = [\underline{y}_m] = [y_{m,n}] \end{aligned}\right\} \tag{2.19}$$

with

$$B_c^* \equiv \log \mu + \frac{1}{2!} \langle \tilde{\underset{\sim}{y}} [\theta^2_{MN} \underline{\rho}'_s - \langle\underset{\sim}{\theta}\rangle \langle\tilde{\underset{\sim}{\theta}}\rangle] \underset{\sim}{y} + \langle \tilde{\underset{\sim}{\theta}} \underset{\sim}{z} \underset{\sim}{\theta} \rangle\rangle_{H_0} \; ; \quad \theta^2_{MN} \underline{\rho}'_s = \langle \underset{\sim}{\theta} \tilde{\underset{\sim}{\theta}} \rangle \tag{2.19a}$$

cf. (2.12); (2.14), (2.15), where now from (2.7) and (2.14a) we can write explicitly

$$\underline{\langle\theta\rangle} = [\langle a_{on}^{(m)}\rangle \langle s_n^{(m)}\rangle]_{MN} \; ; \quad \underline{\langle\theta\tilde{\theta}\rangle} = [\hat{a}_{nn'}^{(mm')}\rho_{nn'}^{(mm')}]_{(MN)\times(MN)}$$

$$= [\langle a_{on}^{(m)} a_{on'}^{(m')}\rangle \langle s_n^{(m)} s_{n'}^{(m')}\rangle]_{J\times J}, \qquad (2.19b)$$

again with little loss of generality in treating amplitude ($\sim a_o$) and waveform ($\sim s$) as statistically independent.

(2) Incoherent Detection ($\underline{\langle\theta\rangle} = 0$)

$$\boxed{g_{inc}^* = B_{inc}^* + \frac{1}{2!}[\underline{\tilde{y}}\theta_{MN}^2\underline{\rho'_s y} + \langle\underline{\tilde{\theta}}\underline{\tilde{z}}\underline{\theta}\rangle]}, \qquad (2.20)$$

with the bias

$$B_{inc}^* = \log\mu + \frac{1}{4!}\left\langle \sum_{ijkl}^{J} \langle\theta_i\theta_j\theta_k\theta_l\rangle \frac{w_J^{(ijkl)}}{w_J} - 3\left\{\sum_{ij}\langle\theta_i\theta_j\rangle(y_i y_j + z_{ij})\right\}^2 \right\rangle_{H_0} \qquad (2.20a)$$

cf. (A.1-8a) of [12], where

$$w_J^{(ijkl)} \equiv \frac{\partial^4 w_J}{\partial x_i \partial x_j \partial x_k \partial x_l} \; ; \qquad \text{cf. (2.8a) for } y_i,\ z_{ij} \qquad (2.20b)$$

[It is required here that $\langle\theta_j\theta_k\theta_l\rangle=0$, as well as $\langle\theta_j\rangle=0$, if the signals are broadband.]

(3) Composite Detection ($\underline{\langle\theta\rangle} \neq 0$)

It is shown in [12] that the optimum canonical composite threshold detector is simply the sum of the coherent and incoherent threshold algorithms (1) and (2) above, viz.:

$$g_{comp}^* = g_c^* + g_{inc}^* - \log\mu \qquad (2.21a)$$

or,

$$\boxed{g_{comp}^* = (B_c^* + B_{inc}^* - \log\mu) - \langle\underline{\tilde{\theta}}\rangle\underline{y} + \frac{1}{2!}[\underline{\tilde{y}}\theta_{MN}^2\underline{\rho'_s y} + \langle\underline{\theta}\underline{\tilde{z}}\underline{\theta}\rangle]} \qquad (2.21b)$$

where the component bias is

$$B^*_{comp} = B^*_c + B^*_{inc} - \log \mu = \text{Eq. (2.19a)} + \text{Eq. (2.20a)} - \log \mu. \qquad (2.21c)$$

2.3 Asymptotic Optimality (AO)

A sufficient condition for the asymptotic optimality of the properly truncated threshold expansion, g^*_J, of the general (binary) likelihood ratio, here expressed as $\log \Lambda_J$, cf. (2.6a, b), is that g^*_J be asymptotically normally distributed, with means $\mp \sigma^{*2}_{0J}/2$ (respectively under H_0, H_1) and with variances $\text{var}_0\, g^*_J \equiv \sigma^{*2}_{0J}$, e.g., $\sigma^{*2}_{1J} = \sigma^{*2}_{0J}$, as $J(=MN)>>1$, e.g., the pdf's of g^*_J are

$$w_1(g^*_J|H_0) \simeq \frac{e^{-(g^*_J + \sigma^{*2}_{0J}/2)^2/2\sigma^{*2}_{0J}}}{\sqrt{2\pi\sigma^{*2}_{0J}}}\ ; \quad w_1(g^*_J|H_1) \simeq \frac{e^{-(g^*_J - \sigma^{*2}_{0J}/2)^2/2\sigma^{*2}_{0J}}}{\sqrt{2\pi\sigma^{*2}_{0J}}}. \qquad (2.22)$$

[Here the $J(=MN)$ data samples $\{\underset{\sim}{x}\}$ are not necessarily independent; see, in particular, Appendix A.3-3 of [12], for details.] Our earlier results (Appendix A3-6, [12]) also show that the proper bias term, B^*_J, appearing in g^*_J, cf. (2.6b), is always given here by

$$\hat{B}^*_{J\text{-coh,inc}} = -\sigma^{*2}_{0J}/2 = \langle O(\theta^2_J)\rangle_{H_0\text{-coh}};\quad \langle O(\theta^4_J)\rangle_{H_0\text{-inc}}, \qquad (2.23)$$

namely, the bias term may be obtained directly from the terms $O(\theta^2_J)$ in the expansion of $\log \Lambda_J$ averaged over H_0 for coherent detection, and from the terms $O(\theta^4_J)$ for the incoherent cases, which is in turn always equal to the appropriate $-\sigma^{*2}_{0J}/2 = -\text{var}_0\, g^*_J$.

For the composite cases we have, since $B^*_J \equiv B^*_J + \log \mu$, from (2.21c),

$$\hat{B}^*_{J\text{-comp}} = \hat{B}^*_{J\text{-coh}} + \hat{B}^*_{J\text{-inc}} = -\frac{1}{2}\left(\sigma^{*2}_{0J\text{-coh}} + \sigma^{*2}_{0J\text{-inc}}\right). \qquad (2.24a)$$

Moreover, for the composite detectors (2.21a), it can be similarly shown that

$$\sigma^{*2}_{0J\text{-comp}} = \text{var}_0 g^*_{J\text{-comp}} = \sigma^{*2}_{0J\text{-coh}} + \sigma^{*2}_{0J\text{-inc}}, \tag{2.24b}$$

so that once we have established the LOB and AO structures of the associated coherent and incoherent detectors [cf. (2.19), (2.20)] along with their respective $(\text{var}_0\ g^*_J)_{\text{coh,inc}}$, we have $\sigma^{*2}_{0J\text{-comp}}$ directly from (2.24b). (See Appendix A.3-6, [12], esp. Secs. II, III therein, for details.)

2.4 Factorability and Separability

In the general cases of detection and estimation it is not possible to separate the geometry-dependent (i.e., spatially-dependent) elements of the received fields from their statistical characteristics. Moreover, temporal processing (over n) and spatial processing (over m) are likewise entwined, so that it is not possible, for example, to process the output of a single sensor (m) in time and independently combine the result with other sensor outputs to achieve a correct result for decision-making. For arbitrary input signal levels this is the consequence of both the signal intercorrelations and of the noise, similarly (although signal and noise are themselves independent). For threshold signal reception, it is the noise intercorrelations--expressed in the detailed structure of the J-fold pdf $w_J(\underset{\sim}{x})$--which prevent these various types of separability generally.

It is convenient to describe these "separability" concepts somewhat more concisely and precisely: From earlier work ([19], Sec. II, B) we introduce the term "factorability":

I. Factorability: this occurs when it is possible to separate the array (i.e., spatial) geometry from the noise and signal statistics, in the sense that changing one does not alter the other. More precisely, we say* that "factorization is defined as the procedure of resolving

---

* This is a slightly extended paraphrase of the first sentence of Sec. II, B, [19], broadened to include general statistical, i.e., nongaussian situations.

the overall 'structure' or processing operations into a product of two independent (sets of) operators, one of which depends only on the geometrical properties of the sensing array and the other of which depends only on the (temporal) statistical properties of the signal, the internal, and the external noise fields."

Unfortunately, it is almost never possible to achieve factorization, particularly in the threshold signal cases (since in gaussian noise fields [cf. Sec. II, C] the conditions are too strict for realistic application). However, if we relax them, to the following notion of "separability," the latter can often be achieved:

II. Separability: this is said to occur when temporal processing (over n) and spatial processing (over m) can be interchanged, i.e., carried out separately.

Fortunately, this situation arises in the threshold régimes whenever independent sampling of the noise field is possible; (it is desired, of course, that the spatio-temporal coherence of the signal field be maintained, which is ultimately determined by the channel through which the desired signal is propagating). Separability, as defined above, is thus a much less restrictive condition than factorability, with the considerable practical advantage that any desired modifications of the spatial/temporal processing algorithms can be effected without disturbing the other. For the algorithms of Sec. 3 et seq. separability is directly demonstrated. In general, i.e., for arbitrary signal levels, the desired signal correlations do not permit separability, even though it may be possible to sample the noise field independently.

Section 3. Optimum Threshold Detection Algorithms: Independent Space-Time Sampling

As we have already noted above [Sec. 2.2-III], the case of independent sampling is a critically limiting, conservative operation, which we use here and henceforth as providing the desired form of algorithm. Apart from the great simplifications introduced by independent sampling, it is also dictated by the state of our analytical capabilities: the general N^{th}-order

(and for that matter, the MN^{th}-order) pdf's of nongaussian noise are unknown, and in known specific cases are too complex for exploitation.

Accordingly, from the results of Section 2.2-III and (2.17c) we have at once for (statistically) independent sampling of the noise field in both space and time

$$w_J = \exp \sum_{m}^{M} \sum_{n}^{N} \log w_1(x_{m,n}) \; ; \quad \log w_J = \sum_{m=1}^{M} \sum_{n=1}^{N} \log w_1(x_{m,n}) \tag{3.1}$$

from which is it immediately clear that w_J, and $\log w_J$, are <u>separable</u>, in the sense of Section 2.4.

Remembering that $i=(m,n)$, $j=(m',n')$, $(i,j=1, \ldots, MN=J)$ are double number indexes, as noted, we can apply (3.1) to (2.19), to obtain the <u>canonical coherent LOBD algorithm</u>†

$$\boxed{g^*_{coh} = B^*_{coh} - \sum_{m,n}^{M,N} \ell_{m,n} \bar{\theta}_{m,n}} \; ; \quad \bar{\theta}_{m,n} = \langle a^{(m)}_{on} \rangle \langle s^{(m)}_{n} \rangle$$

$$y_i \equiv \ell_{(m,n)} \equiv \frac{\partial \log w_1(x_{m,n}|\mathcal{P}_{m,n})}{\partial x_{(m,n)=i}} , \tag{3.2}$$

where from (A.1-16) of [12] this bias is specifically

$$\boxed{B^*_{coh} = \log \mu - \frac{1}{2} \sum_{m,n}^{M,N} \bar{\theta}^2_{m,n} L^{(2)}_{m,n}} \; . \tag{3.2a}$$

The quantity $L^{(2)}_{m,n}$ is given by

$$\boxed{L^{(2)}_{m,n} \equiv \langle \ell^2_{m,n} \rangle_{H_0} = \int_{-\infty}^{\infty} \left[\frac{w_1'(x_{m,n}|\mathcal{P}_{m,n})}{w_1(x_{m,n}|\mathcal{P}_{m,n})} \right]^2 w_1(x_{m,n}|\mathcal{P}_{m,n}) \, dx_{m,n}, \quad (>0)} \tag{3.3}$$

cf. (A.1-15) of [12], $i \to (m,n)$, where we introduce the parameter set, $\mathcal{P}_{m,n}$, associated with the generally nonstationary, inhomogeneous pdf w_1 here, to emphasize the subscript interpretation of $L^{(2)}_{m,n}$: this is $L^{(2)}$ calculated at

---

† For simplicity, we write $\ell_{m,n}$ for $\ell^{(m,n)}_{m,n}$, (3.2). When $\underset{\sim}{x}$ is stationary, we have $\mathcal{P}_m$, and when $\underset{\sim}{x}$ is both stationary and homogeneous, $\mathcal{P}_{m,n} \to \mathcal{P}$, cf. ¶ ff. (3.7b).

position (element) $\underline{m}$ in space Λ_J and time $\underline{n}$ in $(t_0, t_0+\tau)$, from the ensamble of $\{x_{m,n}\}$ generating w_1.

In a similar way we find from (3.1) that z_{ij}, (2.8a), becomes directly

$$z_{ij} \equiv \frac{\partial^2}{\partial x_i \partial x_j} \log w_J \Big|_{\substack{i=m,n \\ j=m',n'}} = \sum_{m',n'} \sum_{m,n} \frac{\partial^2 \log w_1(x_{m,n}|\mathcal{P}_{m,n})}{\partial x_{m,n}\, \partial x_{m',n'}}$$

$$= \ell'_{m,n} \delta_{mm'} \delta_{nn'} \tag{3.4}$$

Applying (3.4) to (2.21) and using (A.1-20a) of [12], we obtain the canonical incoherent LOBD algorithm

$$g^*_{inc} = B^*_{inc} + \frac{1}{2!} \sum_{m,m'}^{M} \sum_{n,n'}^{N} [\ell_{m,n}\ell_{m',n'} + \ell'_{m,n}\delta_{mm'}\delta_{nn'}] \langle \theta_{m,n}\theta_{m',n'} \rangle \tag{3.5}$$

with

$$B^*_{inc} = \log \mu - \frac{1}{8} \Bigg(\sum_{m,n} \{L^{(4)}_{m,n} - 2L^{(2)2}_{m,n}\} \langle \theta^2_{m,n} \rangle^2 + 2 \sum_{m,m'}^{M} \sum_{n,n'}^{N} L^{(2)}_{m,n} L^{(2)}_{m',n'} \langle \theta_{m,n}\theta_{m',n'} \rangle^2 \Bigg) \tag{3.5a}$$

Here $L^{(4)}_{m,n}$ is defined by $(i \mapsto m,n)$

$$L^{(4)}_{m,n} \equiv \int_{-\infty}^{\infty} \left(\frac{w_1''}{w_1} \right)^2_{m,n} w_1(x_{m,n}|\mathcal{P}_{m,n}) dx_{m,n} = \langle (\ell'_{m,n}\delta_{mm'}\delta_{nn'} + \ell^2_{m,n})^2 \rangle_{H_0}$$

$$= \left\langle \left(\frac{w_1''}{w_1} \right)^2_{m,n} \right\rangle_{H_0} \qquad (> 0), \tag{3.6}$$

cf. (A.1-19b) of [12]. The biases, as well as the data-dependent parts of g*, are seen at once to be separable (cf., Sec. 2.4) in these cases as well,

as a consequence of the independent noise samples.

For the composite detector, we may combine (3.2)-(3.6) to get directly

$$g^*_{comp} = g^*_c + g^*_{inc} - \log \mu = \text{Eq. (3.2)} + \text{Eq. (3.5)} - \log \mu \tag{3.7}$$

which can be written explicitly as

$$g^*_{comp} = \{B^*_c + B^*_{inc} \log \mu\} - \sum_{m,n}^{M,N} \ell_{m,n}\bar{\theta}_{m,n} + \frac{1}{2}\sum_{m,m'}^{M}\sum_{n,n'}^{N} [\ell_{m,n}\ell_{m'n'} + \ell'_{m,n}\delta_{mm'}\delta_{nn'}]\langle\theta_{m,n}\theta_{m',n'}\rangle \tag{3.7a}$$

with

$$B^*_{comp} \equiv B^*_c + B^*_{inc} - \log \mu = \log \mu - \frac{1}{8}\sum_{m,n}^{M,N}\{4\langle\theta_{m,n}\rangle^2 L^{(2)}_{m,n} + \langle\theta^2_{m,n}\rangle^2[L^{(4)}_{m,n} - 2L^{(2)2}_{m,n}]\} - \frac{1}{4}\sum_{m,m'}^{M}\sum_{n,n'}^{N} L^{(2)}_{m,n} L^{(2)}_{m',n'}\langle\theta_{m,n}\theta_{m',n'}\rangle^2 \tag{3.7b}$$

Again, we have separability in the sense of Sec. 2.4, for these composite cases also.

When the data $(x_{m,n})$ are stationary, we can drop the subscript n on $L^{(2)}_{m,n}$, $L^{(4)}_{m,n}$ and $\langle\theta_{m,n}\theta_{m',n'}\rangle = \langle\theta_m\theta_{m'}\rangle_{|n-n'|}$. If the data are also homogeneous, we can similarly drop the subscript m on $L^{(2)}$, $L^{(4)}$, and $\langle\theta_{m,n}\theta_{m',n'}\rangle = \langle\theta_i\theta_j\rangle$, $i=|m-m'|$, $j=|n-n'|$, etc., and these $L^{(2)}$, $L^{(4)}$ factors may be removed from under the summation signs.† Note, as expected, that in the special case here of a single element or aperture ($M=1$) our results above reduce to the earlier expressions of Refs. [10]-[12].

Finally, we note that when the total noise is gaussian, e.g., we have the normalized pdf's

---

† See footnote, page 19.

$$w_1(x_{m,n}|\mathcal{P}_{m,n}) = \frac{e^{-x_{m,n}^2}}{\sqrt{2\pi}} \tag{3.8}$$

(where $x_{m,n} = X_{m,n}/\sqrt{\psi_n^{(m)}}$, so that $\overline{x_{m,n}^2} = 1$), we readily obtain

$$L_{m,n}^{(2)} = 1; \qquad L_{m,n}^{(4)} = 2 \tag{3.9}$$

cf. Sec. A.1-3, [12]. [Because of the normalization and the fact that $X_{m,n}$ is gaussian ($\langle X_{m,n}\rangle=0$), $L_{m,n}^{(2)}$, etc. are automatically independent of (m,n), which is not generally true in the (3 or more parameter) nongaussian cases.]

Section 4. Diagrams and Interpretations: The LOBD with Independent Sampling

The optimum threshold algorithms (3.2), (3.5), and (3.7) above may be interpreted in canonical fashion, when we separate the temporal and spatial processing, and the linear from the nonlinear portions of the resulting operations. From this, in turn, we can obtain a general insight into the significance of the processing and why it can often be so much more effective than the so-called conventional systems, which are optimized against gaussian noise fields only.

Because of the separability of the temporal and spatial processing in these threshold algorithms, stemming from the postulated space-time independence of the noise samples here, we have a choice between processing in space at each given time instant ($\sum_{m,m'}$) and then processing in time ($\sum_{n,n'}$), or the more usual approach of temporal processing of the received data at a particular spatial element, with subsequent processing over space. We shall choose the latter here.

Accordingly, from earlier analyses [[20], Chapter 4, and the Appendix therein], we can establish matched filter structures for the linear portions of the threshold signal processing explicitly indicated in g* for both coherent and incoherent reception, cf. (3.2), (3.5) above. This is important, because such structures provide a guide to the actual realization of the physical entities which are needed to carry out the indicated processing, either directly as a computational program or by building the specialized

minicomputer which represents the operations involved. We note that the results here apply for both broad and narrow-band signals. We consider first the coherent cases:

4.1 Coherent Reception:

We consider a typical m^{th} sensor and examine the resultant temporal processing. Here we have the situation shown in Fig. 4.1 for these optimum spatio-temporal detectors. First, in the optimum case, the imput sampled data $\{x_{m,n}\}$ are non-linearly processed, to yield $y_{m,n} = \ell_{m,n}$, cf. (3.2). This new sample [where $y_{m,n} = y_m(t_n) = \ell(x_m(t_n))$, etc., of course], is then passed through a (linear) "matched filter," where the weighting function of this filter is

$$\boxed{h_M^{(m)}(T-t_n;T)\Delta t = \langle a_o^{(m)}(t_n)s^{(m)}(t_n)\rangle, \quad 0 \leq t_n \leq T; \quad = 0 \text{ elsewhere}} \tag{4.1}$$

so that

$$\psi_{m,N}^{(1)*} \equiv \sum_{n=1}^{N} \langle a_{on}^{(m)} s_n^{(m)} \rangle \ell_{m,n} = \sum_{n=1}^{N} y_m(t_n) h_M^{(m)}(T-t_n;T)\Delta t \tag{4.2}$$

(which in continuous form becomes, on (0-,T+), the linear functional

$$\psi_{m,N}^{(1)*} \equiv \psi_{m,T}^{(1)*}(x(t)) = \int_{0-}^{T+} y_m(t) h_M^{(m)}(T-t,T)dt. \tag{4.3}$$

The matched filters are shown in Fig. 4.1. The filter, $h_M^{(m)}$, is a form of delay-line filter, with suitable weighting ($\sim h_M^{(m)}$) and a read-out at t=T from whenever we choose to start the particular sampling for the interval (t_o, t_o+T). From this, in turn, we than combine (i.e., add) all these resultant (m=1,...,M) outputs according to (3.2) to form g_{coh}^*, which is then compared to a threshold, in the manner of (2.2), for a decision, cf. Fig. 4.1. We have called such filters "Bayes matched filters of the 1st kind, Type 1," cf. Sec. 4.2, [20], which is, of course, recognized as a special form of (cross-) correlation filter. Note, in particular, that these (matched) filters depend only on the desired input signal statistics--here the first-order statistics, because of coherent threshold reception.

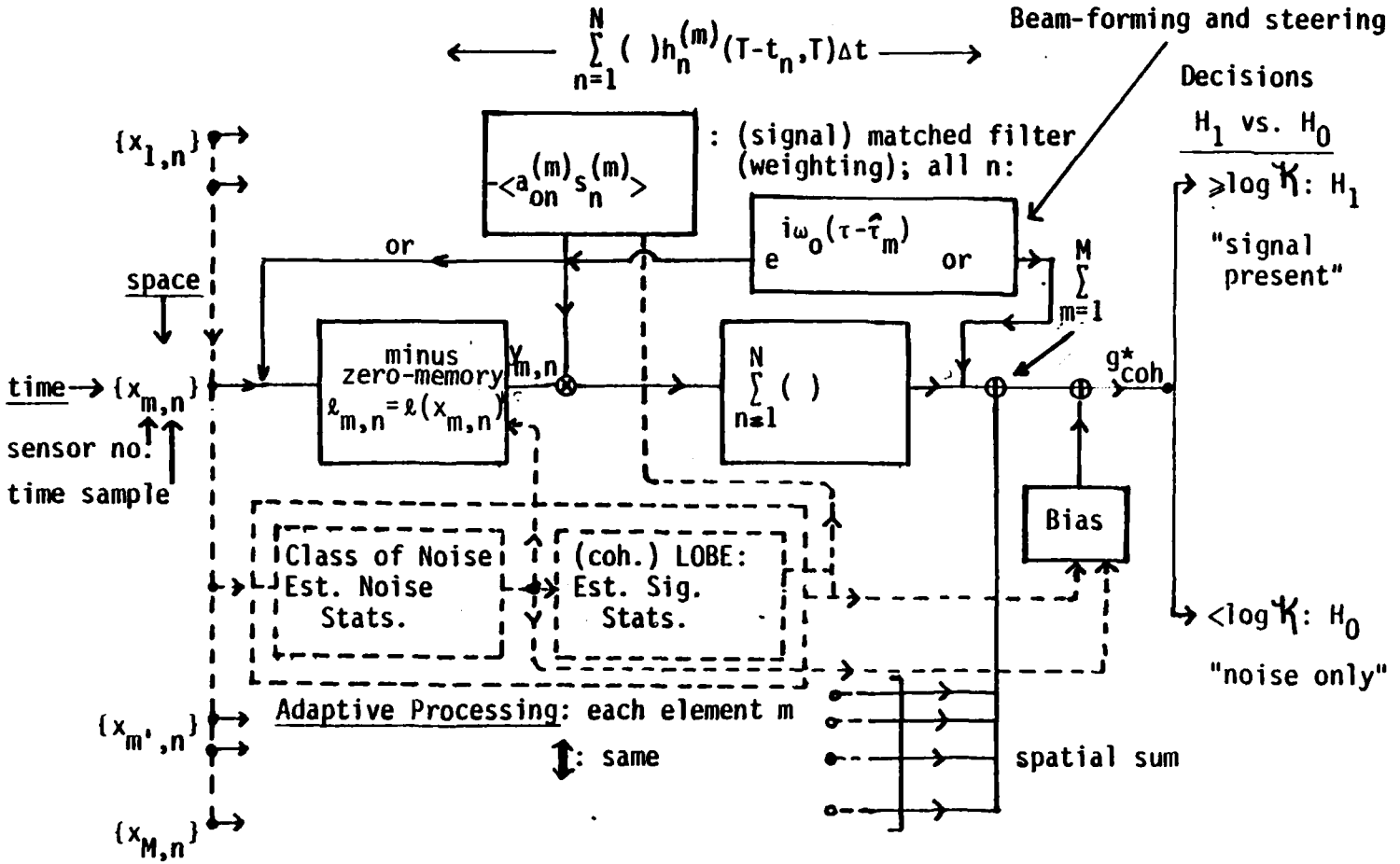

Figure 4.1 Canonical structure of the locally optimum (and AO) space-time threshold detector Eq. (3.2) for general signals in general (nongaussian) noise fields, for binary "on-off" coherent signal detection, H_1 vs. H_0, showing matched filter structures. [The associated adaptive portions of the system, by which the noise and signal parameters are estimated, when such data are not available a priori, is shown by the dotted lines; see also [22].] Note the summation over parallel space elements ($\sum_m$) to yield g^*_{coh}, with the beam-forming and steering factors.

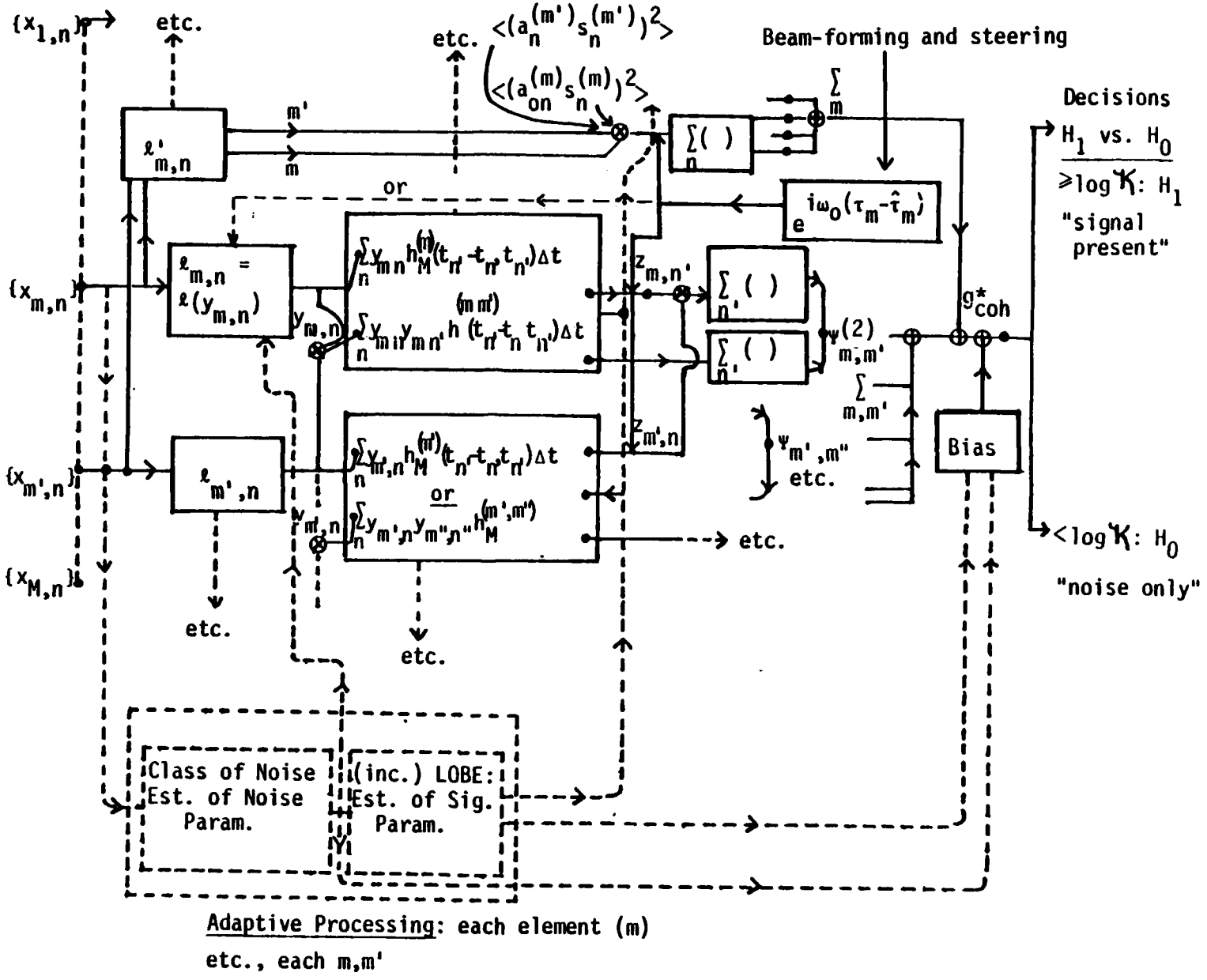

Figure 4.2 Canonical structure of the locally optimum (and AO) space-time threshold detector (3.5), as expressed by (4.5), or (4.7), in (4.8), for binary "on-off" incoherent signal detection (H_1 vs. H_0), showing alternative matched filter structures. [Each spatial element (m) has an adaptive processing unit, analogous to the coherent cases, cf. Fig. 4. .]. The spatial summations are over all pair products $\psi^{(2)}_{m,m'}$, to yield g^*_{coh}, cf. (4.8). Note the beam-forming and steering elements

4.2 Incoherent Reception

Here we have a more complex situation than the coherent cases above, namely the type of phenomenon: a set of highly non-linear operations in the sampled data, to obtain $\ell_{m,n}, \ell_{m',n'}$, and $\ell'_{m,n}$, cf. (3.5). The results of these are then passed into a second-order nonlinear system, a typical element of which can be expressed in the manner of Fig. 4.2, either as a combination of time-varying (linear) filter and zero-memory miltiplication, or as another time-varying (linear) filter and appropriate multiplications, in each instance plus a (weighted) nonlinear functional of the received data. The results of these operations are then summed over all pairs of spatial elements (e.g., $\sum_{m,m'}$), as indicated.

Our first point here is that the linear "matched filter" operations $h_M^{(m)}$, $h_M^{(m')}$ can be represented in two equivalent realizable† forms. The first is given by

$$h_M^{(m \text{ or } m')}(t_{n'}-t_n,t_{n'}) \equiv \text{sol. of } \sum_{\ell=1}^{N} h_M^{(m)}(t_\ell-t_n,t_\ell)h_M^{(m')}(t_\ell-t_{n'},t_\ell)\Delta t$$

$$\begin{cases} = \langle a_{on}^{(m)} a_{on'}^{(m')} s_n^{(m)} s_{n'}^{(m')} \rangle, & \{t_o \leq t_\ell \leq T;\ \ell=1, \ldots, N\} \\ = 0, \text{ elsewhere,} \end{cases} \tag{4.4}$$

where $h_M^{(m \text{ or } m')}$, [m,m' = 1, ..., M], are formally the set of simultaneous solutions of (4.4). Thus, we can write

$$\begin{aligned} \psi_{m,m'}^{(2)}(\underline{y})^* &\equiv \sum_{n,n'}^{N} y_{m,n} y_{m',n'} \langle a_{on}^{(m)} a_{on'}^{(m')} s_n^{(m)} s_{n'}^{(m')} \rangle \\ &= \sum_{n'} \left(\sum_{n} y_{m,n} h_M^{(m)}(t_{n'}-t_n,t_{n'})\Delta t \sum_{p} y_{m,p} h_M^{(m')}(t_{n'}-t_p,t_{n'})\Delta t \right) \qquad (4.5) \\ &= \sum_{n'} z_{m,n'} z_{m',n'} \ ; \quad \therefore (z_{m,n'} \equiv \sum_{n} y_{m,n} h_M^{(m)}(t_{n'}-t_n,t_{n'})\Delta t, \text{ etc.}) \end{aligned}$$

---

† This means operations only on the past of the data input.

The filters, $h_M^{(m)}(t_{n'}-t_n,t_{n'})$, are real, time-varying, and realizable: we call them Bayes matched filters of the second kind, Type 1; (cf. Fig. 4.3, [20] also).

An alternative and simpler form of matched filter, particularly useful in the case of narrow-band (as well as broad-band) input signals, is used, along with a multiplier (in the manner of Fig. 4.2), and is represented by

$$\hat{h}_M^{(m,m')}(t_{n'}-t_n,t_{n'})\Delta t \equiv \langle Z_n^{(m)} Z_{n'}^{(m')*}\rangle = \langle a_{on}^{(m)} a_{on'}^{(m')} s_n^{(m)} s_n^{(m')}\rangle, \quad t_{n'} > t_n$$
$$= 0, \qquad t_{n'} < t_n \qquad (4.6)$$

so that now (4.5) can be written equivalently

$$\psi_{m,m'}^{(2)}(y)^* = \sum_{n,n'}^{N} y_{m,n} y_{m',n'} \hat{h}_M^{(m,m')}(t_{n'}-t_n,t_{n'})\Delta t; \qquad (4.7)$$

(we note that $\hat{h}_M^{(m,m')} \neq h_M^{(m \text{ or } m')}$.) This filter is also real, realizable, time-varying, and as in the coherent cases, cf. (4.1) above, depends only on the signal statistics, now the second-order statistics, because of the incoherent (threshold) reception made.

The complete processing algorithm now requires two additional operations: the addition of the term $\frac{1}{2}\sum_{m,n} \ell'_{m,n}\langle\theta^2_{m,n}\rangle$, cf. (3.5), and the summations $(\sum_{m,m'})$ over pairs of spatial elements (or arrays) (m,m'), to give us finally

$$g(\underline{x})^*_{inc} = \underbrace{\{\log \mu - \hat{B}^*_{inc}\}}_{(\equiv B^*_{inc} = \text{bias})} + \frac{1}{2!}\sum_{m,m'}^{M} \psi_{m,m'}^{(2)}(y)^* + \frac{1}{2!}\sum_{m}^{M}\left(\sum_{n}^{N} \ell'_{m,n}\langle\theta^2_{m,n}\rangle\right), \qquad (4.8)$$

as sketched in Fig. 4.2.

4.3 Operational Interpretation

At this point it is important to point out a number of general properties of the canonical LOBD's described above, We observe that:

(1). For coherent and incoherent detection -- with independent noise samples--the matched filter depends only on signal statistics and structure;

(2). The matched filter (by definition) is always linear, but may or may not be realizable, in the sense of operating only on the "past" of the received data [cf. Chapter 4, [20]];

(3). A variety of equivalent matched filters can be obtained, to represent the data functionals $\psi^{(1)}, \psi^{(2)}$, etc.;

(4). The general functional description of the component LOBD elements here is as follows:

(i). A typical component (m) first "matches" the receiver to the (nongaussian, or gaussian) noise or interference, in that it adapts--i.e., estimates the parameters of the noise statistics [which may be Class A (B), or gaussian] to generate nongaussian functionals, e.g., $\ell_{m,n}$, $\ell'_{m,n}$ of the input data; as shown in Figs. 4.1, 4.2. [See [4], [6] for illustrative noise examples in the analogous EM applications.]

(ii). Next, the m^{th} LOBD component then "matches" the signal--as it is a priori known or structured at the receiver--to this new input ($\ell_{m,n}$, $\ell'_{m,n}$, etc.), to form an appropriate correlation detector for the nongaussian functional $\ell_{m,n}$, etc. These "matched" filters are, by definition, always linear and usually realizable in the causal sense. Thus, there is always a double "matching" process involved: first to the noise, and then the signal to the (transformed) noise. [In the conventional or "classical" cases of gaussian noise, the first operation, (i), reduces to a single linear operation of data transmission, and the second to the classical "matched filter" [21].]

(iii). For incoherent detection there is an additional, third operation, which follows the matching process, (ii), above. This is usually a nonlinear operation plus (temporal) summation, where the additional nonlinearity involves a suitable multiplication; cf. (4.5), (4.7) and Fig. 4.2.

(iv). Finally, for both coherent and incoherent detection there is a spatial summation over the (m=1, ..., M) inputs sampling the field. In the coherent cases, this is a simple summation, cf. (3.2), but for incoherent reception all pair-products of each m^{th} LOBD component are to be formed and then summed, to give the desired quantity to be compared against the detection thresholds, cf. Figs. 4.1, 4.2. This pair product formation is a direct consequence of the incoherent mode of detection and the multiplicity of separate spatial sensors.

(v). When there is some signal epoch (or carrier-phase) information available at the receiver, then the composite detector is to be employed, cf. (3.7). This is simply the direct linear sum of the coherent and incoherent LOBD's described above, with their respective matched filters and associated nonlinear elements.

Figures 4.1, 4.2 show the general formalism of LOBD signal detection, for coherent and incoherent reception, respectively. In general, these threshold receivers are adaptive: they adjust their performance to the character of the noise in which they are immersed. Note that the adaptive portion of the signal processing consists of (1), a determination of the noise statistics followed by (2), a possible signal estimation (LOBE: Locally Optimum Bayes Estimator). The first operation, (1), is used to provide the form of $\ell_{m,n}$, ℓ'_{m-n}, as indicated. The second, (2), may be needed to estimate [22] such signal parameters as $\langle a_{on}^{(m)} s_n^{(m)} \rangle$, $\langle a_{on}^{(m)} a_{on}^{(m')} \rangle$, etc., cf. (3.2), (3.5). In any case, it is this feature of adaptivity which provides the often very large superiority of these detectors over conventional ones.

An important point here is that the noise field has analytically defined functional forms, $w_1(x|H_0)_A$, cf. Sec. 7ff., so that (in any case) the $\ell_{m,n}$, $\ell'_{m,n}$, etc. can be calculated without recourse to the estimation of w_1 itself on the basis of limited sample-size: only parameter estimates are required, or they may be themselves calculated, when the acoustic interference scenario is specified. Of course, a further (very considerable) advantage of knowing the noise class is the ability to determine and compare performance for specified parameter values [cf. Sec. 11ff.].

Finally, we remark that the general resolution of these detection operations into simple combinations of (linear) signal matched filters and (zero-memory) nonlinear noise matched filters stems entirely from the condition of independent spatial and temporal sampling of the noise field, which sets a conservative upper bound on performance in most instances; (see, moreover, Sec. 5.4 for a further discussion). Without the ability to "factor" the general noise pdf $w_J(\underline{x})$, Sec. 2.2-II, no canonical operational forms appear possible in the threshold cases, let alone for general signal levels.

Section 5. Optimum Threshold Performance: Canonical M-Element Results

From the results of [10], [12] we can at once present the limiting canonical expressions for the detector performance under the large-sample threshold condition required in the optimum detection of weak-signals in our general noise environments. Independent samples are postulated, so that these performance relations give conservative results: if, in addition, the correlation structures of the noise were included, some (small) further improvement would be obtained [cf. Sec. 2.2-III, Sec. 3 earlier, and VII, Sec 12.3 ff.]. Specifically, for the Neyman-Pearson (or fixed false-alarm) detectors appropriate here, we have (cf. (2.31) of [12]) for the probability of correct signal detection:

$$P_D^* \simeq \frac{p}{2}\left\{1 + \Theta\left[\frac{\langle g^*\rangle_1 - \langle g^*\rangle_0}{\sqrt{2}\,\sigma_0^*} - \Theta^{-1}(1 - 2\alpha_F^*)\right]\right\} = p(1 - \beta^*), \tag{5.1}$$

cf. (2.5), with the associated conditional correct signal detection probability

$$p_D^* \equiv 1 - \beta^* = P_D^*/p \quad \frac{1}{2}\left\{1 + \Theta\left[\frac{\langle g^*\rangle_1 - \langle g^*\rangle_0}{\sqrt{2}\,\sigma_0^*} - \Theta^{-1}(1- 2\alpha_F^*)\right]\right\} \tag{5.1a}$$

$$\alpha_F^* \simeq \frac{1}{2}\left\{1 + \Theta\left[\frac{\langle g^*\rangle_0 - \log K}{\sqrt{2}\,\sigma_0^*}\right]\right\}. \tag{5.1b}$$

Here $\Theta(x) \equiv (2/\sqrt{\pi})\int_0^x e^{-t^2}dt = \mathrm{erf}(x)$ and $\langle\ \rangle_{1,0}$ denote the averages (over the test statistic or processing algorithm, g^*, cf. Sec. 3) with respect to H_1: S+N, or H_0=N. The quantity $\sigma_0^* \equiv (\mathrm{var}_0 g^*)^{\frac{1}{2}}$, the rms value of g^* under H_0, and α_F^* is the (preset) false-alarm (or Type I error) probability, cf. (2.5) et seq.

From the results of Sec. 2.3 earlier, we note that our LOBD's of Sec. 3 above are AO as well, for large samples, regardless of the mode of detection. A sufficient condition that these optimum algorithms (g*) are AO is that they are asymptotically normally distributed, expressed by the formalism $G(\log \mu \mp \sigma_o^{*2}/2;\ \sigma_o^{*2})$, where (-/+) refers to the averages of g* under H_0 or H_1, respectively. In fact, it is readily shown (cf. Appendix A-3, [12]) that, for all modes (i.e., coherent, incoherent, and composite),

$$\langle g^* \rangle_1 - \langle g^* \rangle_0 \doteq \sigma_o^{*2}/2 - (-\sigma_o^{*2}/2) = \sigma_o^{*2}; \quad [\langle g^* \rangle_1 \equiv \langle g^* \rangle_{H_1}, \text{ etc.}] \tag{5.2}$$

so that (5.1a) becomes explicitly

$$\boxed{p_D^* \equiv 1 - \beta^* \approx \frac{1}{2}\{1 + \Theta[\sigma_o^*/\sqrt{2} - \Theta^{-1}(1 - 2\alpha_F^*)]\}} \tag{5.3}$$

with†

$$\alpha_F^* \approx \frac{1}{2}\left\{1 - \Theta\left[\frac{\sigma_o^*}{2\sqrt{2}} + \frac{\log(\mathcal{K}/\mu)}{\sqrt{2}\,\sigma_o^*}\right]\right\}\ ; \quad \beta^* = \frac{1}{2}\left\{1 - \Theta\left[\frac{\sigma_o^*}{2\sqrt{2}} - \frac{\log(\mathcal{K}/\mu)}{\sqrt{2}\,\sigma_o^*}\right]\right\} \tag{5.3a}$$

[where for given σ_o^* (implying a fixed space-time sample size) and threshold $(\mathcal{K}/\mu)$ one has the corresponding desired fixed false-alarm probability, α_F^*, characteristic of the "on-off" Neyman-Pearson observer employed in this study.]† Several conditions on the applicability of this canonical (optimum threshold) performance measure are noted below in III, Section 5.2.

Finally, it is convenient to rewrite (5.3) as

$$\frac{\sigma_o^*}{\sqrt{2}} = \Theta^{-1}(2p_D^* - 1) + \Theta^{-1}(1 - 2\alpha_F^*) \equiv C_{NP} \equiv \sqrt{B_{NP}^*} \tag{5.3b}$$

for those cases where p_D^*, α_F^* are prechosen, and we are interested in determining the associated minimum detectable signal (cf. Sec. 5.1ff.).

---

† See Eqs. (9.2a, b) ff. The key point here is that choosing α_F^* = means setting a threshold, which in turn requires the correct bias $(\hat{\beta}_J^*)$, which must be properly determined to realize the AO condition for these algorithms under the usual small-signal and therefore, large sample (J>>1) conditions.

5.1 Processing Gains and Minimum Detectable Signals (General)

The key quantity specifying AO performance, as well as the correct bias B_J^* [cf. Sec. 3], is the variance σ_o^{*2}, which is shown in Appendix A.1 of [12] to be

$$\sigma_o^{*2} = -2(B_J^* - \log \mu) = -2\hat{B}_J^* . \tag{5.4}$$

Specifically, we have (Appendix A.1, [12]):

I. Coherent Detection

$$\sigma_{o\text{-coh}}^{*2} = \sum_m^M \sum_n^N L_{m,n}^{(2)} \overline{a_{on}^{(m)2}}\,\overline{s_n^{(m)2}} . \tag{5.5}$$

Next, in order to proceed more profoundly into the analysis and physical interpretation of the structure and performance of these (optimum threshold) detection algorithms, it is necessary to define a processing gain, Π^*, and minimum detectable signal, $\langle a_o^2\rangle_{min}^*$. This is done generally as follows (cf. Sec. 6.2, [12]), by writing

$$\sigma_{o\text{-coh}}^{*2} \equiv 2\Pi_{coh}^* \langle a_o^2\rangle_{min\text{-coh}}^* . \tag{5.6}$$

To apply this relation to (5.5) in the general case of nonstationary noise, etc., we rewrite (5.6) here as

$$\boxed{\sigma_{o\text{-coh}}^{*2} = 2\left\{ NM\, L_{MN}^{(2)} \sum_m^M \sum_n^N \frac{\overline{a_{on}^{(m)2}}\,\overline{s_n^{(m)2}}}{2N} \cdot \frac{\ell_{m,n}^{(2)}}{M} \right\}; \quad \ell_{m,n}^{(2)} \equiv L_{m,n}^{(2)} \Big/ L_{MN}^{(2)}} \tag{5.7}$$

where now

$$\boxed{\therefore \Pi_{coh}^* \to \Pi_{MN\text{-coh}}^* \equiv NM\, L_{MN}^{(2)}; \quad \langle a_o^2\rangle_{min\text{-coh}}^* \to \langle a_{o\text{-}MN}^2\rangle_{min\text{-coh}}^* \equiv \sum_{m,n}^{M,N} \frac{\overline{a_{on}^{(m)2}}\,\overline{s_n^{(m)2}}\,\ell_{m,n}^{(2)}}{2MN}} \tag{5.8a}$$

in which

$$\boxed{L_{MN}^{(2)} \equiv \sum_{m,n}^{M,N} L_{m,n}^{(2)}/MN, \qquad MN \equiv J.} \tag{5.8b}$$

In this general situation where both signal and noise may be nonstationary and inhomogeneous, it is clear that the minimum detectable signal, (5.8a), depends on the noise structure ($\sim \ell^{(2)}_{m,n}$) as well as on overall sample-size. Here $\langle a^2_{o\text{-}MN}\rangle^*_{min\text{-}coh}$ is an averaged quantity, over time and the array (space), as one would expect. This, the processing gain here is directly proportional to the overall number of (independent) samples, J=MN, and the average non-gaussian factor, $L^{(2)}_{MN}$ (≥ 1), cf. (3.9). Accordingly, as expected, increasing the number of independent samples (J) improves performance as $\sigma^*_{o\text{-}coh} \simeq \sqrt{J} = \sqrt{MN}$, i.e., as the square root of the number of (independent) samples. Furthermore, the more nongaussian the interference (for the same mean intensities as gauss noise) the larger $L^{(2)}_{MN}$. As we shall see in Part IIff., $L^{(2)}_{MN}$ can be quite large $O(10^2\text{-}10^4$ or more) in typical acoustic environments. The relation of aperture or array size in space to the number of spatially independent samples (M) is discussed below in Sec. 5.4.

Finally we note the rôle of beam-forming, where $\langle s^{(m)}_n\rangle$ ($= \langle s(t_n - \tau_m; \underline{\theta})\rangle$) is maximized by proper choise of delay τ_m for each element of the M-element array formed by applying such delays. Thus, beam-forming, as well as sample size, plays an important part in making $(\sigma^*)^2$ larger, and performance error smaller.

II. Incoherent Detection

In a similar way (cf. Appendix A.1-2, [12], and (3.5a) in (5.4)), we have for the variance $\sigma^{*2}_{o\text{-}inc}$ for incoherent detection

$$\sigma^{*2}_{o\text{-}inc} = \frac{1}{4} \sum_{m,m'}^{M} \sum_{n,n'}^{N} \overline{\theta^2_{m,n}}\ \overline{\theta^2_{m',n'}} \left\{ (L^{(4)}_{m,n} - 2L^{(2)2}_{m,n})\ \delta_{mm'}\delta_{nn'} + (2\, L^{(2)}_{m,n}\, L^{(2)}_{m',n'}) \right\} \hat{m}^{(m,m')2}_{nn'}\ \rho^{(mm')2}_{nn'} \qquad (5.9)$$

where

$$\hat{m}^{(mm')}_{nn'} \equiv \frac{\overline{a^{(m)}_{on}\, a^{(m')}_{on'}}}{\left\{ \overline{a^{(m)2}_{on}} \cdot \overline{a^{(m')2}_{on'}} \right\}^{\frac{1}{2}}}\ ; \quad \rho^{(mm')}_{nn'} = \overline{s^{(m)}_n s^{(m')}_{n'}}\ ; \quad \overline{s^{(m)2}_n} = 1 \qquad (5.9a)$$

(by normalization)

so that $|\hat{m}| \leq 1$; $|\rho| \leq 1$.

For processing gain and minimum detectable signal here we use the defining relations

$$\sigma^{*2}_{o\text{-inc}} \equiv 2\langle a_o^2\rangle^{*2}_{\text{min-inc}}\, \Pi^{*}_{\text{inc}} = 2(\langle a^2_{o\text{-}MN}\rangle^{*}_{\text{min-inc}})^2 \Pi^{*}_{MN\text{-inc}} \tag{5.10}$$

suggested by (6.6) and (6.22) of [12]. These components of $\sigma^{*2}_{o\text{-inc}}$ are formally obtained, paralleling the coherent cases (I) above, where we now write compactly (j=m,n), (j'=m',n'). Thus, from (5.9) we get

$$\sigma^{*2}_{o\text{-inc}} = \frac{1}{4}\sum_{J}\sum_{J'} \overline{\theta_J^2}\;\overline{\theta_{J'}^2}\left\{(L_J^{(4)} - 2L_J^{(2)2})\delta_{JJ'} + 2L_J^{(2)}L_{J'}^{(2)}\right\}\hat{m}^2_{JJ'}\rho^2_{JJ'} \tag{5.11}$$

which can be transposed formally to

$$\sigma^{*2}_{o\text{-inc}} = 2\,\langle a^2_{o\text{-}MN}\rangle^{*2}_{\text{min-inc}}\left\{\frac{MN}{8}L^{(4)}_{MN}\left[\sum_{m,n}\langle \hat{a}^{(m)2}_{n|MN}\rangle^2\, \ell^{(4)}_{m,n}/MN\right.\right.$$

$$\left.\left. + \sum_{m,m'}\sum_{n,n'}\frac{2(1-\delta_{mm'}\delta_{nn'})}{MN}\hat{\ell}^{(2)}_{m,n}\hat{\ell}^{(2)}_{m',n'}\overline{\hat{a}^{(m)2}_{n|MN}}\;\overline{\hat{a}^{(m')2}_{n'|MN}}\;\hat{m}^{(mm')2}_{nn'}\rho^{(mm')2}_{nn'}\right]\right\} \tag{5.12}$$

where we write

$$\left.\begin{aligned} &\hat{\ell}^{(2)}_{m,n} \equiv L^{(2)}_{m,n}/(L^{(4)}_{MN})^{1/2};\quad \ell^{(4)}_{m,n} \equiv L^{(4)}_{m,n}/L^{(4)}_{MN}\ ;\quad L^{(4)}_{MN} \equiv \sum_{m,n} L^{(4)}_{m,n}/MN\ ; && (5.13a)\\ &\langle a^2_{o\text{-}MN}\rangle^{*}_{\text{min-inc}} \equiv \left(\sum_{m,n}\frac{\overline{a^{(m)2}_{on}}^2}{MN}\right)^{1/2}\ ;\quad \overline{\hat{a}^{(m)2}_{n|MN}} \equiv \overline{a^{(m)2}_{on}}\Big/\langle a^2_{o\text{-}MN}\rangle^{*}_{\text{min-inc}}. && (5.13b)\end{aligned}\right\}$$

Comparing (5.12) with (5.10) shows that <u>the processing gain</u> $\Pi^{*}_{MN\text{-inc}}$ <u>is given by the expression in the braces { } of (5.12)</u>. (The amplitude factors $\langle\hat{a}^{(m)2}_{n/MN}\rangle$, $\hat{m}^{(mm')}_{nn'}$ in the overall processing gain are normalized, cf. (5.9a), (5.13b). In general, we cannot escape having amplitude-dependent quantities in the processing gain for these incoherent cases generally, and particularly since not only is signal level ($\sim a^{(m)}_{on}$) involved, but the signal correlation

structures, as well $(\sim\hat{m},\rho)$. Increasing the processing gain (and $\therefore \sigma_o^{*2}$) is further accomplished by beam-forming, as in the coherent cases above. Beam-forming here requires choosing path-delay differences $|\tau_m - \tau_{m'}|$ between elements so as to maximize $\rho^{(mm')}$, i.e., form a beam normal to the desired signal wavefront [cf. Sec. 6ff.].

Finally, for the composite detector (3.7), it has been shown that (Appendix 3, [12])

$$(\sigma^*_{comp})^2 = (\sigma^*_{coh})^2 + (\sigma^*_{inc})^2 \tag{5.13c}$$

so that inserting (5.7) and (5.12) yield $(\sigma^*_{comp})^2$ directly.

A. Stationary Cases

In the stationary (but not necessarily homogeneous) cases, which fortunately are effectively the practical cases in most instances, we can achieve a considerable reduction of $\sigma^{*2}_{o\text{-}inc}$ along the lines of (5.10) above, now on a per channel basis. Thus, we let (for each m)

$$\langle a^{(m)2}_{o\text{-}N}\rangle^*_{min\text{-}inc} \equiv \left\{\sum_n \overline{a^{(m)2}_{on}}^2 \Big/ N\right\}^{\frac{1}{2}} = \overline{a^{(m)2}_o}; \quad \langle \hat{a}^{(m)2}_{n|MN}\rangle = \langle \hat{a}^{(m)2}_N\rangle = 1, \tag{5.14}$$

cf. (5.13b), because of stationarity (independence of n,n'). Accordingly, (5.12) can be expressed as

$$\sigma^{*2}_{o\text{-}inc}\Big|_{stat} = \sum_{m,m'} 2\langle a^{(m)2}_{o\text{-}N}\rangle \langle a^{(m')2}_{o\text{-}N}\rangle \left\{\frac{N}{8}\sqrt{L^{(4)}_m L^{(4)}_{m'}}\,\delta_{mm'} + \frac{2L^{(2)}_m L^{(2)}_{m'}}{8}\sum_{n,n'}(1-\delta_{mm'}\delta_{nn'})\hat{m}^{(mm')2}_{|n-n'|}\rho^{(mm')2}_{|n-n'|}\right\}$$

$$= \sum_{m,m'} 2\langle a^{(m)2}_{o\text{-}N}\rangle^*_{min\text{-}inc}\langle a^{(m')2}_{o\text{-}N}\rangle^*_{min\text{-}inc}\left\{\frac{N}{8}\sqrt{L^{(4)}_m L^{(4)}_{m'}}\left[\delta_{mn} + \frac{2L^{(2)}_m L^{(2)}_{m'}}{N\sqrt{L^{(4)}_m L^{(4)}_{m'}}}\sum_{n,n'}(1-\delta_{mm'}\delta_{nn'})\hat{m}^{(mm')2}_{|n-n'|}\rho^{(mm')2}_{|n-n'|}\right]\right\} \tag{5.15}$$

which shows that the quantity in the braces { } of (5.15) is indeed a processing gain (m,m'). In fact, if we let

$$\hat{\ell}_m^{(2)} \equiv L_m^{(2)} \Big/ \sqrt{L_m^{(4)}} \; ; \quad \ell_m^{(4)} \equiv L_m^{(4)} \Big/ L_M^{(4)} \; ; \quad L_M^{(4)} \equiv \sum_m L_m^{(4)} \Big/ M \tag{5.16}$$

we can rewrite (5.15) compactly as

$$\boxed{\sigma^{*2}_{o\text{-}inc}\Big|_{stat} = 2MNL_M^{(4)} \sum_{m,m'}^{M} \langle a_{o\text{-}N}^{(m)2} \rangle^*_{min\text{-}inc} \langle a_{o\text{-}N}^{(m')2} \rangle^*_{min\text{-}inc} \pi_{inc}^{(mm')*}} \tag{5.17}$$

where $\pi_{inc}^{(mm')*}$ is the <u>mutual</u> or interelement <u>processing gain per element</u>, specified by

$$\boxed{\pi_{inc}^{(mm')*} \equiv \frac{\sqrt{\ell_m^{(4)} \ell_{m'}^{(4)}}}{8M} \left\{ \delta_{mm'} + \frac{2\hat{\ell}_m^{(2)} \hat{\ell}_{m'}^{(2)}}{N} \sum_{nn'}^{N} (1 - \delta_{mm'}\delta_{nn'}) \hat{m}_{|n-n'|}^{(mm')2} \rho_{|n-n'|}^{(mm')2} \right\}} \tag{5.18}$$

In matrix form we can write (5.17) even more compactly, viz.:

$$\boxed{\sigma^{*2}_{o\text{-}inc}\Big|_{stat} = 2MNL_M^{(4)} \cdot (\underline{\tilde{A}}^*_{N\text{-}inc} \underline{\pi}^*_{inc} \underline{A}^*_{N\text{-}inc})} \tag{5.19}$$

where $\underline{A}^*_{N\text{-}inc} = [\langle a_{o\text{-}N}^{(m)2} \rangle^*_{min\text{-}inc} \equiv \overline{a_o^{(m)2}}]$ is the (column) vector of mean-square signal amplitudes into the (m=1, 2, ..., M) elements, while π^*_{inc} is the (symmetrical) M×M matrix of interelement processing gains. Furthermore, if we let

$$\langle a^2_{o\text{-}MN} \rangle^*_{min\text{-}inc} = \max_m \langle a_o^{(m)2} \rangle = \sup_m \langle a_o^{(m)2} \rangle \tag{5.20}$$

so that we can write (the column vector)

$$\underline{A}_{N\text{-}inc} \Big/ \sup_m \overline{a_o^{(m)2}} \equiv [\hat{a}^2_{o\text{-}m}] \equiv \underline{\hat{a}}^2_o, \qquad 0 \leq \hat{a}^2_{o\text{-}m} \leq 1 \; , \tag{5.21}$$

with some $\langle a_o^{(m)2} \rangle > 0$. This then enables us to recast (5.19) now as

$$\boxed{\sigma^*_{o\text{-inc}|\,stat} = 2 \left| MNL_M^{(4)} \left(\underset{\sim}{\tilde{a}}^2_o \underset{\sim}{\pi}^*_{inc} \underset{\sim}{\hat{a}}^2_o \right) \right| \left(\langle a^2_{o\text{-}MN} \rangle^*_{min\text{-}inc} \right)^2} \qquad (5.22)$$

which is in the desired form (5.10) if we write the overall processing gain as

$$\boxed{\Pi^*_{MN\text{-inc}|\,stat} \equiv MNL_M^{(4)} \cdot \underset{\sim}{\tilde{a}}^2_o \underset{\sim}{\pi}_{inc} \underset{\sim}{\hat{a}}^2_o ;} \qquad MN \equiv J \qquad (5.23)$$

(We remark that $\underset{\sim}{\tilde{a}}^2_o \underset{\sim}{\pi}^*_{inc} \underset{\sim}{\hat{a}}^2_o > 0$, $\underset{\sim}{\tilde{A}}^*_{N\text{-inc}} \underset{\sim}{\pi}^*_{inc} \underset{\sim}{A}^*_{N\text{-inc}} > 0$: these quadratic forms are positive definite, as is, of course, required since $\sigma^{*2}_{o\text{-inc}} \equiv var_o g^*_{inc} > 0$.) In our present formulation the minimum detectable signal is taken to be the largest of the minimum detectable signals in the M-branches of the array.

B. Bounds

It is possible to bound the overall processing gain. We consider two limiting cases:

Case I: Completely Incoherent Signals, all elements: $\rho^{(mm')}_{|n-n'|} = \delta_{nn'}$

$$\therefore \pi^{(mm')*}_{inc} = \ell^{(4)}_m \, \delta_{mm'}/8M \qquad (5.24)$$

so that (5.23) becomes

$$\Pi^*_{MN\text{-inc}|\,stat} = MNL_M^{(4)} \left(\sum_m \frac{\hat{a}^4_{o\text{-}m} \ell^{(4)}_m}{8M} \right) = N \sum_m \frac{\hat{a}^4_{o\text{-}m} L^{(4)}_m}{8M} = O(MNL_M^{(4)}). \qquad (5.25)$$

Case II: Completely Coherent Signals, all elements: $\rho = \hat{m} = 1$ (all m,n',n,n')

$$\therefore \pi^{(mm')*}_{inc} = \frac{\ell^{(4)}_m}{8M} \delta_{mm'} + \frac{2L^{(2)}_m L^{(2)}_{m'}}{8ML^{(4)}_M N} \delta_{mm'} \sum'_{n,n'} 1 \cdot 1 + \frac{2L^{(2)}_m L^{(2)}_{m'} (1-\delta_{mm'})}{8ML^{(4)}_M N} \sum_{n,n'} 1 \cdot 1 \qquad (5.26a)$$

$$= \frac{\delta_{mm'}}{8M} \left[\ell^{(4)}_m + \frac{2L^{(2)}_m L^{(2)}_m}{L^{(4)}_M} (N-1) \right] + \frac{(1-\delta_{mm'}) L^{(2)}_m L^{(2)}_{m'} N}{4ML^{(4)}} \, . \qquad (5.26b)$$

Accordingly, we obtain on applying (5.26b) to (5.23)

$$\Pi^{*}_{MN\text{-inc}}\big|_{stat} = MNL_M^{(4)}\left\{ \sum_{\hat{m}}^{M} \frac{\hat{a}^4_{o-m}}{8M}\left[\rho_m^{(4)} + \frac{2L_m^{(2)^2}(N-1)}{L_M^{(4)}}\right] + N \sum_{m,m'}^{M,'} \frac{\hat{a}^2_{o-m}\hat{a}^2_{o-m'}L_m^{(2)}L_{m'}^{(2)}}{4ML_M^{(4)}} \right\}, \quad (5.27)$$

from which we see that when $M \geq 2$, and particularly if M is at all large, the last term of (5.27) dominates, so that here

$$\Pi^{*}_{MN\text{-inc}}\big|_{stat} = O\left(\left\{MNL_M^{(2)}\right\}^2\right); \qquad L_M^{(2)} \equiv \sum_{\hat{m}} L_m^{(2)}/M; \qquad J \equiv MN. \quad (5.28)$$

Since frequently $L_M^{(2)^2} \sim L_M^{(4)}$, we may say from (5.25) and (5.28) that when the received signal structure is reduced to total (wave form) incoherence in time ($\rho_{|n-n'|} = \delta_{nn'}$), say by doppler spread, the overall processing gain is least $\sim O(MNL_M^{(4)})$ and is greatest, not unexpectedly, when both amplitude ($a_o^{(m)}$) and wave form coherence are maximal in time and over the array, e.g., $\rho = \hat{m} = 1$, i.e., $O((MN)^2 L_M^{(2)^2} = (MN)^2 L_M^{(4)})$. Although we cannot remove at the receiver the deleterious effects of wave form (i.e., time) incoherence, we can attempt to restore spatial coherence of the signal by judicious spatial sampling, provided the signal field has not been excessively perturbed in space, thus gaining possibly a factor M, anyway, in overall processing gain. In general, the structure of $\Pi^{*}_{MN\text{-inc}}$ provides a direct account of the spatio-temporal effects of the medium on the received signal field, subject to potential fading, multipath, and doppler dispersion. For the effects of spatial coherence or incoherence of the noise field, see the remarks in Sec. 5.4ff.

III. Composite Detection

Here the optimum threshold algorithm is given by (3.7) above. It can be shown (Appendix 3, [12]) that

$$\boxed{\mathrm{var}_o g^*_{comp} \equiv \sigma^{*2}_{o\text{-}comp} = \sigma^{*2}_{o\text{-}coh} + \sigma^{*2}_{o\text{-}inc}} \tag{5.29}$$

where $(\sigma^*_{o\text{-}coh})^2$, $(\sigma^*_{o\text{-}inc})^2$ are obtained from the results of I, II, Eq. (5.4) et seq.

Next, we observe that using (5.6), (5.10) in (5.29) we can write

$$\sigma^{*2}_{o\text{-}comp} = 2\overline{a_o^2}\hat{b}_{coh}\Pi^*_{coh} + 2\overline{a_o^2}\hat{b}^2_{inc}\Pi^*_{inc} \tag{5.30a}$$

where now we have generally

$$\hat{b}_{coh} \equiv \sum_{m,n} \frac{\overline{a^{(m)2}_{on}}\ \overline{s^{(m)2}_n}\ \ell^{(2)}_{m,n}}{2MN\ \overline{a_o^2}}\ ; \qquad \hat{b}_{inc} \equiv \left(\sum_{m,n} \frac{\overline{a^{(m)2}_{on}}}{MN\overline{a_o^2}^2} \right)^{1/2}. \tag{5.30b}$$

Here $\hat{b}_{coh}$, $\hat{b}_{inc}$ are normalized expressions which embody various second moment statistics of the signal amplitude.

We now define processing gain and minimum detectable signal using the analogue of (5.30a) from the pair of relations

$$\boxed{\sigma^{*2}_{o\text{-}comp} \equiv 2\langle a_o^2\rangle^*_{min\text{-}comp}\hat{b}_{coh}\Pi^*_{coh} + 2\langle a_o^2\rangle^{*2}_{min\text{-}comp}\hat{b}^2_{inc}\Pi^*_{inc}} \tag{5.30c}$$

$$\boxed{\equiv 2(\langle a_o^2\rangle^*_{min\text{-}comp})^2\Pi^*_{comp}.} \tag{5.30d}$$

From (5.3b) we can also write again

$$\sigma^*_{o\text{-}comp} \Big/ \sqrt{2} = \Theta^{-1}(2p^*_D - 1) + \Theta^{-1}(1 - 2\alpha^*_F) \equiv C_{N.P.} \equiv \sqrt{B^*} \tag{5.31}$$

so that (5.30c,d) are readily solved, to give

$$\boxed{\langle a_o^2\rangle^*_{min\text{-}comp} = \frac{1}{2}\frac{\Pi^*_{coh}\hat{b}_{coh}}{\Pi^*_{inc}\hat{b}_{inc}}\left(\sqrt{1 + \frac{4B^*\Pi^*_{inc}\hat{b}^2_{inc}}{(\Pi^*_{coh}\hat{b}_{coh})^2}} - 1\right)} \tag{5.32}$$

and

$$\pi^*_{comp} = B^* \Big/ \left(\langle a_o^2 \rangle^*_{min\text{-}comp}\right)^2$$

$$= \left[2\sqrt{B^*}\, \pi^*_{inc} \hat{b}^2_{inc} \Big/ \pi^*_{coh} \hat{b}_{coh} \left\{ \sqrt{1 + 4B^* \pi^*_{inc} \hat{b}^2_{inc} \Big/ (\pi^*_{coh} \hat{b}_{coh})^2} - 1 \right\} \right]^2 , \tag{5.33}$$

respectively. The various processing gains may be obtained from (5.8a), (5.12), (5.23), etc., in these M-element cases. [Note that in the purely incoherent cases ($\pi^*_{coh} = 0$) we get $\pi^*_{comp} = \pi^*_{inc}$, as expected.]

5.2 Some Special Results

Other special results are readily obtained from Sec. 5.1 above. We list some of the more important below:

I. Single Element or Beam (M = m = m' = 1)

From (5.5) or (5.7) we have generally

$$\sigma^{*2}_{o\text{-}coh} = 2\left\{ N L_N^{(2)} \cdot \sum_n \frac{\overline{a_{on}^2}\, \overline{s_n^2}\, \ell_n^{(2)}}{2N} \right\}; \quad \ell_n^{(2)} = L_n^{(2)} \Big/ L_N^{(2)}; \quad L_N^{(2)} = \frac{1}{N} \sum_n L_n^{(2)};$$

$$= 2NL_N^{(2)} \langle a_o^2 \rangle^*_{min\text{-}coh} \cdot \tag{5.34}$$

From (5.9), (5.11) we have

$$\sigma^{*2}_{o\text{-}inc} = \frac{1}{4} \sum_{n,n'}^{N} \langle a_{on}^2 \rangle \langle a_{on'}^2 \rangle \left\{ (L_n^{(4)} - 2L_n^{(2)} L_{n'}^{(2)}) \delta_{nn'} + 2L_n^{(2)} L_{n'}^{(2)} \cdot \hat{m}^2_{nn'} \rho^2_{nn'} \right\} \tag{5.34a}$$

$$= 2\langle a_{oN}^2 \rangle^{*2}_{min\text{-}inc} \left\{ \sum_{nn'} \overline{\hat{a}^2_{n/N}} \cdot \overline{\hat{a}^2_{n'/N}} \sqrt{L_n^{(4)} L_{n'}^{(4)}} \left(\delta_{nn'} + \frac{2L_n^{(2)} L_{n'}^{(2)}}{\sqrt{L_n^{(4)} L_{n'}^{(4)}}} (1 - \delta_{nn'}) \hat{m}^2_{nn'} \rho^2_{nn'} \right) \right\}$$

(5.35a)

which again shows the factorization into processing gain × (min. det. signal)^2, as noted above (5.12) in the M-ary cases. Here we have

$$\langle a_{oN}^2 \rangle^*_{\text{min-inc}} \equiv \left\{ \sum_n \overline{a_{on}^2}^2 / N \right\}^{1/2} ; \quad \overline{a_{n/N}^2} \equiv \overline{a_{on}^2} \Big/ \langle a_{oN}^2 \rangle^*_{\text{min-inc}} . \tag{5.35b}$$

When the signal processes are also stationary, (5.34), (5.35) reduce directly to our earlier results [12].

$$\underline{M=1}: \quad \sigma^{*2}_{o\text{-coh}}\big|_{\text{stat}} = 2NL^{(2)} \langle a_o^2 \rangle^*_{\text{min-coh}} ; \quad \langle a_o^2 \rangle^*_{\text{min-coh}} = \frac{\overline{a_o}^2}{2N} \sum_n \overline{s_n}^2 + \overline{a_o}^2 ; \tag{5.36}$$

$$\underline{M=1}: \quad \sigma^{*2}_{o\text{-inc}}\big|_{\text{stat}} = 2\Pi^*_{\text{inc}} \left(\langle a_o^2 \rangle^*_{\text{min-inc}} \right)^2 ;$$

$$\Pi^*_{\text{inc}} = \frac{NL^{(4)}}{8} \left\{ 1 + \frac{2L^{(2)^2}}{L^{(4)}} \sum_{nn'}{}' \hat{m}^2_{|n-n'|} \rho^2_{|n-n'|} \right\} \tag{5.37a}$$

$$= \frac{NL^{(4)}}{8} \left\{ 1 + \frac{2L^{(2)^2}}{L^{(4)}} (Q_N - 1) \right\} \tag{5.37b}$$

with

$$\boxed{Q_N \equiv \frac{1}{N} \sum_{nn'}^{N}{}' \hat{m}^2_{|n-n'|} \rho^2_{|n-n'|} ,} \qquad \text{cf. (6.24), (6.25), [12].} \tag{5.37c}$$

$$\left. \begin{aligned} \underline{M=1}: \quad \sigma^{*2}_{o\text{-comp}}\big|_{\text{stat}} &= 2\langle a_o^2 \rangle^*_{\text{min-comp}} \hat{b}_{\text{coh}} \Pi^*_{\text{coh}} + 2\langle a_o^2 \rangle^{*2}_{\text{min-comp}} \hat{b}^2_{\text{inc}} \Pi^*_{\text{inc}} \\ &\equiv 2\langle a_o^2 \rangle^*_{\text{min-comp}} \Pi^*_{\text{comp}} , \end{aligned} \right\} \tag{5.37d}$$

$$\therefore \langle a_o^2 \rangle^*_{\text{min-comp}} = \text{Eq. (5.22), M=1;} \quad \Pi^*_{\text{comp}} = \text{Eq. (5.33), M=1,} \tag{5.37e}$$

where Π^*_{coh}, Π^*_{inc} are given by (5.36), (5.37a,b), and where now

$$\hat{b}_{coh} = 1 - \eta; \qquad \eta \equiv \text{var}\, a_o/\overline{a_o^2}\,; \qquad \hat{b}_{inc} = 1; \qquad 0 < \eta \leq 1 \tag{5.37f}$$

These results are particularly pertinent for strongly correlated interference fields (in space), cf. the remarks in Sec. 5.4ff.

II. M-ary Stationary and Homogeneous Noise and Signal Fields

In this important case we have $L^{(2)}$, $L^{(4)}$, and $a_{on}^{(m)} \to a_o$, independent of time (n,n'), and of space (m,m') over the domain of the receiving aperture (array), so that (5.5), (5.8), (5.22), (5.23) all reduce to the still simpler results:

A. Coherent Reception

$$\boxed{\sigma^{*2}_{o\text{-coh}}\Big|_{\substack{\text{stat}\\ \text{homog}}} = 2MNL^{(2)}\left\{\overline{a_o}^{-2}\sum_{mn}\frac{\overline{s_n^{(m)2}}}{2MN}\right\}, \qquad MN = J} \,, \tag{5.38}$$

$$\langle a_o^2\rangle^*_{\text{min-coh}} = \overline{a_o}^2\sum_{m,n}\overline{s_n^{(m)2}}\Big/2MN; \qquad \pi^*_{coh} = MNL^{(2)} = JL^{(2)} \tag{5.38a}$$

where we keep the m-index on $s_n^{(m)}$, since this denotes reception at the m^{th}-element of the array; (see Sec. 6ff. for details).

B. Incoherent Reception

$$\sigma^{*2}_{o\text{-inc}}\Big|_{\substack{\text{stat}\\ \text{homog}}} = 2\,MNL^{(4)}(\underline{\tilde{1}}\,\underline{\pi}^*_{inc}\,\underline{1})\overline{a_o^2}^2, \qquad \underline{1} = [1] \tag{5.39}$$

$$\therefore \langle a_o^2\rangle^*_{\text{min-inc}} = \langle a_o^{(m)2}\rangle^*_{\max_m} = \overline{a_o^2}\,; \qquad \hat{a}_o^2 = \overline{a_o^{(m)2}}\Big/\overline{a_o^{(m)2}}\Big|_{\max_m} = 1; \quad \overline{a_o^{(m)2}} = \overline{a_o^2} \tag{5.39a}$$

with the interelement processing matrix

$$\underline{\pi}^*_{inc} = \left[\frac{1}{8M}\left\{\delta_{mm'} + \frac{2L^{(2)2}}{NL^{(4)}}\sum_{n,n'}(1-\delta_{mm'}\delta_{nn'})\hat{m}^2_{|n-n'|}\rho^{(mm')2}_{|n-n'|}\right\}\right] = [\pi_{mm',nn'}], \tag{5.39b}$$

where again we keep the indexes (mm') on ρ, since these denote interelement wave form correlations. Thus, the dependence on array element (m,m') remains in the normalized signal wave form because of the path delays τ_m applied to each receiving element vis-à-vis a common reference, e.g., "beam-forming" (see Sec. 6 ff. for details). Accordingly, (5.39) becomes explicitly

$$\sigma^{*2}_{o\text{-inc}}\Big|_{\substack{\text{stat}\\ \text{homog}}} = 2\overline{a_o^2}^2 \left[MNL^{(4)} \sum_{m,m'}^{M} \frac{1}{8M} \right\} \delta_{mm'} + \frac{2L^{(2)^2}}{NL^{(4)}} \sum_{n,n'}^{N} (1-\delta_{mm'}\delta_{nn'}) m^2_{|n-n'|} \rho^{(mm')^2}_{|n-n'|} \left\} \right] = 2\overline{a_o^2}^2 \, \Pi^*_{inc} \,, \tag{5.40}$$

where the overall processing gain, Π^*_{inc}, is now given by the expression in the brackets [ ]. In all of the above both noise and signal fields are assumed to be homogeneous as well as stationary.

C. Composite Reception

Here we use (5.38) and (5.40) in (5.29) to get explicitly

$$\sigma^{*2}_{o\text{-comp}}\Big|_{\substack{\text{stat}\\ \text{homog}}} = 2\, MNL^{(2)} \overline{a_o^2} \hat{b}_{coh} + 2\, MNL^{(4)} \overline{a_o^2}^2 \sum_{m,m'}^{M} \frac{1}{8M} \right\} \delta_{mm'} + \frac{2L^{(2)^2}}{NL^{(4)}} \sum_{n,n'}^{N} (1-\delta_{mm'}\delta_{nn'}) \hat{m}^2_{|n-n'|} \rho^{(m-m')^2}_{|n-n'|} \left\} \right) \tag{5.41}$$

for these totally homogeneous and stationary cases, with now

$$\hat{b}_{coh} = (1 - n) \sum_{m,n} \frac{\overline{s^{(m)}}^2}{2MN} \,, \qquad [\text{cf. (5.30b)}] \;; \quad [0 < n \equiv \frac{\text{var } a_o}{\overline{a_o^2}} \leq 1]. \tag{5.41a}$$

For the minimum detectable signal, $\langle a_o^2 \rangle^*_{min\text{-}comp}$, and associated processing gain, Π^*_{comp}, we apply (5.38a), (5.40) to (5.32) and (5.33), where (5.41a) gives $\hat{b}_{coh}$ and $\hat{b}_{inc} = 1$.

5.3 Conditions on the Measures of Performance

With the discrete sampling employed here, there is one fundamental condition for the asymptotic optimality (AO) of these LOB detectors, and hence on the validity of the performance measures (p_D^*, α_F^*, β^*) described above at the beginning of Section 5. This condition is that these LOBD-AO algorithms, g*, [cf. Sec. 3.4], must yield equal variances under both H_0, H_1 (as $J >> 1$), viz.:

$$var_1 g^* \doteq var_0 g^*, \quad \text{or } var_1 g^* = var_0 g^* + F_1(M,N;\langle a_o^2 \rangle^*_{min}), \tag{5.42}$$

or since $\langle a_o^2 \rangle^*_{min} > 0$ practically,

$$\therefore \sigma_o^{*2} = var_0 g^* >> F_1(M,N;\ \langle a_o^2 \rangle^*_{min}). \tag{5.42a}$$

Moreover, condition (5.42a) equivalently establishes upper bounds on the magnitude of the (small) minimum detectable signal, $\langle a_o^2 \rangle^*_{min}$, since generally $F_1/\sigma_o'^2 = \langle a_o^2 \rangle^*_{min}\ (x_o^*, \text{ or } y_o^*)^{-1} << 1$, where x_o^*, y_o^* are respectively bounding quantities determined from the explicit structure of $var_0 g^*$, $var_1 g^*$, for coherent and incoherent detection. Thus, we may state that

$$(0 <)\langle a_o^2 \rangle^*_{min\text{-}coh} << x_o^*\ ; \qquad (0 <)\langle a_o^2 \rangle^*_{min\text{-}inc} << y_o^* \tag{5.43}$$

cf. Secs. 6.4, 6.5, [12], where the strong inequality (<<) is usually taken to be O(10-15 db).

By setting i=(m,n), j=(m',n'), noting that $\sum_{ij}{}' \rightarrow \sum_{mm'} \sum_{nn'}{}'$ (i.e., $i \neq j$ does not imply $m \neq m'$, as we can readily check for M=m=m'=1), and applying these relations to (A.2-15a) of [12], we readily find in the limiting case of stationary and homogeneous fields [cf. II of Sec. 5.2 above] that for coherent detection

$$x_o^* = L^{(2)} \Big/ \left| \frac{L^{(2,2)}}{2} - (1-\eta)L^{(2)^2} + \frac{L^{(2)^2}}{MN} \sum_{mm'} \sum_{nn'} [\hat{m}_{|n-n'|} - (1-\eta)] \right| \tag{5.44}$$

where we have set $s_n^{(m)} = \sqrt{2}$, etc., taking advantage of the coherent signal structure at each sample point. Here $0 < 1-\eta \leq 1$, $\eta = \text{var } a_o / \overline{a_o^2}$, with $\eta \sim 1$ corresponding to deep fading while $\eta = 0$ represents no fading at all. Fading, accordingly, lowers this upper limit. For no or rapid fading the last terms of the denominator of (5.44) vanishes, while it becomes $\approx -L^{(2)^2}$ for slow fading.

Here $L^{(2,2)}$ is defined by

$$L^{(2,2)} \equiv 2\left\langle \left(\frac{w_1'}{w_1} \right)^4 \right\rangle_{H_0} = 2\langle \ell^4 \rangle_o \quad (> 0). \tag{5.44a}$$

In a similar way we can readily show that for the incoherent modes of reception, the upper bounds y_o^*, cf. (5.43), may be obtained directly from (A.2-41) of [12] again, with the extensions $i \to m,n$; $j \to m',n'$, $k \to m'',n''$. Writing

$$Q_N^{(m,m')} \equiv \frac{1}{N} \sum_{n,n'}^{N} \hat{m}^2_{|n-n'|} \rho^{(mm')^2}_{|n-n'|} \tag{5.45a}$$

$$R_N^{(m,m',m'')} \equiv \frac{1}{N} \sum_{n,n',n''}^{N'''} \left\{ 4\hat{m}_{|n-n'|} \hat{m}_{|n'-n''|} \hat{m}_{|n''-n|} \rho^{(mm')}_{|n-n'|} \rho^{(m'm'')}_{|n'-n''|} \rho^{(m''m)}_{|n''-n|} - 2\,\hat{m}^2_{|n'-n''|} \rho^{(m'm'')^2}_{|n'-n''|} \right\} \tag{5.45b}$$

for the assumed stationary and homogeneous noise and signal fields [cf. II,B of Sec. 5.2], we have

$$y_o^* = \frac{\left| L^{(4)} + \frac{2L^{(2)^2}}{M} \left[\sum_{mm'}' Q_N^{(mm')} + \sum_{m} (Q_N^{(mm)} - 1) \right] \right|}{\left| \frac{L^{(6)}}{2} + 6L^{(2)}L^{(2,2)} \cdot \sum_{mm'}^{M} \frac{Q_N^{(mm')}}{M} + L^{(2)^3} \sum_{mm'm''}^{M} \frac{R_N^{(m,m',m'')}}{M} \right|} \tag{5.46}$$

which is the extension of the general result (A.2-42), [12], for M=1, viz.,

$$y_o^*\big|_{M=1} = \frac{L^{(4)} + 2L^{(2)^2}(Q_N - 1)}{\left| \frac{L^{(6)}}{2} + 6L^{(2)}L^{(2,2)}Q_N + L^{(2)^3}R_N \right|} : \underline{\text{single element or array}}, \tag{5.47}$$

with

$$L^{(6)} \equiv \langle (w_1''/w_1)^3 \rangle_0 = \langle (\ell' + \rho^2)^3 \rangle_\theta \quad \gtrless 0. \tag{5.47a}$$

We may specialize (5.46) along the lines of (A.2-42b)-(A.2-42f), [12], when coherent or incoherent signals are used. We may also extend these results to the important cases where the signal levels [$\sim a_o^{(m)}$] vary across the array, in the manner of Sec. 5.1A above.

In recent earlier work [10], [11] we have required a second condition on $\langle a_o^2 \rangle^*_{min}$, stemming from the fact that coherent performance cannot be inferior to incoherent performance under otherwise the same conditions of sample-size, signal and noise fields, etc. This is a valid condition, provided continuous sampling in (space and) time is employed, but does not hold for the discrete sampling cases generally. The basic reason for the latter is that the additional information about the noise (embodied in $L^{(2)}$ and $L^{(4)}$) and the noise and signal interactions (in $Q_N^{(mm')}$, etc.) can more than compensate for the effects of the loss of signal epoch or "carrier" frequency phase data characteristic of incoherent detection, so that for the same controls (decision probabilities, sample-size) $\langle a_o^2 \rangle^*_{min\text{-}inc}$ can be less than $\langle a_o^2 \rangle^*_{coh}$; see Sec. 6.3, B III of [12] for further discussion.

5.4 Remarks on Independent Sampling

In this study we postulate independent temporal and spatial sampling of the noise fields. Since the noise fields are basically poisson processes in time and space [as we shall see in Part IIff.], the usual temporal sampling at 1/B second intervals†-which gives (statistically) independent samples for band limited gaussian noise--does not generally result in independent samples for poisson processes of comparable bandwidth. For Class A and B noise

---

† B = bandwidth of data samples ($\underset{\sim}{x}$) at output of each sensor.

([1]-[7]) the temporal sampling rate must be slower: O(1.5/B), or (2.0 or more/B), respectively for Class A and Class B noise, to ensure essentially independent samples (see [9], OT-Rpt. 75-67). Because of the truly impulsive nature of Class B noise it is not possible to obtain strictly independent samples, but it is possible to obtain nearly independent quantities if the sampling rate is larger than the decay-time T_d of the receiver's linear front-end stages, so that the resultant transient overlap is small. By "larger," we mean $T_{sample} > T_d$, with T_d such that a transient produced by an entering impulse dies down to, say, a few hundredths of its maximum value (in the receiver). Thus, we employ here "sparse" sampling in time, to justify our postulate of temporal independence in the development of the threshold algorithms above.

For spatial independence we must examine the relevant spatial statistics of the noise field. In theory this demands a joint M^{th} order ($M >> 1$) determination of the field amplitudes over the spatial region to be sampled by our M-element set of sensors (or arrays). In practice, this is beyond our powers, and we must usually be content to determine the spatial covariance function K_I of the field, placing our sensors at the zero's of this function, i.e., at those points where K_I vanishes, or failing this, where K_I is small vis-à-vis $K_{I\text{-max}}$. Again, we require a "sparse" spatial sampling also, here.

In practice, however, it may be difficult to obtain the number (N) of needed independent temporal samples: while we may choose N (>> 1) nominally independent time samples, in effect we may have only $N' < N$ [but with $N' >> 1$ so that the Central Limit Theorem still applies and the AO condition can be reasonably approximated, cf. beginning of Sec. 5 above.] The result, of course, is degraded performance, now with fewer effectively independent samples ($N' < N$). Moreover, taking many, correlated noise samples, will improve performance very little O(1 or 2 db) over that obtained using only the independent samples in the same time interval (t_o, t_o+T). The reason, of course, is that the effective statistical sample--i.e., the number of <u>independent</u> noise elements--has not been noticeably enlarged. This applies also to continuous sampling on the interval in the limit. In any case, except for gaussian noise processes, the needed N^{th} order pdf's of the interference are not known, so that they cannot be applied specifically to our canonical threshold detection algorithm (2.6b). Moreover, we would not wish to do so because of the monumental complexity of the resulting algorithms, stemming

from the added correlations (of all orders), which, as we have just noted, yield very little further improvement. The manageable simplicity of the threshold structure with independent samples is a major justification for its use. [See VII, Sec. 12.3 ff.]

Similar remarks apply for spatial samples: we postulate M independent elements (or arrays), where in practice we may have only $1 \leq M' < M$ such elements effectively. If the noise field is completely correlated over the domain of the M sensors, then, of course, $M' = 1$, and the best we can do is to combine the M elements in such a way or to form a beam, effectively at a point in the domain. We gain nothing further from the spatial distribution of elements. [The same observation applies if each m "element" is itself an array, so that we now combine these to form a composite array, again effectively at a single location in the correlated noise field.] In these cases our analysis for a single element ($M = 1$), or single array [Sec. 5.2, I] then applies.

In summary, we employ:

(1) Threshold detection algorithms which are LOB and AO when the space and time samples of the received noise field are independent and sufficiently numerous ($J = MN >> 1$) so that performance may be calculated from the asymptotically normal nature of the algorithm [cf. beginning of Sec. 5 above].

(2) We employ these same algorithms when only ($J > J'(=M'N' >> 1$) of the samples are effectively independent. [These algorithms are no longer strictly optimum, but are equated to the equivalent LOB and AO procedures for J' independent samples. In principle, the actual value of J' may be found empirically by matching the actual performance, for given minimum detectable signal and probability controls, with that of the analytically determined performance, under J' independent samples and the same signal and noise conditions.]

(3) As we have already noted above, when J' independent noise samples are obtainable, sampling more densely in the space-time interval, i.e., ($J'' > J$) will (slightly) improve performance. It is in this sense that we say that algorithms with (only) independent samples are "conservative": they yield a lower bound, i.e., a somewhat inferior performance (viz. larger error probabilities, etc.) than would

ideally be obtained from either the optimum or the now suboptimum algorithm using J" (> J) samples, not all of which are independent.

5.5 Principal Results of Part I

At this point it is useful to note briefly the principal results obtained in Sections 2-5 (Part I). These are:

(1) A canonical M-sensor (or array) formulation of optimum threshold detection theory, in the binary ("on-off") state-desired signal or not--for general signals and noise fields, which are not usually gaussian [Sec. 2].

(2) The explicit development of the theory for independent space-time sampling of the noise field [Sec. 3], where it is shown that the resulting threshold algorithms, g_J^*, are separable [cf. Sec. 2.4], i.e., the temporal and spatial processing can be interchanged. Three modes of operation are considered: coherent, incoherent, and composite detection.

(3) For threshold detection the algorithms may be interpreted in terms of nonlinear zero-memory filters matched to the noise, which are combined with conventional matched filters for the signal to produce a test statistic, g_J^*, which is in turn compared to a threshold for the desired decision process [Sec. 4]. For incoherent and composite detection all pair products of spatial channels (m,m') are required, cf. Fig. 4.2. It is emphasized that these algorithms are also adaptive, requiring a parallel estimation of appropriate noise field parameters and first- and second-order signal statistics, cf. Sec. 4.3.

(4) Optimum threshold performance is explicitly obtained in canonical form [Sec. 5]. The key structural parameter here is the variance (under H_0) of the appropriate algorithm, g_J^*, viz., $(\sigma_0^*)^2 = \mathrm{var}_0 g_J^*$. Since $(\sigma_0^*)^2 \sim J(=MN)$, increasing the number of independent samples rapidly increases $(\sigma_0^*)^2$, and, correspondingly, detector performance. Beam-forming also plays a central rôle in increasing σ_0^{*2} and hence improving performance. For coherent detection beam forming can increase σ_0^{*2} by maximizing the sampled wave form, $\langle s_n^{(m)} \rangle = (\langle s(t_n - \tau_m, \theta) \rangle)$ by proper choice of delay (τ_m). For incoherent and composite

detection beam-forming similarly achieves this by maximizing the interelement correlation function $\rho\left(\begin{smallmatrix} mm' \\ n-n' \end{smallmatrix}\right)$ of the signal wave form. (See Secs. 5.2, 5.3). Various important special cases are derived, including the case of a single element or beam. The general formulation includes such physical features as fading, doppler spreading field amplitude variation over the spatial elements, nonstationarity and inhomogeneity, as well as the relevant statistical structure of the interfering noise field and general signal wave forms.

In Part II following, we shall apply these canonical results to specific underwater acoustic signal and interference environments.

Part II. Application to Underwater Acoustic Signal and Interference Environments

Continuing our "top-down" approach--from the general or canonical formulation to progressively more explicit developments--in order to implement our optimum detection algorithms and evaluate receiver performance, we now need to construct appropriate statistical-physical models of desired signals and interference environments. The strength of this approach is that it provides analytically tractable results, which can be (and have been) experimentally well established (the latter mostly in the analogous EMI cases ([1]-[7]), with some recent work on modeling ice-noise*).

The advantage of having an analytical model for the pdf's appearing in the signal processing algorithms [cf. Secs. 3, 5] that only a few noise distribution parameters need to be estimated [cf. Sec. 4] and applied in the derived analytic forms [$\ell_{m,n}$, $\ell'_{m,n}$, etc.]. This is opposed to an estimation of the entire pdf, which may be particularly difficult on the "tails" of the distributions, where the number of data "events" becomes comparatively rare [23]. Furthermore, analytic operations (differentiation, integration) may be performed without error on these analytical models, whereas this is not the case with empirically derived pdf's, differentiation, for example, increasing the error for finite samples, which latter are always the case in practice.

Here in Part II we proceed first (Sec. 6), with the development of received signal models, including the effects of a number of array structures on these signals. Section 7 provides the appropriate analytic (i.e., statistical-physical) noise models, including some examples of typical received data and calculations of wave-number spectra of the interference field. In Section 8 we present several explicit optimum threshold detection algorithms based on the results of Sections 6 and 7. (These are among the algorithms which we shall ultimately wish to implement and test: see "Recommendations," Sec. 12.) Specific optimum threshold performance, minimum detectable signals, etc., along with a variety of results for some common suboptimum detectors are summarized in Sections 9 and 10, and

---

* D. Middleton, Tech. Rpt. in preparation for NUSC (Research & Technology), 1983.

compared in Section 11. Section 12 completes the Report with a concise account of the major results, their implications, and a resumé of technical recommendations for exploitation of the present work in various analytical and empirical follow-on efforts.

Section 6. The Received Signal

From Sec. 3 of [1], and in particular from Eq. (3.35) therein, we can express the signal received at the $m^{\underline{th}}$ element of our initially arbitrary array of M elements by the following relations:

$$s^{(m)}(t) \doteq \mathrm{Re}\left\{ \frac{S_{0T} e^{i\mu\omega_0(t-\varepsilon-\underline{R}_0\cdot\underline{r}_m/c_0\mu)} |Q_{RT}^{(m)}| a(t-\tau_m) e^{i\phi_a(t-\tau_m)}}{|\underline{R}_p-\underline{r}_m|^{\gamma}} \cdot \hat{s}_0\left(\frac{t-\varepsilon}{\mu} - |\underline{R}_0-\underline{r}_m|/\mu c_0 - \frac{\phi_T(f_0)}{\mu}\right)\right\} \tag{6.1a}$$

$$= \frac{A_0^{(m)}(t)}{\sqrt{2}} s^{(m)}(t-\varepsilon;\theta_m) = a_0^{(m)}(t) s^{(m)}(t-\varepsilon;\theta_m)\sqrt{\psi^{(m)}(t)} \tag{6.1b}$$

cf. (2.7a,b). Our principal assumptions here are:

(i). Narrow-band signals from the source and at the receiving element;

(ii). Far-field reception--the receiving elements are in the Frauenhofer region of the source;

(iii). Small doppler (and for the moment the receiver is stationary in space).

[The narrow-band condition is easily removed for multiple harmonic signals, cf. Sec. 6.2 ff.: one has appropriately modified beam pattern structures, for $2f_0$, $3f_0$, etc. Extensions to moving receiver arrays is straightforward [25], and is reserved for a later study.] For (6.1a,b) we can also write

$$A_0^{(m)}(t) \equiv \left\{ S_{0T} a^{(m)}(t) |Q_{RT}^{(m)}| \sqrt{2} \left| e^{i\phi_a^{(m)}(t)} \hat{S}_0\left(\frac{t-\varepsilon}{\mu} - |R_0-r_m|/\mu c_0 - \phi_T/\mu\right)\right| \right/ \lambda_m^{\gamma}$$

instantaneous peak amplitude, cf. (2.7); (6.2a)

$$a_o^{(m)}(t) \equiv A_o^{(m)}(t)\Big/\sqrt{2\psi^{(m)}(t)} = \text{normalized signal amplitude cf. (2.7);} \tag{6.2b}$$

$$s^{(m)}(t...) = \cos\{\mu\omega_o[t-\varepsilon-|R_o-r_m|/\mu c_o] + \phi_a^{(m)} + \phi_o\left(\frac{t-\varepsilon}{\mu} - |R_o-r_m|/\mu c_o\right)$$

$$-\phi_T(f_o)/\mu\}. \tag{6.2c}$$

The normalizations are chosen so that $\langle s^2\rangle = \langle s^2(t-\varepsilon;\theta)\rangle_{\varepsilon,..} = 1$, and that $\overline{a^{(m)}(t)^2}$ = normalized signal intensity at the $m^{\underline{th}}$ array element, or the input signal-to-noise (intensity) ratio (at time t) at that element .

Specifically, we define the various elements of (6.1)-(6.2) by

$S_{oT} = \hat{S}_{oT}\hat{\lambda}_o^{\gamma}$ = an amplitude (A'), with dimensions $[A'] = [A][T^{\gamma}]$, where $S_{oT}(=[A])$ has the same dimensions as the received wave S(t). Here,

$\hat{\lambda}_o$ = a reference "distance" (from the signal source) at which $\hat{S}_{oT}$ is calibrated, expressed in units of <u>time</u>, i.e., $r_o(=[L]) = c_o\lambda_o$, with

c_o = speed of (wavefront) propagation, so that $\hat{\lambda}_o = [T]$ (seconds);

$\mu = 1+\beta$ = a doppler factor, $\beta = \underset{\sim}{i}_o\cdot\underset{\sim}{v}_s/c_o$; $|\beta^2|\ll 1$, where $\underset{\sim}{v}_s$ is the (constant) velocity of the signal source with respect to the (fixed) receiver's frame of reference (O_R), cf. Fig. 6.1.

$\omega_o = 2\pi f_o$ = angular (central) frequency of the (narrow-band) signal;

$\lambda_o = c_o/f_o$ = wavelength of the propagating wave with frequency f_o.

ε = an epoch, representing the time difference between the observer's time scale and some reference point on the emitted signal waveform. Thus, for <u>coherent reception</u>, $\varepsilon=\varepsilon_o$, a known quantity at the receiver, while for <u>incoherent reception</u> ε is randomly distributed over some interval, such that $\langle s\rangle_{\varepsilon} = 0$ for purely incoherent reception, while $\langle s\rangle_{\varepsilon} \neq 0[\neq s(t-\varepsilon_o,\underset{\sim}{\theta}_m)$ for partially incoherent observation].

(6.3a)

$\underset{\sim}{r}_m = \underset{\sim}{R}_o - \underset{\sim}{R}_m$ = vector distance from receiver reference O_R to $m^{\underline{th}}$ element, cf. Fig. 6.1.

$\lambda = |\underset{\sim}{R}_o - \underset{\sim}{R}|/c_o$ = distance (measured in time) of source from $P(\underset{\sim}{R})$; distance along path of source from $P(\underset{\sim}{R})$ ($\nabla c \neq 0$), e.g., "path distance," cf. Figs. 6.1, 6.2.

$T_o = R_o/c_o$ = distance of the source from O_R; or "path distance" ($\nabla c \neq 0$).

$\lambda_m = |\underset{\sim}{R}_o - \underset{\sim}{r}_m|/c_o = \frac{R_m}{c}$ = distance of $m^{\underline{th}}$ element from O_R.

γ = (av.) law of propagation, which takes into account the effective spreading, diffraction, and focusing action of the medium, i.e., av. gradient effects on the propagating energy. Here $\gamma>0$ and $\gamma=1/2$ for cylindrical spreading; $\gamma=1$ for spherical spreading, and is usually greater than unity for diffraction, e.g., $\gamma=3/2$, 2, or more for propagation over "mountain ridges," etc.

$|\mathcal{Q}_{RT}^{(m)}| = |\mathcal{Q}_T|\,|\mathcal{Q}_R^{(m)}|$ = product of the (here dimensionless) moduli of the beam patterns of the source (T) and of the $m^{\underline{th}}$ receiving element in the array. $|\mathcal{Q}_T|$ may be highly directional, but is usually well-modeled by that of a point-source, i.e., an omni-directional pattern. (For $|\mathcal{Q}_R^{(m)}|$ see Secs. (6.1), (6.2)ff.) (6.3

$\phi_T = \phi_T(f_o)$ = phase angle of the (complex) pattern, $\mathcal{Q}_T$, of the desired signal source.

$\psi^{(m)}(t)$ = total intensity of the noise (gauss + non-gauss) at the $m^{\underline{th}}$ element and at time t; in the usually stationary cases, $\psi^{(m)}(t) = \psi^{(m)}$, cf. (2.1).

$\hat{S}_o(t\ldots) = |\hat{S}_o|e^{i\Phi_o}$ = (complex) envelope of the assumed narrow-band signal. (By "narrow-band" here is meant a bandwidth which is a factor O(5-10 or more) less than the central or "carrier" frequency f_o, cf. (6.3a) above.

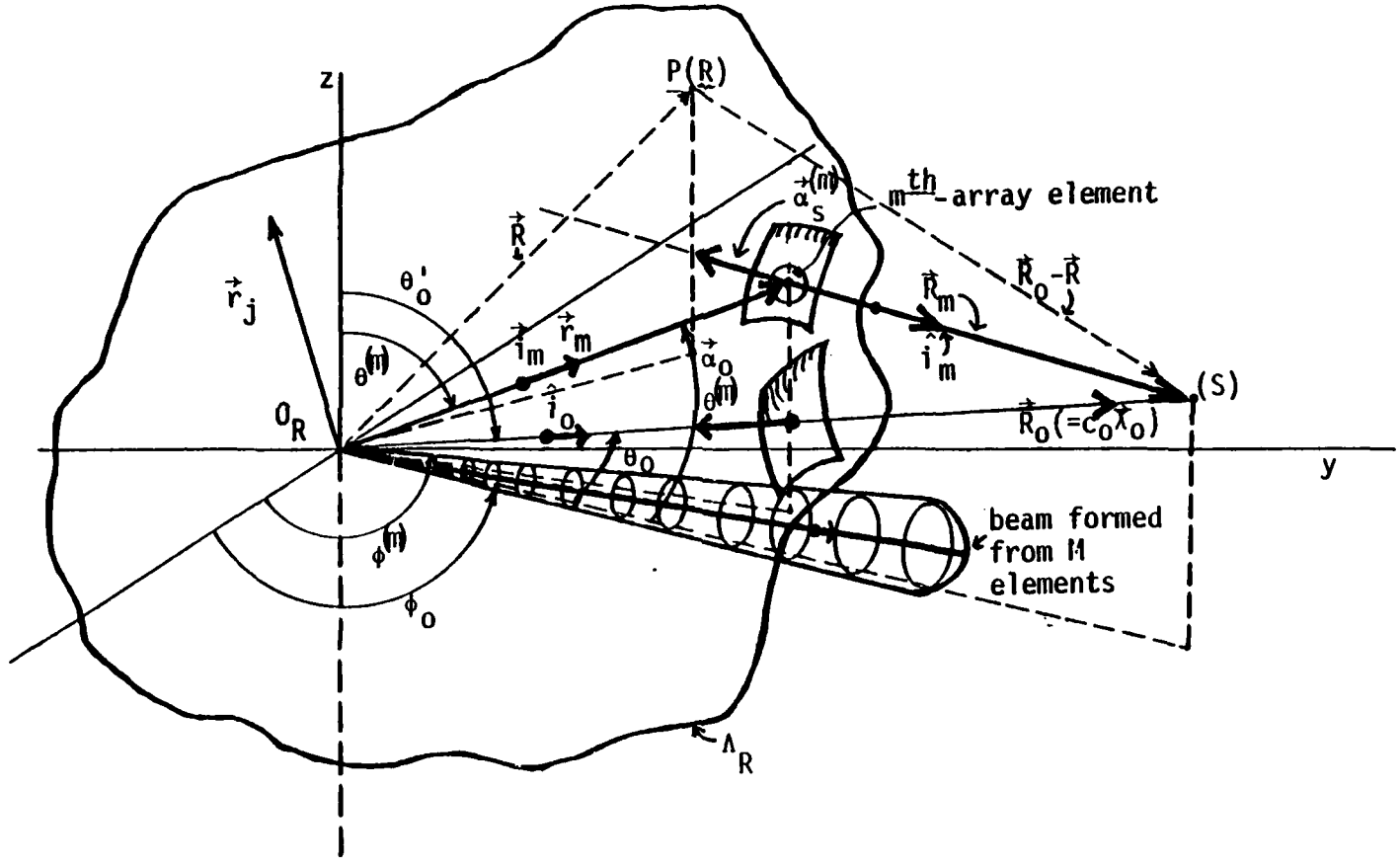

Figure 6.1. Geometry of signal source, m^{th} array element, and reference (O_R) system; Λ_R is the domain of the array.

$\underset{\sim}{\theta}_m$ = a set of signal parameters, some dependent on the particular array element (m) and others not, as indicated by a comparison of (6.1a,b).

τ_m = a key parameter is the path delay τ_m, from the $m^{\underline{th}}$ element to the chosen reference point, O_R, cf. Fig. 6.1;

$a^{(m)}(t) = a(t-\tau_m)$ = a dimensionless fading factor amplitude, as seen at the $m^{\underline{th}}$ element, which can produce an amplitude modulation.

$\phi_a^{(m)}(t) = \phi_a(t-\tau_m)$ = the phase component of the fading, which can produce a phase modulation at the $m^{\underline{th}}$ element. (6.3b)

Equation (6.1) is partially phenomenological in that is employs a localized fading effect,

$$a^{(m)}(t)e^{i\phi_a^{(m)}(t)},$$

and a non-integral spreading term (λ_m). The precise structure of $a^{(m)}(t)$, $\phi_a^{(m)}(t)$, and its statistics, and the appropriate value of γ, must therefore be determined ultimately by experiment. This, of course, does not vitiate the analytic and quantitative nature of Eq. 6.1. (For experimental events and associated theory, see [26]-[28].)

We proceed next to the development of beam-forming and beam-steering for these signals.

6.1 Beam-Forming and Beam-Steering

Our task here is to examine general linear beam formation for our initially arbitrary array of M elements in space (cf. Fig. 6.1) [viz. $\overline{\theta}_{m,n}$ in (3.2)]. Higher-order beam formation (what we shall call product beams), which arise in the structure of incoherent reception [viz. $<\theta_{m,n}\theta_{m',n'}>$ in (3.5)], are discussed in Sec. 8ff.

To describe the effects of the path delays τ_m, and to develop a resultant beam by suitable insertion of compensating delays and steering components, we introduce the delay per unit distance of signal wavefront, $\alpha_s^{(m)}$, where

$$\underset{\sim}{\alpha}_s^{(m)} = \underset{\sim}{i}_x\alpha_{sx}^{(m)} + \underset{\sim}{i}_y\alpha_{sy}^{(m)} + \underset{\sim}{i}_z\alpha_{sz}^{(m)};\quad |\alpha_s^{(m)}| = \sqrt{\left\{(\alpha_{sx})^2+(\alpha_{sy})^2+(\alpha_{sz})^2\right\}^{(m)}} = (c_o^{(m)})^{-1} \tag{6.4}$$

with

$$c_o^{(m)} = \underset{\sim}{\alpha}_s^{(m)}/|\underset{\sim}{\alpha}_s^{(m)}|^2;\quad \theta^{(m)} = \cos^{-1}(\alpha_{sz}^{(m)}/|\underset{\sim}{\alpha}_s^{(m)}|);\quad \phi^{(m)} = \tan^{-1}(\alpha_{sy}^{(m)}/\alpha_{sx}^{(m)});$$

$$= \pi/2 \leq \theta^{(m)} \leq \pi/2;\quad 0 \leq \phi^{(m)} \leq (2\pi \text{ or } \pi) \tag{6.4a}$$

where $\underset{\sim}{c}_o^{(m)}$ is the velocity of propagation of the signal wavefront. [Since we allow for possible variations of these quantities with the location of the array elements in the medium (about O_R), we write $\underset{\sim}{\alpha}_s \to \underset{\sim}{\alpha}_s^{(m)}$, $\underset{\sim}{c}_o \to \underset{\sim}{c}_o^{(m)}$, etc.] Figure 6.1 shows a typical source and receiver geometry for this general array configuration (arbitrary locations of $\underset{\sim}{r}_m$, $\underset{\sim}{r}_j$).

Since $|\underset{\sim}{R}_o - \underset{\sim}{r}_m| = R_o - \hat{\underset{\sim}{i}}_o \cdot \underset{\sim}{r}_m$, $R_o >> |r_m|$, with $\hat{\underset{\sim}{i}}_o = \underset{\sim}{R}_o/|\underset{\sim}{R}_o|$, we can write

$$\boxed{\left|\frac{\underset{\sim}{R}_o - \underset{\sim}{r}_m}{c_o}\right| \doteq \frac{R_o}{c_o} - \frac{\hat{\underset{\sim}{i}}_o \cdot \underset{\sim}{r}_m}{c_o} = T_o + \underset{\sim}{\alpha}_s^{(o)} \cdot \underset{\sim}{r}_m};\quad \underset{\sim}{\alpha}_s^{(o)} \equiv -\hat{\underset{\sim}{i}}_o/c_o;\ T_o = R_o/c_o \tag{6.5}$$

$$\boxed{\tau_m \doteq \hat{\underset{\sim}{i}}_o \cdot r_m/c_o}. \tag{6.5a}$$

[In general, the path delay from the $m^{\underline{th}}$ element to O_R is

$$\tau_m = -\underset{\sim}{\alpha}_s^{(m)} \cdot \underset{\sim}{r}_m,\quad \text{where } \underset{\sim}{\alpha}_s^{(m)} = \underset{\sim}{i}_m/c_o^{(m)}, \tag{6.6}$$

but, since $\underset{\sim}{\alpha}_s^{(m)} = \underset{\sim}{\alpha}_s^{(m)}(-\underset{\sim}{R}_o + \underset{\sim}{r}_m) = -\hat{\underset{\sim}{i}}_m/c_o^{(m)} = \underset{\sim}{\alpha}_s^{(m)}(-\underset{\sim}{R}_o) = -\hat{\underset{\sim}{i}}_o/c_o$, because $|\underset{\sim}{R}_m|$, $R_o >> L_{max}$, $|r_m|$, where L_{max} is the maximum dimension of the array, we have here $\underset{\sim}{\alpha}_s^{(m)} = -\underset{\sim}{i}_m/c_o^{(m)} \doteq \underset{\sim}{\alpha}_s^{(o)}$, (6.5), with $c_o^{(m)} = c_o$. and $\therefore \tau_m \doteq -\hat{\underset{\sim}{i}}_o \cdot \underset{\sim}{r}_m/c_o$, cf. (6.5a). [If the variations in c_o are large over the array, or if the far-field conditions assumed here are not in force, then the actual values of $\underset{\sim}{\alpha}_s^{(m)}$ must be used, and additional terms in the expansion of $|\underset{\sim}{R}_o - \underset{\sim}{r}_m|$ must be employed.] Similarly, we have in the amplitude factor of the received signal

$$|\underset{\sim}{R}_o - \underset{\sim}{r}_m|^{-\gamma} = R_o^{-\gamma}; \quad \lambda^{-\gamma} = (R_o/c_o)^{-\gamma} . \tag{6.7}$$

The unit vector $\hat{\underset{\sim}{i}}_o$ is explicitly here

$$\hat{\underset{\sim}{i}}_o = \hat{\underset{\sim}{i}}_x \cos\phi_o \cos\theta_o + \hat{\underset{\sim}{i}}_y \sin\phi_o \cos\theta_o + \hat{\underset{\sim}{i}}_z \sin\theta_o, \tag{6.8}$$

and the unit vector $\hat{\underset{\sim}{i}}_m$ is similarly expressed on setting $\phi_o \to \phi_o^{(m)}$, $\theta_o \to \theta_o^{(m)}$ therein.

With (6.5), (6.7) in (6.1) we can now write the signal at the $m^{\underline{th}}$ array element as†

$$s^{(m)}(t) = \mathrm{Re}\left\{ S_{OT} \frac{|\mathcal{A}_T| e^{i\mu\omega_o(t-\varepsilon-T_o/\mu)}}{\lambda_o^{\gamma}} \, a(t-\tau_m) e^{i\phi_a(t-\tau_m)} \right.$$

$$\left. \cdot \hat{s}_o\left(\frac{t-\varepsilon}{\mu} - \frac{T_o}{\mu} + \frac{\tau_m}{\mu} - \frac{\phi_T}{\mu}\right) \cdot |\mathcal{A}_R^{(m)}| e^{i\omega_o \hat{\underset{\sim}{i}}_o \cdot \underset{\sim}{r}_m / c_o} \right\}. \tag{6.9}$$

From (6.9) we note that

$$\mathcal{A}_R^{(m)}(\underset{\sim}{\nu}_o, f_o) \equiv |\mathcal{A}_R^{(m)}(f_o)| e^{i\underset{\sim}{k}_o \cdot \underset{\sim}{r}_m} = |\mathcal{A}_R^{(m)}(f_o)| e^{2\pi i \underset{\sim}{\nu}_o \cdot \underset{\sim}{r}_m};$$

$$\underset{\sim}{\nu}_o \equiv \hat{\underset{\sim}{i}}_o / \lambda_o = \hat{\underset{\sim}{i}}_o f_o / c_o , \tag{6.10}$$

where $\mathcal{A}_R^{(m)}$ is the effective <u>beam pattern of the $m^{\underline{th}}$ element</u>, referred to O_R, and $\underset{\sim}{\nu}_o$ is the spatial frequency associated with the temporal frequency f_o. It is convenient to introduce a normalizing factor $A = \max_m |A_m| = \max_m |\mathcal{A}_R^{(m)}(f_o)|$, so that with

$$t - \varepsilon - T_o/\mu \equiv \hat{t} \tag{6.11}$$

---

† If the array is not too large and the input signal sufficiently narrow band, so that in

$$\hat{s}_o\left(\frac{\hat{t}+\tau_m-\phi_T}{\mu}\right) \doteq \hat{s}_o(\hat{t}-\phi_T) + \hat{s}_o \tau_m + \ldots$$

only the first term is significant, e.g.,

$$\hat{s}_o\left(\frac{\hat{t}+\tau_m-\phi_T}{\mu}\right) \doteq \hat{s}_o(t),$$

then the signal envelope is generally independent of the array element (m).

we can rewrite (6.9) as†

$$\boxed{s^{(m)}(t) \doteq \mathrm{Re}\left\{ \frac{(AS_{OT})e^{i\mu\omega_o t}}{\lambda_o^{\gamma}} \hat{S}_o\left(\frac{t+\tau_m-\phi_T}{\mu}\right) a^{(m)}(t) e^{i\phi_a^{(m)}(t)} \mathcal{Q}_R^{(m)}(\underset{\sim}{\nu}_o, f_o)_{norm} \right\}}; \tag{6.12}$$

$$\mathcal{Q}_{norm}^{(m)} \equiv \mathcal{Q}^{(m)}/A .$$

To form a beam we simply add the output (6.12) of the m elements, here referred to a common origin of space (O_R) and hence of time. In addition, we can steer the resultant beam by applying a path delay, $\hat{\tau}_m$, for each m-element output. This inserted delay is explicitly

$$\hat{\tau}_m = \hat{\underset{\sim}{i}}_{oR} \cdot \underset{\sim}{r}_m / c_o, \quad \text{with } \underset{\sim}{\nu}_{oR} \equiv \hat{\underset{\sim}{i}}_{oR} f_o / c_o = \hat{\underset{\sim}{i}}_o / \lambda_o , \tag{6.13}$$

so that the resultant output of this receiving beam is now (with τ_m replaced by $\tau_m - \hat{\tau}_m$ in (6.12))

$$S_R(t;\underset{\sim}{\theta}) = \sum_m s^{(m)}(t;\underset{\sim}{\theta}) = \mathrm{Re}\left\{ \frac{e^{i\mu\omega_o \hat{t}} AS_{OT}}{\lambda^{\gamma}} \sum_m a_m(t-\tau_m+\hat{\tau}_m) e^{i\phi_a(t-\tau_m+\hat{\tau}_m)} \right.$$

$$\left. \cdot \hat{S}_o(\hat{t}-\tau_m+\hat{\tau}_m;\ldots) \mathcal{Q}_R^{(m)}(\underset{\sim}{\nu}_o - \underset{\sim}{\nu}_{oR}, f_o)_{norm} \right\} \tag{6.14a}$$

$$= \mathrm{Re}\left\{ \frac{e^{i\mu\omega_o \hat{t}} AS_{OT}}{\lambda^{\gamma}} \sum_m \hat{A}_m(t) \mathcal{Q}_R^{(m)}(\underset{\sim}{\nu}_o - \underset{\sim}{\nu}_{oR}, f_o)_{norm} \right\} \tag{6.14b}$$

where $\hat{A}_m(t)$ is at once evident by comparison with (6.14a). We can write further

$$\boxed{S_R(t;\underset{\sim}{\theta}) = \mathrm{Re}\left\{ \frac{e^{i\mu\omega_o t} AS_{OT}}{\lambda^{\gamma}} \mathcal{Q}_R'(\underset{\sim}{\nu}_o - \underset{\sim}{\nu}_{oR}, f_o(t) \right\}, \qquad \hat{t} = t - \varepsilon - T_o/u} \tag{6.15a}$$

where

$$\mathcal{Q}_R' = \sum_m \hat{A}_m(t) \mathcal{Q}_R^{(m)}(\underset{\sim}{\nu}_o - \underset{\sim}{\nu}_{oR}, f_o)_{norm} \tag{6.15b}$$

---

† See footnote, page 58.

is the time-weighted, or time-variable (complex) beam pattern of the receiving array.

This weighting, or "modulation," is produced by the variable inputs at each array element, reflecting the fact that the signal wavefront is not generally uniform over the array. These time-variable, unequal inputs produce, in effect, a dynamic "shading" of the simple beam which would be obtained if these inputs were identical at each array element. Alternatively, for example, if the fading $[\sim a^{(m)} e^{-i\phi_a^{(m)}}]$ and signal envelope are independent of element location (and properties), we see that our more general result (6.15) reduces directly to

$$S_R(t;\theta) = \mathrm{Re}\left\{[e^{i\mu\omega_o\hat{t}}\frac{AS_{OT}a(t)}{\lambda^Y}e^{i\phi_a(t)-i\phi_T}]\sum_m \mathcal{A}_R^{(m)}(\underset{\sim}{\nu}_o-\underset{\sim}{\nu}_{oR},f_o)_{norm}\right\} \quad (6.16)$$

with $\underset{\sim}{\theta}$ representing the various (random) parameters of the received waveform. This we can write alternatively, and more compactly, as

$$S_R(t;\underset{\sim}{\theta}) = \mathrm{Re}\left\{e^{i\mu\omega_o\hat{t}}\cdot\frac{a(t)\hat{G}_o}{\lambda^Y}\mathcal{A}_R(\underset{\sim}{\nu}_o-\underset{\sim}{\nu}_{oR},f_o)\right\}\ ;\quad \hat{G}_o \equiv AS_{OT}/\sqrt{2} \quad (6.16a)$$

$$= \frac{a(t)\hat{G}_o}{\lambda^Y}|\mathcal{A}_R(\underset{\sim}{\nu}_o-\underset{\sim}{\nu}_{oR},f_o)|\sqrt{2}\cos(\mu\omega_o\hat{t}+\phi_a(t)-\phi_T-\phi_R) \quad (6.16b)$$

or

$$S_R(t;\underset{\sim}{\theta}) = A_o(t)s(t;\underset{\sim}{\theta}). \quad (6.16c)$$

Here the instantaneous amplitude and normalized signal waveform are explicitly (cf. (6.2))

$$A_o(t) \equiv \frac{a(t)\hat{G}_o|\mathcal{A}_R|}{\lambda^Y}\ ;\quad s(\hat{t};\underset{\sim}{\theta}) \equiv \sqrt{2}\cos(\mu\omega_o\hat{t}+\phi_a(t)-\phi_T-\phi_R)\ . \quad (6.17)$$

This unmodulated beam pattern is directly [(6.16a,b) vs. (6.16)]:

$$\mathcal{A}_R(\underset{\sim}{\nu}_o-\underset{\sim}{\nu}_{oR},f_o) = \sum_m \mathcal{A}_R^{(m)}(\underset{\sim}{\nu}_o-\underset{\sim}{\nu}_{oR},f_o)_{norm} = |\mathcal{A}_R|e^{-i\phi_R}\ , \quad (6.18)$$

where $|\mathcal{A}_R|$ and ϕ_R are respectively the modulus and phase of this (complex) pattern. Using (6.10) in (6.18) we can write in more detail

$$\boxed{a_R(\underset{\sim}{\nu}_o - \underset{\sim}{\nu}_{oR}, f_o) = \sum_m \frac{A_m(f_o)}{A} e^{2\pi i(\underset{\sim}{\nu}_o - \underset{\sim}{\nu}_{oR})\cdot \underset{\sim}{r}_m}} \; ; \quad A_m(f_o) \equiv |a_R^{(m)}(f_o)|, \tag{6.19}$$

which represents a time-invariant but weighted or "shaded" beam, if A_m depends on m.

Finally, we note that all the beams formed above are examples of adaptive beam forming [29], where beam formation depends on a posteriori information, i.e., in some sense on the received data. The simplest form is that involving steering ($\sim \underset{\sim}{\nu}_{oR}$, cf. (6.19); the more complex forms are signal processing beams, where in addition to steering the weightings of the elements depend on the received data and some chosen processing algorithm(s). As we shall see in Sec. 8 following, threshold detection requires beam formation of this latter type.

6.2 Two Beam-Forming Examples: Signals Only

Although signal and noise ultimately are combined nonlinearly in the threshold detection algorithms [cf. Sec. 3 above and Sec. 8ff.], it is nevertheless informative to consider beam forming for signals alone, to illustrate simple adaptive beam forming concepts. To this end, we shall consider the two cases of a vertical and a horizontal m-element array, as sketched in Fig. 6.2, where beam steering is employed.

1. Linear* Vertical Array

We postulate equal spacing, $\Delta\ell$, between elements, and employ $2M_o+1(=M)$ elements, with the spatial (and temporal) reference at O_R at the middle element (m=0), Thus, we now have for the linear vertical array

$$\underset{\sim}{r}_m = \hat{\underset{\sim}{i}}_z m\Delta\ell \qquad (-M_o, \ldots, m, \ldots M_o) , \tag{6.20}$$

and from (6.8), (6.10), (6.13) we have

$$\left.\begin{aligned} \underset{\sim}{\nu}_o\cdot\underset{\sim}{r}_m = (f_o/c_o)m\Delta\ell \sin\theta_o \; ; \quad \underset{\sim}{\nu}_{oR}\cdot\underset{\sim}{r}_m &= |\nu_{oR}|\hat{\underset{\sim}{i}}_{oR}\cdot\hat{\underset{\sim}{i}}_z\, m\Delta\ell \\ &= (f_o/c_o)\, m\Delta\ell \sin\vartheta_{oR} . \end{aligned}\right\} \tag{6.21}$$

---

* The term "linear" here and subsequently refers to the geometry of the array, not to its possible signal processing attributes.

Accordingly, from (6.14) the receiving beam pattern becomes specifically here

$$\left.\begin{aligned} \mathcal{A}_R(\underset{\sim}{\nu}_o - \underset{\sim}{\nu}_{oR}, f_o)_{vert} &= \sum_{m=-M_o}^{M_o} \frac{A_m}{A}\, e^{2\pi i m \Delta \ell \Delta \nu_z}\ ; \\ \Delta\nu_z &= (f_o/c_o)(\sin\theta_o - \sin\theta_{oR}). \end{aligned}\right\} \quad (6.22)$$

Let us consider next the case of (real) uniform weighting, with $A_m = A(>0)$. The resulting series in (6.22) can easily be summed, using

$$\sum_{1}^{M_o} \rho^m = (1 - \rho^{M_o+1})/(1-\rho) - 1. \quad (6.23)$$

We get

$$\mathcal{A}_{R\text{-vert}} = \sum_{m=1}^{M_o} e^{2\pi i m\Delta} + \sum_{m=1}^{M_o} e^{-2\pi i m\Delta} + 1, \qquad \Delta \equiv \Delta\ell\Delta\nu_z \quad (6.24a)$$

$$= 2\,\mathrm{Re}\left(\frac{1 - e^{2\pi i(M_o+1)\Delta}}{1 - e^{2\pi i\Delta}}\right) - 1$$

$$\therefore \boxed{\mathcal{A}_{R\text{-vert}} = \cos 2\pi M_o\Delta + \frac{\sin 2\pi M_o\Delta \sin 2\pi\Delta}{1 - \cos 2\pi\Delta}}\ , \quad (6.24b)$$

which is real. Now we note that if $\Delta = k = 0, \pm 1, \ldots,$

$$\Delta\nu_z = k/\Delta\ell, \qquad \text{or} \qquad \sin\theta_{oR} = \sin\theta_o - k/\Delta\ell \quad (6.25)$$

then

$$\therefore \mathcal{A}_{R\text{-vert}} = 1 + 2M_o = M\ , \quad (6.26)$$

which is the maximum "gain" of the beam. Not surprisingly, this gain is just equal to the total number of elements (M). This is achieved for the main beam, $\Delta = k = 0$, or when

$$\theta_{oR} = \theta_o \ ,$$

i.e., when the beam is directed (i.e., "steered" in elevation) at the source, as it appears ($\hat{\underset{\sim}{i}}_o$) in the vicinity of the array, cf. Figs. 6.1, 6.2.

II. Linear Horizontal Array

The element configuration here is shown in Fig. 6.2. In this situation we have

$$\underset{\sim}{r}_m = \hat{\underset{\sim}{i}}_x m\Delta\ell \ , \tag{6.27}$$

so that

$$(\underset{\sim}{\nu}_o - \underset{\sim}{\nu}_{oR}) \cdot \underset{\sim}{r}_m = m\Delta\ell\Delta\nu_x = m\Delta\ell(f_o/c_o)\ (\cos\phi_o \cos\theta_o - \cos\phi_{oR} \cos\theta_{oR}) \tag{6.28}$$

from (6.8), $\theta_o \to \theta_{oR}$, etc. With uniform weighting once more ($A_m = A$) we have (6.24b) for the (real) beam pattern, where now instead of $\Delta\nu_z$ we have

$$\Delta\nu_x = k/\Delta\ell, \quad \text{or } [\phi_o = \phi_{oR};\ \theta_o = \theta_{oR};\ k = 0] \ , \tag{6.29}$$

yielding again the maximum gain $Q_{R\text{-}horiz|max} = M$, cf. (6.26), in the direction of the source.

6.3 Various Signal Models, $S^{(m)}(t;\underset{\sim}{\theta})$

In our present applications we are concerned primarily with signals which are sinusoidal, or are combinations of sinusoids. Moreover, as we have seen above in Sec. 6.1, for beam forming we require the signal structure at the individual elements of the array, cf. (6.12). Thus, for the signals received at the $m^{\underline{th}}$ array element, including the path delay $\hat{\tau}_m$ for steering, cf. (6.13) in (6.12), we have for the $S^{(m)}(t;\underset{\sim}{\theta})$ in (6.14):

I. Single Component at $m^{\underline{th}}$ Element

$$\boxed{S^{(m)}(t;\underset{\sim}{\theta}) = \frac{a^{(m)}(t-\Delta\tau_m)G_o^{(m)}}{\lambda^{\gamma}}\sqrt{2}\cos\left[\mu\omega_o(t-\epsilon)-\omega_o T_o+\omega_o\Delta\tau_m+\phi_a^{(m)}(t-\Delta\tau_m)-\phi_T-\phi_R^{(m)}\right]}$$

since $\hat{S}_o = e^{i\omega_o\Delta\tau_m}$ here, with (6.30)

$$\left.\begin{aligned}\Delta\tau_m &= (\hat{\underset{\sim}{i}}_o - \hat{\underset{\sim}{i}}_{oR})\cdot\underset{\sim}{r}_m/c_o = (\underset{\sim}{\nu}_o - \underset{\sim}{\nu}_{oR})\cdot\underset{\sim}{r}_m/f_o \quad , \quad (6.13)\\ G_o^{(m)} &= AS_{OT}|\mathcal{Q}_R^{(m)}|/\sqrt{2};\ \mu = 1 + f_d/f_o = 1 + \hat{\underset{\sim}{i}}\cdot\underset{\sim}{\nu}_s/c_o\end{aligned}\right\} \quad (6.30a)$$

Somewhat more compactly, (6.30) can be rewritten

$$\boxed{S^{(m)}(t;\underset{\sim}{\theta}) = A_o^{(m)}(t)\sqrt{2}\cos\left[\omega_o\mu t+\Phi^{(m)}(t)\right]} \quad , \quad (6.31)$$

which defines $A_o^{(m)}(t)$, $\Phi^{(m)}(t)$ here on comparison with (6.30), viz.:

$$A_o^{(m)}(t) \equiv \frac{a^{(m)}(t-\Delta\tau_m)G_o^{(m)}}{\lambda^{\gamma}}\ ;\quad \Phi^{(m)}(t) \equiv \omega_o\Delta\tau_m + \phi_a^{(m)}(t-\Delta\tau_m) - \phi_T - \phi_R^{(m)};$$

$$\hat{t} = t-\epsilon-T_o/\mu\,. \quad (6.31a)$$

II. Multipath at $m^{\underline{th}}$ Element

$$S^{(m)}(t;\underset{\sim}{\theta}) = \frac{G_o^{(m)}\sqrt{2}}{\lambda^{\gamma}}\{a_1^{(m)}\cos(\omega_o\mu_1\hat{t}_1+\phi_1^{(m)}) + a_2^{(m)}\cos(\omega_o\mu_2\hat{t}_2+\phi_2^{(m)}) + \ldots + a_k^{(m)}\cos(\omega_o\mu_k\hat{t}_k+\phi_k^{(m)})\} \quad (6.32)$$

where

$$\mu_k = 1 + f_{dk}/f_o;\quad \hat{t}_k = t-\epsilon-T_{ok}/\mu_k;\quad \phi_k^{(m)} = \omega_o\Delta\tau_{m,k} + \phi_a^{(m)}(t-\Delta\tau_{m,k}) - \phi_T - \phi_R^{(m)} \quad (6.32a)$$

$k = 1, \ldots, K$ and K = no. of (resolvable) multipath components, in which now

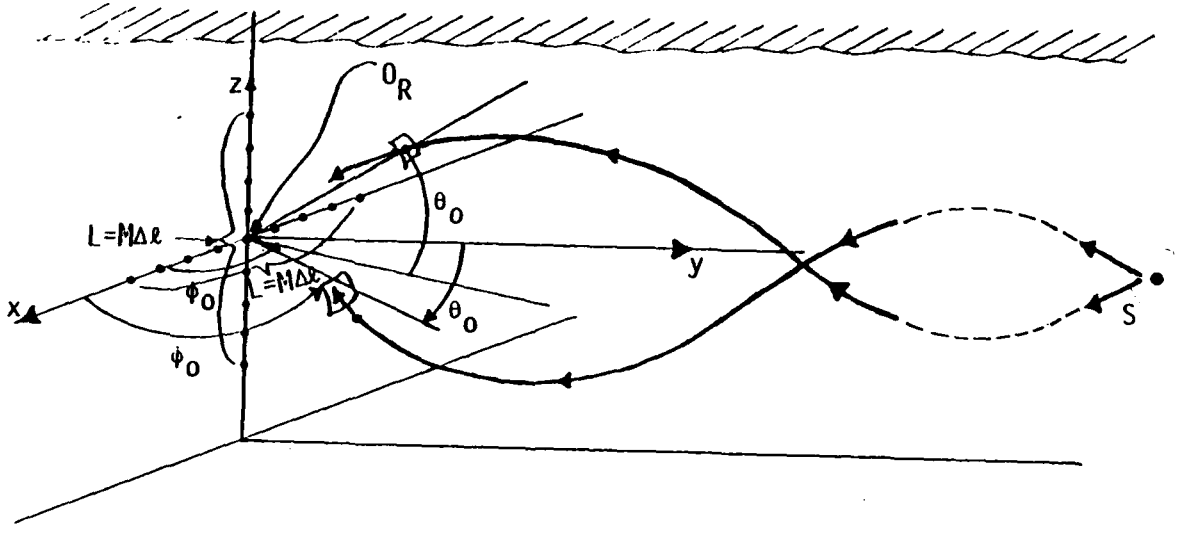

Figure 6.2. Vertical and horizontal arrays, with several multipaths from the source, impinging on the arrays.

$$\Delta\tau_{m,k} = (\hat{\underset{\sim}{i}}_{ok} - \hat{\underset{\sim}{i}}_{oR}) \cdot \underset{\sim}{r}_m / c_o, \qquad \text{cf. (6.30a)}, \tag{6.32b}$$

and where f_{dk} is the (source) doppler on the $k^{\underline{th}}$ path. It is assumed in this model that the spreading loss ($\sim\lambda^{-\gamma}$) is essentially the same for each resolvaable path. [If this is not the case, one simply replaces $\lambda^{-\gamma}$ by $\lambda_k^{-\gamma}$ in each component.] Moreover, it is required here that

$$\sum_k \overline{a_k^{(m)2}} = \overline{a^{(m)2}}, \tag{6.33}$$

namely, that all the multipath components yield the same total signal level as would occur if there were only a single component (Case I above). In practice, K = 2 or 3 is often sufficient to describe this type of signal. A particularly important point here is that $\hat{\underset{\sim}{i}}_o = \hat{\underset{\sim}{i}}_{ok}$: each component wavefront impinges on the $m^{\underline{th}}$ array element from generally different directions, i.e., $\hat{\underset{\sim}{i}}_{ok} \neq \hat{\underset{\sim}{i}}_{ok'}$, $k \neq k'$, as sketched in Fig. 6.2. Still more elaborate signal models can be constructed along these lines.

III. Broad-Band Signals (at $m^{\underline{th}}$ Element)

The broad-band signals encountered here usually consist of a sinusoid [cf. (6.31)] and several of its harmonics. Since the aperture (or array) elements are frequency sensitive, we may combine several terms like (6.31), suitably adjusted to take this frequency dependence into account. We have (under the usual assumptions that the medium is linear and negligibly dispersive)

$$s^{(m)}(t;\underset{\sim}{\theta}) = \sum_{\ell=1}^{L} A_o^{(m)}(t)_\ell \sqrt{2} \cos\left[\ell\omega_o \mu t + \phi^{(m)}(t)_\ell\right] \tag{6.34}$$

where now

$$A_o^{(m)}(t)_\ell = a^{(m)}(t-\Delta\tau_m)_\ell G_{o\ell}^{(m)}/\lambda^\gamma; \quad \phi^{(m)}(t)_\ell = \ell\omega_o \Delta\tau_m + \phi_a^{(m)}(t-\Delta\tau_m) - \phi_{T\ell} - \phi_{R\ell}^{(m)}. \tag{6.34a}$$

The fading may be frequency sensitive, and the beam patterns certainly are,

viz., $G_{o\ell}^{(m)} = AS_{OT}^{(\ell)}|Q_R^{(m)}(\ell f_o)|/\sqrt{2}$, cf. (6.30a), and $\hat{S}_{OR} = e^{i\ell\omega\Delta\tau_m}$ here, with $\phi_{T\ell} = \phi_T(\ell f_o)$, etc., with $S_{OT}^{(\ell)}$ representing the level of the $\ell^{\underline{th}}$ harmonic, cf. (6.3a).

This model is readily extended to include different angles of arrival of the various harmonic wavefronts: $\hat{\underline{i}}_o \to \hat{\underline{i}}_{o\ell}$ in (6.30a), so that $\Delta\tau_m \to \Delta\tau_m^{(\ell)} = (\hat{\underline{i}}_o - \hat{\underline{i}}_{oR})\cdot\underline{r}_m/c_o$, where beam steering is done for the fundamental $\ell=1$, i.e., for f_o. Steering for other harmonics is accomplished by setting $\hat{\underline{i}}_{oR} \to \hat{\underline{i}}_{oR}^{(\ell)}$, $\ell\geq 2$ in $\Delta\tau_m^{(\ell)}$. The further conplexity of multipath may be incorporated by using (6.32) for each component of (6.34). We leave the details to a later study.

6.4 Second-Order Space-Time Moments of the Signal Field: Examples

In order to take advantage of array gain we must strive to obtain as uniform (or correlated) a signal wave field over the array as possible. This is necessary but not sufficient: the accompanying noise or interference field must also be taken into account at the same time. Ideally, we would like to place the array elements to achieve maximum signal *coherence* <u>*and*</u> *minimum* noise coherence over the aperture. As we shall see in Sec. 7 ff, however, this is not usually possible. In any case, we aim for signal coherence and the capability of beam forming and steering, even though the associated noise field may be similarly correlated across the array.

Accordingly, to derive a useful measure of the spatial coherence of the incoming signal field over the array, let us consider the second-order, second-moment function of the acoustic signal field in the vicinity P(R) of our aperture, cf. Fig. 6.1. Here (and henceforth in this first study) we shall confine our attention to single-component signals [I, Sec. 6.3] for the purpose of quantitative illustration. Thus, the signal field at $P(\underline{R})$ is given by

$$p_s(\underline{R},t) = \frac{Ba(\underline{R},t)}{R_o^{\gamma}}\ \mathrm{Re}\left\{ e^{i\omega_o\mu[t-\epsilon-\hat{\underline{i}}_o\ (\underline{R}_o-\underline{R})/\mu c_o] - i\phi_a(\underline{R},t) - i\phi_T} \right\}, \quad (6.35)$$

where the array (and $P(\underline{R})$) are in the far-field of the signal source. On the reasonable assumption of stationarity and local homogeneity, we find that the desired field statistic here is

$$M_{2S}(R_1,t_1;R_2,t_2) \equiv \langle p_s(\underset{\sim}{R}_1,t_1)p_s(\underset{\sim}{R}_2,t_2)^*\rangle_{\varepsilon,\mu,a,\phi_a,\hat{\underset{\sim}{i}}_o}$$

$$= \frac{1}{2} B^2 \left\langle \frac{1}{R_o^{2\gamma}} \right\rangle \mathrm{Re}\left\{ M_a(\rho,\tau) \langle e^{i\omega_o \mu\tau} \rangle_\mu \langle e^{\omega_o \hat{\underset{\sim}{i}}_o \cdot \underset{\sim}{\rho}/c_o} \rangle_{\hat{\underset{\sim}{i}}_o} \right\}, \tag{6.36}$$

$$\underset{\sim}{\rho} = \Delta\underset{\sim}{R} = \underset{\sim}{R}_2 - \underset{\sim}{R}_1; \quad \tau = t_2 - t_1,$$

with B an appropriate amplitude. [Here (*) denotes the complex conjugate: in this instance p_s is real, $p_s^* = p_s$, but see (7,6)ff.] Specifically, we have

$$\left.\begin{aligned} M_a(\rho,\tau) &\equiv \langle a(\underset{\sim}{R}_1,t_1)a(\underset{\sim}{R}_2,t_2)e^{i\phi_a(\underset{\sim}{R}_2,t_2)-i\phi_a(\underset{\sim}{R}_1,t_1)}\rangle \\ &= A(\underset{\sim}{\rho},\tau)e^{-i\phi_a(\underset{\sim}{\rho},\tau)}; \end{aligned}\right\} \tag{6.37a}$$

$$D_1(\omega_o\tau) \equiv \langle e^{i\omega_o\mu\tau}\rangle_\mu = e^{i\omega_o\tau}\langle e^{i\omega_d\tau}\rangle_{\omega_d} = e^{i\omega_o\tau}F_i(i\tau)_{\omega_d}; \tag{6.37b}$$

$$E_1(k_o\Delta R) \equiv \langle e^{i\omega_o \hat{\underset{\sim}{i}}_o\cdot\rho/c_o}\rangle_{\hat{\underset{\sim}{i}}_o} = \langle e^{ik_o\rho g(\theta_o,\phi_o)}\rangle_{\theta_o,\phi_o}; \tag{6.37c}$$

$$k_o = \omega_o/c_o = 2\pi/\lambda_o; \qquad \rho = |\underset{\sim}{\rho}| = |\underset{\sim}{R}_2 - \underset{\sim}{R}_1|,$$

where $A(\underset{\sim}{\rho},\tau)$, $\Phi_a(\underset{\sim}{\rho},\tau)$ are real; $F_1(i\tau)_{\omega_d}$ is the characteristic function of the random (angular) doppler frequency (ω_d); and $g(\theta_o,\phi_o)$ is the appropriate function of the angles between $\hat{\underset{\sim}{i}}_o$, cf. (6.8), and $\Delta\underset{\sim}{R} \equiv \underset{\sim}{\rho} = \underset{\sim}{R}_2 - \underset{\sim}{R}_1$. Note that $D_1(0)$, $E_1(0)$ are unity. Stationarity and homogeneity of the signal and/or noise field, of course, do <u>not</u> insure uniformity of the field here, in the vicinity of the array, cf. (6.30), (6.37).

To see how the signal field is structured in space (~ρ) let us next determine (6.37c) for the vertical and horizontal arrays. From (6.8) we have (cf. Fig. 6.2)

(i) Vertical array: $\underset{\sim}{\rho} = \underset{\sim}{\Delta R} = \hat{\underset{\sim}{i}}_z \Delta R$; $\therefore \hat{\underset{\sim}{i}}_o \cdot \underset{\sim}{\rho} = \Delta R \sin \theta_o$; (6.38a)

(ii) Horizontal array: $\underset{\sim}{\rho} = \underset{\sim}{\Delta R} = \hat{\underset{\sim}{i}}_x \Delta R$; $\therefore \hat{\underset{\sim}{i}}_o \cdot \underset{\sim}{\rho} = \Delta R \cos \phi_o \cos \theta_o$. (6.38b)

The value of (6.37c) depends on the state of knowledge regarding (θ_o, ϕ_o) at the array (i.e., receiver). We distinguish a variety of cases:

I. Distant Source; Known Angles of Wavefront Arrival $(\theta_o = \hat{\theta}_o;\ \phi_o = \hat{\phi}_o)$

Here we know (θ_o, ϕ_o) at the array, e.g., $\theta_o = \hat{\theta}_o$, $\phi_o = \hat{\phi}_o$, so that on setting $\tau = 0$ in (6.36) we have from (6.38a) for the correlation structure of the signal field

(i) Vertical array: $$M_{2s}(\underset{\sim}{\rho}, 0) = \frac{B^2}{2} \left\langle \frac{1}{R_o^{2\gamma}} \right\rangle A(\underset{\sim}{\rho}, 0) \cos [k_o \Delta R \sin \hat{\theta}_o - \Phi_a(\underset{\sim}{\rho}, 0)] \tag{6.39}$$

which shows the effects of fading across the array. Thus, to maximize M_{2s} by suitable spacing of the array elements, i.e., choice of $\Delta R(\neq 0)$, we must know A and Φ_a over the array. However, in many situations of interest the fading may be treated as uniform across the array elements, so that A, Φ_a are constants. Then (6.39) is maximized by setting

$$\Delta R = (2\pi m + \Phi_a)/k_o \sin \hat{\theta}_o ; \qquad (\hat{\theta}_o \neq 0) : \tag{6.40}$$

the elements (along $\hat{\underset{\sim}{i}}_z$) should be spaced according to (6.40), where $m \geq 2$ for multiple unit spacings. If $\theta_o = 0$, i.e., the array is parallel to the signal wavefront, the magnitude of M_{2s} is independent of ΔR and any element spacing is permitted. Note that beam steering ($\sim \hat{\underset{\sim}{i}}_{oR}$) plays no rôle here: it is the actual physical location of the elements in the signal field which is significant in the choice of element spacing.

Similarly, we have using (6.38b) in (6.36)

(ii) Horizontal array: $$M_{2s}(\underset{\sim}{\rho}, 0) = \frac{B^2}{2} \left\langle \frac{1}{R_o^{2\gamma}} \right\rangle A(\underset{\sim}{\rho}, 0) \cos [k_o \Delta R \cos \hat{\phi}_o \cos \hat{\theta}_o - \hat{\Phi}_a(\rho, 0)], \tag{6.41}$$

and again, for uniform fading we see that the element spacing is now determined by

$$\boxed{\Delta R = (2\pi m+\phi_a)/k_o \cos\hat{\phi}_o \cos\hat{\theta}_o}\ , \qquad (\hat{\theta}_o,\hat{\phi}_o\neq\pi/2). \tag{6.42}$$

When $\hat{\phi}_o=\pi/2$, i.e., the array is broadside to the signal wavefront, M_{2s} is independent of element spacing.

Finally, for uniform fading ϕ_a may be set equal to zero, so that M_{2s} is again maximized, independent of ΔR, whenever $\hat{\theta}_o=0$ and $\hat{\phi}_o=\pi/2$, i.e., the signal wavefront is parallel to the array in question.

II. Distant Source; Unknown Angles of Wavefront Arrival

Here we have again the situation sketched in Fig. 6.2, where now the angles of signal wavefront arrival are subject to some probability distribution density, $w_1(\theta_o,\phi_o)$, so that

$$E_1(k_o\Delta R) = \int_0^{\pi} d\phi_o \int_{-\pi/2}^{\pi/2} d\theta_o\, e^{ik_o\underline{i}_o\cdot\underline{\rho}} w_1(\theta_o,\phi_o)\,. \tag{6.43}$$

Many possibilities, of course, are available. To make a selection of pdf(w_1) that is appropriate, we must invoke experiment, but the following densities appear reasonable and typical:

$$[-\pi/2\leq\theta_o\leq\pi/2;\quad 0\leq\phi_o\leq\pi]$$

$$\left.\begin{aligned} w_1(\theta_o,\phi_o)_I &= \frac{1}{\pi}\cdot\frac{1}{\pi} && :(\text{uniform})\\ w_1(\theta_o,\phi_o)_{II} &= \left\{\frac{\cos\theta_o}{2}\cdot\frac{\sin\phi_o}{2}\right\} \\ w_1(\theta_o,\phi_o)_{III} &= \frac{2}{\pi}\cos^2\theta_o\cdot\frac{\sin\phi_o}{2} \end{aligned}\right\}. \tag{6.44}$$

Accordingly, we obtain for the vertical and horizontal arrays above, from (6.44) in (6.43):

$$E_1(k_o\Delta R)_I \;|_{vert} = \frac{1}{\pi}\int_{-\pi/2}^{\pi/2} e^{ik_o\Delta R \sin\theta_o} d\theta_o = \frac{a}{\pi}\int_0^{\pi/2} \cos(k_o\Delta R \sin\theta)d\theta$$

$$= J_o(k_o\Delta R)\,; \qquad (6.45a)$$

$$E_1(k_o\Delta R)_{II}\,|_{vert} = \frac{1}{2}\int_{-\pi/2}^{\pi/2} \cos\theta_o\, e^{ik_o\Delta R \sin\theta_o} d\theta_o = \frac{1}{2}\int_{-1}^{1} e^{ik_o\Delta Rz} dz$$

$$= \frac{\sin k_o\Delta R}{k_o\Delta R}\,; \qquad (6.45b)$$

$$E_1(k_o\Delta R)_{III}|_{vert} = \frac{2}{\pi}\int_{-\pi/2}^{\pi/2} \cos^2\theta_o\, e^{ik_o\Delta R \sin\theta_o} d\theta_o$$

$$= \frac{2}{\pi}\left(\int_0^{\pi/2} e^{ik_o\Delta R \sin\theta}\cos^2\theta_o d\theta_o + \int_0^{\pi/2} e^{-ik_o\Delta R \sin\theta_o}\cos^2\theta_o d\theta_o\right)$$

$$= \frac{J_1(k_o\Delta R) + iH_1(k_o\Delta R)}{k_o\Delta R} + \frac{J_1(-k_o\Delta R) + iH_1(-k_o\Delta R)}{-k_o\Delta R}$$

$$= J_1(k_o\Delta R)/(k_o\Delta R/2)\,, \qquad (6.45c)$$

where H_1 is a Struve function [cf. [24], Sec. 8] (which is an even function of its argument).

We have also

$$E_i(h_o\Delta R)_I \;|_{horiz} = \frac{1}{\pi^2}\int_{-\pi/2}^{\pi/2} d\theta_o \int_0^{\pi} e^{ik_o\Delta R \cos\theta_o \cos\phi_o} d\phi_o$$

$$= \frac{2}{\pi}\int_0^{\pi/2} J_o(k_o\Delta R \cos\theta_o)d\theta_o = J_o^2(k_o\Delta R/2) \qquad (6.46a)$$

cf. [30], p. 681, No. 4. Similarly, we get

$$E_1(k_o R)_{II\,|\,horiz} = \frac{1}{4}\int_{-\pi/2}^{\pi/2} \cos\theta_o d\theta_o \int_0^{\pi} \sin\phi_o\, e^{ik_o\Delta R \cos\theta_o \cos\phi_o} d\phi_o$$

$$= \frac{1}{2}\int_{-\pi/2}^{\pi/2} \frac{\sin(k_o\Delta R \cos\theta_o)}{k_o\Delta R} d\theta_o = \int_0^{\pi/2} \frac{\sin(k_o\Delta R \cos\theta_o)}{k_o\Delta R} d\theta_o$$

$$= \frac{\pi}{2} H_0(k_o\Delta R)/k_o\Delta R\,, \qquad (6.46b)$$

where the Strüve function, $H_0(k_o\Delta R)$, is given by

$$H_0(k_o\Delta R) = \sum_{n=0}^{\infty} \frac{(-1)^n \left(\frac{k_o\Delta R}{2}\right)^{2n+1}}{\Gamma(n+3/2)\Gamma(n+3/2)}, \qquad (6.46c)$$

cf. [24], Eq. (35), and is shown in Fig. 13 of [24]; (as required, when $\Delta R=0$, $E_1(0)=1$). Finally, for Case III we obtain

$$E_1(k_o R)_{III|\,horiz} = \frac{1}{\pi}\int_{-\pi/2}^{\pi/2} \cos^2\theta_o d\theta_o \int_0^{\pi} \sin\phi_o\, e^{ik_o\Delta R \cos\phi_o \cos\theta_o} d\phi_o$$

$$= \frac{4}{\pi}\int_0^{\pi/2} \cos\theta_o \frac{\sin[k_o\Delta R \cos\theta_o]}{k_o\Delta R} d\theta_o$$

$$= 2J_1(k_o\Delta R)/k_o\Delta R\,, \qquad (6.46d)$$

which is the same as $E_1(k_o\Delta R)_{III|vert}$, cf. (6.45c). Note, however, that E_1 differs generally in the horizontal and vertical cases, cf. (6.45a,b) vs. (6.46a,b).

6.5 Degraded Beam Formation

From the above we see at once that the random angles of arrival of the signal wavefront heavily degrade the beam gain [(6.26) etc.]. This is because the signal field is noticeably nonuniform along the array in

these cases, as can be seen from (6.45), (6.46): it is not possible to find element spacings such that all elements remain strongly correlated. On the other hand, when the desired signal wavefront comes in at nearly fixed angles (Case I above, cf. (6.40), (6.42)), the desired wavefront coherence can be almost fully obtained with the appropriate element spacing.

This degrading of the beam processing because of the non-uniformity of the signal field at the array can be demonstrated rather easily by computing the corresponding second-order second-moment function of the beam output--i.e., the array-processed received signal S_R. We consider the somewhat simpler situation of uniform fading across the array and use (6.16), (6.19) in

$$M_{S_R}(\tau) = \frac{1}{2}\left\langle \frac{1}{\lambda^{2\gamma}} \right\rangle \hat{G}_o^2 \quad \mathrm{Re}\left\{ M_a(\tau) \quad D_1(\omega_o\tau) < |Q_R(\underset{\sim}{\nu}_o - \underset{\sim}{\nu}_{oR}, f_o)|^2 > \underset{\sim}{\hat{i}}_o \right\} \qquad (6.47)$$

cf. (6.36), (6.37). The average over the beam pattern becomes for Case I above just $|Q_R|^2$, as before, and maximum beam gain is achieved if $A_m = A$, cf. Sec. 6.2, (6.23) et. seq.: the beam is pointed in the direction of the arriving (nonrandom) signal wavefront.

However, in the random cases we obtain

$$< |Q_R|^2 >_{\underset{\sim}{\hat{i}}_o = \theta_o, \phi_o} = \sum_{mm'} \frac{A_m A_{m'}^*}{A^2} < e^{(2\pi i/\lambda_o)(\underset{\sim}{\hat{i}}_o - \underset{\sim}{\hat{i}}_{oR}) \cdot (\underset{\sim}{r}_m - \underset{\sim}{r}_{m'})} >_{\theta_o, \phi_o} . \qquad (6.48)$$

As an example, let us postulate the vertical array (6.20), so that the average in (6.48) becomes explicitly

$$\left\langle Q_R^{(m)} Q_R^{(m')*} \right\rangle_{vert} \equiv < e^{2\pi i \Delta_{mm'}(\sin\theta_o - \sin\theta_{oR})} >_{\theta_o}$$

$$= e^{-2\pi i \Delta_{mm'} \sin\theta_{oR}} < e^{2\pi i \Delta_{mm'} \sin\theta_o} >_{\theta_o} ; \qquad (6.49a)$$

$$\Delta_{mm'} = \frac{(m-m')\Delta\ell}{\lambda_o} ,$$

which, if we use, say, Case I (6.45a), reduces to

$$\langle a_R^{(m)} a_R^{(m')*} \rangle_{vert} = e^{-2\pi i \Delta_{mm'} \sin\theta_{oR}} J_o(2\pi\Delta_{mm'}) . \qquad (6.49b)$$

We see at once that the presence of the J_o factor prevents our obtaining the desired maximum gain of the steered beam (where the exponent remains $2\pi i\Delta_{mm'}(\sin\theta_o - \sin\theta_{oR})$. Instead, there is an interelement "shading," as represented by $J_o(2\pi\Delta_{mm'})$, which reduces the coherent element gain significantly and consequently seriously distorts the resulting beam and our ability to achieve effective steering. In fact, this beam-"smearing" effectively destroys the beam.

Fortunately, however, the desired signal wavefront normally has some specified direction, i.e., is non-random in direction, so that there is negligible beam degradation (other than possible fading over the array), and we can obtain, for the signal, wavefront coherence along our array by suitable element spacings, as noted above for Case I, cf. (6.40), (6.42). As we shall see in Section 7.2, it is the random angular arrival of the various individual signals comprising the interference which can produce highly non-uniform fields over our array. This, in turn, offers the possibility of spatial noise incoherence, permitting the desired independent sampling in space of the noise field, cf. Sec. 5.4.

Section 7. Some Statistical-Physical Models of Underwater (Ocean) Acoustic Interference (ACI) Environments

Here we develop: (1), the first-order probability density of the acoustic interference (ACI) which accompanies our desired signal; and (2), various expressions for this noise field, including the second-order second-moment function of the field, as well, cf. (6.36). The ACI environment also includes a gaussian component, in addition to the usually significant nongaussian term. The former arises from the presence of a large number of more or less comparable, independent sources, whose composite effect is statistically normal by virtue of the Central Limit Theorem (CLT). The latter is distinguished on the average by a few, strong structured sources (in time), active at any given moment. [See [4]-[6] for the details of noise model-building here.] Figure 7.1 shows an ACI environment, as "seen" by a receiving beam.

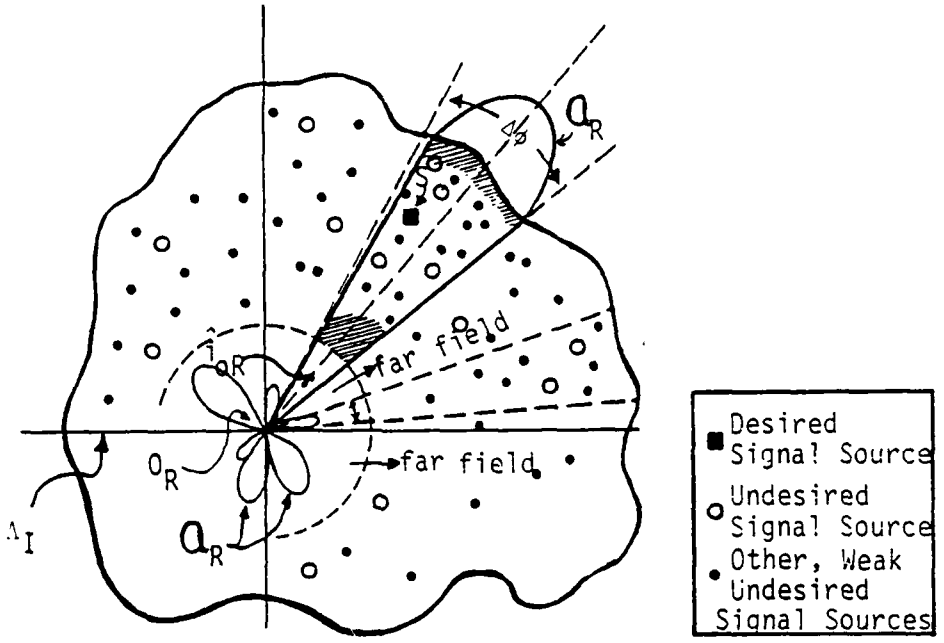

Fig. 7.1. Schema (in 2-dimensions) of an ACI environment, showing a desired signal, several strong "structured" undesired signal sources, and a comparatively large number of "weak" sources (in the main beam).

7.1 Acoustic Interference (ACI) Scenarios and Class A and B Noise

The acoustic interference (ACI) scenario consists of the following principal elements:

(i). the propagation law [$\lambda^{-\gamma}$, cf. (6.1)-(6.3)];

(ii). the density of potentially emitting sources. $\sigma_s(\lambda) \sim \lambda^{-u} w_1(\phi)$, or $\lambda^{-u} w_1(\theta,\phi)$, in Λ_I, cf. Fig. 7.1;

(iii). the (first-order) statistics of the fading parameters (a, ϕ_a), cf. (6.1);

(iv). the average emission characteristics of the sources, as embodied in the "overlap index" A_A, or A_B, which measure the

average "on-time" of a typical emission; (see [4]-[6] for details. Thus, the overlap-index is defined as the average number of emission "events" (e.g., interfering signals) impinging on the receiving element in question, times the mean duration of a typical source emission [cf. Sec. 2.2, [4]].

(v). the structure of the typical interfering signal amplitude, $A_o^{(m)}(t)$, and waveform $s^{(m)}(t)$, (6.2), which includes beam patterns and fading effects.

(vi). the statistics of any other pertinent parameters in the typical source model.

As we shall see in Sec. 7.3 below, these scenario elements enable us to calculate a priori the various "macro"-parameters of the required (first-order) pdf of the received interference.

Finally, we note that there are two principal types of nongaussian interference: (I), Class A noise, which is coherent in the receiver (here the array elements) in that this noise produces negligible transients therein; (II), and Class B noise, which is alternatively "incoherent," producing essentially only transient responses. The former is non-impulsive, obeying the relation $\overline{T}_I \Delta f_{ARI} >> 1$, where Δf_{ARI} is the effective bandwidth of the combined array element + linear front-end stages of the receiver (detector) and $\overline{T}_I$ is the mean duration of a typical (coherent) emission of the interfering source. [In narrow-band communication and sonar (radar) receivers ARI denotes the aperture ⊗RF⊗IF stages, as successive linear components.] Class B noise, on the other hand, is usually highly impulsive, where $\overline{T}_I \Delta f_{ARI} \tilde{<} 1$: the linear front-end stages of the receiver are shock-excited by the independent succession of input impulses or short emissions. Examples of Class A interference here are sustained surface ship noises like propellor and other nearly periodic emissions or biological sources, such as whales and other marine mammals, while Class B interference may arise from ship transients, "snapping" shrimp, and other marine sources of short acoustic emissions. Marine oil-exploration systems and the like are also a common source of both Class A and B interference, depending on the devices employed.

In addition to the above classes of often highly nongaussian noise, there is always a gaussian component, consisting of external noise which

has no obvious structure, generated by the superposition of large numbers of essentially comparable sources, and (thermal) noise generated in the receiving elements. In most practical applications this latter component is quite small compared to the externally generated, nongaussian sources, where the latter occur. [See Sec. 7.3ff. for details; also [4], [6], [7].] The present study will consider principally narrow-band Class A noise, specifically so in the numerical examples, cf. Sec. 11ff, but the methods and analytic results are canonical with respect to the particular noise and signals involved, as we have noted above.

7.2 Noise Field Statistics

The basic statistical model is poissonian: it is reasonably postulated that each interfering source emits independently of the others, and that while the probability of more than one emission at any given instant is small, there are a large number of potential emitters available. [See Section 2 of [6] for a full development of Class A models in the narrow-band cases.]

Accordingly, we can write for the interference pressure field,

$$p_{N_o}(\underline{R},t) = \int_{\underline{Z}=\underline{\Lambda}\times\underline{\theta}} \mathcal{L}(R,t|\underline{\lambda},t'|\underline{\theta})dN(\underline{Z}) \tag{7.1}$$

where $\mathcal{L}$ is a typical field solution for a single source (in Λ_I); $\underline{\theta}$ denotes all (random) parameters associated with this typically emitted field component. Here Λ denotes the spatial-temporal radiation emissions domain of "radiation events," and $dN(\underline{Z})$ is a counting functional, e.g.,

$$dN(\underline{Z}) = \sum_{k}^{K} \delta(\underline{\lambda}-\underline{\lambda}_k)\delta(\underline{\theta}-\underline{\theta}_k)\delta(t-t_k)$$

for K discrete sources potentially emitting at time t_k in Λ_I. Here $dN(\underline{Z})$ is poissonian, e.g.,

$$dN(\underline{Z}) = dN(\Lambda=1;t_k,\underline{\theta}) = \sigma_s(\underline{\lambda})d\Lambda_I w_1(\underline{\theta})w_1(t')\delta(t'-t_k)dt'd\underline{\theta}$$

for one-emission (at $t'=t_k$) in the small spatio-temporal interval $d\Lambda_I dt'$, with $dN(\Lambda\geq 2; t_k; \underline{\theta}) \to 0$ as $d\Lambda_I \to 0$, etc., [1]. Thus, for k simultaneous radiation events in $d\Lambda_I dt'$ we have

$$dN(\underline{Z}:\Lambda=k; t_k, \underline{\theta}) = \frac{(d\underline{Z})^k e^{-d\underline{Z}}}{k!}, \qquad k\geq 0, \tag{7.2}$$

where $d\underline{Z} = \sigma_s d\Lambda_I d\underline{\theta} dt' w_1(\underline{\theta}) w_1(t')$, etc., and t' is accordingly a random emission time or epoch.

Since the interference consists of the superposition of individual pressure fields generated by signal sources like that of the desired signal, we may use (6.35) for $\mathcal{L}$ in (7.1) above, viz.,

$$\mathcal{L}(R,t|\underline{\lambda},t'|\underline{\theta}) = \frac{B_a(\underline{R},t-t')}{R_o^\gamma} \; \mathrm{Re}\left\{ e^{i\omega_o \mu[t-t'-\hat{\underline{i}}_o\cdot(\underline{R}_o-\underline{R})/\mu c_o]} \right.$$
$$\left. -i\hat{\phi}_a(\underline{R},t-t')-i\phi_T \right\}. \tag{7.3}$$

Now $\hat{\underline{i}}_o (=\hat{\underline{i}}_o(\theta_o,\phi_o)$ and R_o are random variables over the source space Λ_I, while $(t',\underline{\theta})$ are random over time, with a, μ, ϕ_a likewise space-time stochastic. We assume here that far-field conditions prevail: all the interfering sources lie effectively in the far-field (or Fraunhofer) region vis-à-vis the receiving array (in the vicinity of $P(\underline{R})$, cf. Figs. 7.1 and 6.1). Moreover, $\mathcal{L}$ consists of two components:

$$\mathcal{L} = \mathcal{L}_I + \mathcal{L}_G, \tag{7.4}$$

a nongaussian part, $\mathcal{L}_I$, obeying poisonnian statistics with a small overlap index $A_{(A\text{ or }B)}$, $<<O(10)$, and a gaussian component, $\mathcal{L}_G$, structurally similar to (7.3) [if the source mechanism is the same], but with $A_{(A\text{ or }B)}$ large, $O(\geq 10)$.

It can be shown [1] that the $J^{\underline{th}}$-order characteristic function of $P_{N_o}(\underline{R},t)$, (7.1), can be formally written*

---

* This formulation assumes independently emitting sources in time, at least. The spatial locations need not be independent, but usually are physically. In scattering models, as distinct from these ambient emission cases here, the result (7.5) applies only to (k=1)-order of interactions, i.e., independent radiation "events," as distinct from multiple scattering ($k\geq 2$); see [31].

$$F_J(i\xi_1, \ldots, i\xi_J; t_1, \ldots, t_J|\underline{Z}) = \exp\left[\int_{\underline{Z}} <\hat{\varphi}(\underline{\lambda};\underline{\theta})(e^{\sum_j^J i\xi_j \hat{\mathcal{L}}(t_j;\underline{\lambda},\underline{\theta})} - 1)>_{\underline{\theta}} d\underline{\lambda} \right] \quad (7.5)$$

$$J \geq 1,$$

in which the process density $\hat{\rho}$ is specified from the ACI scenario; and from which we can readily obtain the various lower-order moments (cf. Sec. 7.2ff.). To obtain the various $J^{\underline{th}}$-order pdf's, w_J, the central technical problem here lies in the evaluation (and approximation) of the exponent of (7.5), cf. [4], and particularly Sections 3-6 of [6]. We shall give only final results here, cf. Sec. 7.3ff., in the critically important case of J=1, i.e., independent space-time sampling, as explained in II, Sec. 2.2, and Sec. 5.4.

7.3 Second-Order Space-Time Moments of the Interference Field

These moments follow directly from (7.5) on differentiation and noting that the process density $\rho(\underline{\lambda};\underline{\theta})d\underline{\lambda}d\underline{\theta} = d\underline{\lambda}w_1(\underline{\lambda})w_1(\underline{\theta}')d\underline{\theta}'dz_o$, so that the space-time covariance of these poisson fields becomes explicitly (cf. (4.8) of [1], for example, writing $\mathcal{L} = \mathrm{Re}\,\hat{\mathcal{L}}$):

$$K_{N_o}(\underline{R}_1,t_1;\underline{R}_2,t_2) = \overline{\mathcal{L}_1\mathcal{L}_2} - \overline{\mathcal{L}_1}\,\overline{\mathcal{L}_2} = A_{(A\text{ or }B)} \int_0^{(z_o,\infty)} dz_o \int w_1(\underline{\theta}')d\underline{\theta}' \int_{\Lambda_I} w_1(\underline{\lambda})d\underline{\lambda}$$

$$\cdot \tfrac{1}{2}\,\mathrm{Re}\,\hat{\mathcal{L}}(\underline{R}_1,t_1|\underline{\lambda},\underline{\theta}',z_o)\hat{\mathcal{L}}(\underline{R}_2,t_2|\underline{\lambda},\underline{\theta}',z_o)^*>_{z_o} \quad (7.6)$$

with $\underline{\theta}'$ all other (random) parameters in $\mathcal{L}$, e.g., $\underline{i}_o$, a, ϕ_a, ν, etc. (and where for Class B noise we use the infinite limit in z_o). Here $\hat{\mathcal{L}}$ is the complex field, given by

$$\hat{\mathcal{L}}(\underline{R},t|\underline{\lambda};\underline{\theta}',z_o) = \frac{\hat{S}_{OT}}{\lambda^\gamma} \int_{-\infty}^{\infty} \hat{S}_T(f|z_o)_a\, \mathcal{Q}_T(\underline{\lambda}|f)\, e^{i\omega\mu(\hat{t}-|\underline{R}_o-\underline{R}|/\mu c_o)}\, df, \quad (7.7)$$

where the source is treated as effectively a point source, with, however, a nonuniform beam pattern, $\mathcal{Q}_T$, and where

$$\hat{S}_T(f|z_o)_a \equiv \int_{-\infty}^{\infty}\left(\int_{-\infty}^{\infty} a(t-\tau)s_T^{\perp}(\tau)d\tau\right)e^{i\phi_a(t-\tau)}d\tau\; e^{-i\omega t}dt \qquad (7.8)$$

represents the interaction of the source waveform S_T with an effective fading mechanism, $ae^{i\phi_a}$, expressed in frequency space, and an average spreading law ($\sim\lambda^{-\gamma}$), cf. Sec. 6.1. [It is the underlying poissonian statistics which give the field covariance, K_{N_o}, its particular form (7.6), cf. p. 49 of [1].]

In our present cw narrow-band examples, Eq. (7.3) = Re $\hat{\mathcal{E}}$), we see that (7.6) reduces directly to

$$\boxed{K_{N_o}(\underset{\sim}{R}_1,t_1;\underset{\sim}{R}_2,t_2) = A_{\binom{A}{B}}\frac{B^2}{2}\left\langle\frac{1}{R_o^{2\gamma}}\right\rangle \mathrm{Re}\left\{M_a(\underset{\sim}{\rho},\tau)\,\langle e^{i\omega_o\mu\tau}\rangle_{\mu}\cdot\langle e^{ik_o(\hat{\underset{\sim}{i}}_o\cdot\underset{\sim}{\rho})}\rangle_{\theta_o,\phi_o}\right\}} \qquad (7.9)$$

$$\tau = t_2 - t_1; \quad \gamma > 0; \quad \underset{\sim}{\rho} = \underset{\sim}{R}_2 - \underset{\sim}{R}_1,$$

cf. (6.36), (6.37), for Class A or B noise. The interference is stationary and homogeneous (in the 2nd-order, or covariance, sense, at least), as a consequence here of the assumed cw character of the emissions, and the postulated stationary and homogeneous nature of the fading and source dopplers. That (7.9) has a form similar to (6.36) is not surprising, accordingly. [But remember here that

$$M_{N_o}(\underset{\sim}{R}_1,t_1;\underset{\sim}{R}_2,t_2) = K_{N_o}(\underset{\sim}{R}_1,t_1;\underset{\sim}{R}_2,t_2) + \overline{p_1}\cdot\overline{p_2} \quad (\neq M_{2s},\ (6.36)) \qquad (7.10)$$

with

$$\overline{p}_{1,2} = A_{(A\text{ or }B)}\,\mathrm{Re}\left\langle\int_0^{(z_o,\infty)} dz_o \int w_1(\theta')d\theta' \int_{\Lambda_I} w_1(\underset{\sim}{\lambda})d\underset{\sim}{\lambda}\,\hat{\mathcal{E}}(\underset{\sim}{R}_{\binom{1}{2}},t_{\binom{1}{2}}|\underset{\sim}{\lambda};\underset{\sim}{\theta}',z_o)\right\rangle_{z_o} \qquad (7.11)$$

because of the poissonian statistics of the noise vs. the single, desired signal source.]

If the noise mechanism is the same as for the few, outstanding sources on the average, the noise background produced by many unresolved sources is gaussian, with a covariance and mean component structure given by (7.9), (7.11), respectively, but with large values of $A_{(A\text{ or }B)}$ (and small values of the scale factor B, cf. (7.3)), reflecting the fact that the gaussian background is usually small compared to the nongaussian contribution. Thus, we can write

$$K_{N_o} = K_I(\underset{\sim}{R}_1,t_1;\underset{\sim}{R}_2,t_2) + K_G(\underset{\sim}{R}_1,t_1;\underset{\sim}{R}_2,t_2) \tag{7.12}$$

for (7.9).

Let us examine the effects of the different wavefront angles at which the various source fields can impinge upon a given array (cf. Sec. 6.4). We simplify the discussion somewhat, for purposes of illustration, by the assumption that $M_a(\underset{\sim}{\rho},\tau)$ is spatially uniform over the array in question. Here II of Sec. 6.4 applies at once for the averages over (θ_o,ϕ_o). Thus, from (6.43) - (6.46d) we can obtain a variety of results, depending on the appropriate distribution of (θ_o,ϕ_o), cf. (6.44). Also, it is possible that the nongaussian (I) and gaussian (G) ambient components may obey different distributions [cf. (6.44)], depending on the propagation conditions. However, as an example, we shall assume the same distributions. Accordingly, (6.44) leads here to (6.45) for the linear vertical array, and (6.46) for the linear horizontal array. Only for $w_1(\theta_o,\phi_o)_{II}$ is it possible to obtain field nulls for all element spacings, e.g., $k_o\Delta R=q\pi$, or $\Delta R=q\pi/k_o=q\lambda_o/2$, in the vertical case. The other distribution (densities) $w_1(\theta_o,\phi_o)$ do not possess this regularity: some elements can be placed at the covariancenulls of the field, while others necessarily fall in regions where $K_{N_o}\neq 0$, so that the effective number of "independent" spatial samples (M') is less, and possibly much less, than the number (M) of array elements, e.g., $1\leq M'<(<)M$.

We remark that "independence," as defined here, is specified in terms of the zeros of the covariance of the noise process. As is well known, this is practically equivalent to full statistical independence, i.e., $w_M(\underset{\sim}{x})=\prod_{m=1}^{M} w_1(x_m)$, for instance, when the noise is gaussian, namely for

the G-component of the interference, cf. (7.12). It does not, however, guarantee statistical independence in the nongaussian cases, which are significant here: higher order correlations exist, to weaken the effects of this second-order independence, so that basing a determination of independent spatial sampling, as in the associated situation of temporal sampling, on second-order independence is incomplete. More "sparse" spatial sampling, i.e., much wider separation of array elements, may be needed to achieve the needed independence, which in turn yields the hoped for spatial sampling gains ($\sim M$ vs. $M' \geq 1$).*

As an example of the modified beam performance [cf. Sec. 6.5] produced with respect to the incoming noise field, we have the analogue of (6.47) here. Using (6.16)-(6.19) for the typical received narrowband interfering signal (after beam-forming (i.e., Σ_m), in (7.1), we have

$$N_I(t;\underline{\theta}) = \int_{\underline{Z}=\underline{\Lambda}\times\underline{\theta}} S_R(t|\underline{\lambda},t',\underline{\theta})dN(\underline{Z}) \tag{7.13}$$

for the nongaussian component, for example, of the received interfering input. The corresponding covariance of the received array output is, cf. (6.47):

$$K_{N_o}(\tau)_R = \frac{1}{2} B^2 A_{(A \text{ or } B)} \left\langle \frac{1}{R_o^{2\gamma}} \right\rangle \mathrm{Re}\left\{ M_a(\tau) D_1(\omega_o \tau) \left\langle |Q_R(\underline{\nu}_o - \underline{\nu}_{oR}, f_o)|^2 \right\rangle_{\underline{i}_o} \right| \tag{7.14}$$

where $\langle |Q_R|^2 \rangle$ is given by (6.48), subject to various choices of pdf $w_1(\vartheta_o, \varphi_o)$, according to (6.44). The averages in (6.48) become, for example,

---

* The full procedure for determining such space intervals for Class A noise is sketched in Sec. 3.2, [9], in Tech. Rpt. OT-75-67, June, 1975 in the temporal cases. The spatial cases may be handled in the same way, provided the field is governed spatially by a poisson distribution of sources. If this is the case, which is physically likely--the sources are sparse and independent in location, then we have an example of spatial Class B noise, since the sources are effectively points in Λ_I, i.e., are "spatial impulses," analogous to the temporal impulse or very short, independent emissions of Class B time waves, which produce transients in comparatively narrow band receivers. We reserve the development of spatial Class A and B noise models to a subsequent study.

$$\langle a_R^{(m)} a_R^{(m')*} \rangle_{\text{vert:I,II}} = e^{-2\pi i \Delta_{mm'} \sin\theta_{oR}} \left\{ J_o(2\pi\Delta_{mm'}) \text{ or } \frac{\sin(2\pi\Delta_{mm'})}{2\pi\Delta_{mm'}} \right\} \tag{7.15}$$

with

$$\Delta_{mm'} = (m - m')\Delta\ell/\lambda_o \tag{7.15a}$$

cf. (6.49b). Thus, $\Delta\ell=[z_{oq}/2\pi(m-m')]\lambda_o$, $m\neq m'$, is a possible spacing of elements, where z_{oq} is the $q^{\underline{th}}$ zero of the function in question, here J_o or $(\sin x)/x$. Clearly, unless z_{oq} is independent of q, it is not possible to avoid "beam smearing" or degradation. For "vertical$_{II}$," however, we can always choose $z_{oq}=\pi(m-m')$, so that $\Delta\ell=\lambda_o/2$ (or multiples thereof), and maximum gain (~M) is obtained from the array. In general, however, the beam is degraded, and in effect those are only $1\leq M'(<M)$ independent spatial samples.*

7.4 First-Order Probability Density of the Interference

In order to implement the threshold algorithms of Sections 3-5, we must determine, first, the analytical form of the first-order pdf, $w_1(x_{mn})$, of the interference, and, next, measure or calculate from the a priori data of the ACI scenario (above) the relevant parameters of this pdf, generally, at each discrete spatial sample point (m) (for t in the observation period).

Accordingly, the received noise waveform (at each array element m=1,...,M), at time t, is

---

* We remark that it is always possible to obtain (second-order) spatially independent noise samples by a suitable transformation of the spatially sampled data, $\underset{\sim}{x}$. Thus, if $C_x=[\overline{xx^+}]$ is the known (MxM) spatial covariance (at given time t_n), we can choose an (MxM) transformation $\underset{\sim}{A}$, yielding $\underset{\sim}{y}=\underset{\sim}{A}\underset{\sim}{x}$, such that $C_y=\overline{yy^+}=\underset{\sim}{A}\overline{xx^+}\underset{\sim}{A}^+=\underset{\sim}{A}\underset{\sim}{C}_x\underset{\sim}{A}^+$ and $\underset{\sim}{C}_y$ is diagonal, e.g., $\underset{\sim}{C}_y=[\overline{y_i y_j}\delta_{ij}]$. The transformed inputs are now uncorrelated. Several problems, however, arise in the practical implementation of $\underset{\sim}{A}$: (i), the choice of $\underset{\sim}{A}$ is not unique and can lead to computational instabilities in going from $\underset{\sim}{x}\to\underset{\sim}{y}$ and determining $\underset{\sim}{C}_y$; (ii), the same transformation, $\underset{\sim}{A}$, must be applied to the desired signal in the threshold processing algorithms of Sec. 3, which can produce difficult modifications of the needed matched filters [cf. Sec. 4]. Also, there is always the question of the degree of statistical independence achieved by a second-order approach when the noise process is nongaussian; see the remarks in the preceeding footnote.

$$X^{(m)}(t;\underset{\sim}{\theta}) = \int_{\underset{\sim}{Z}} S^{(m)}(t|\underset{\sim}{\lambda};t',\underset{\sim}{\theta}')dN(\underset{\sim}{Z}) \qquad [\underset{\sim}{\theta} = (\underset{\sim}{\theta}',t')] \tag{7.16}$$

cf. (7.1), (7.13), which is a superposition of the individual (interfering) source emissions, cf. Fig. 7.1, and $dN(\underset{\sim}{Z})$ is a poisson counting functional, as before. To calculate the desired pdf $w_1(x_{mn})$ we must first obtain the corresponding characteristic function (c.f.) of the instantaneous amplitudes, X, of the Class A or Class B interference, plus a gaussian component, from

$$F_1(i\xi|X^{(m)})_{A+G} = e^{-\sigma_G^2\xi^2/2-A_A+A_AH_1(i\xi)_A}, \tag{7.17a}$$

$$F_1(i\xi|X^{(m)})_{B+G} = e^{-\sigma_G^2\xi^2/2+A_BH_1(i\xi)_B}, \tag{7.17b}$$

where $H_{1A,B}$ are the c.f.'s of a single, typical emitting source, e.g.,

$$\langle e^{i\xi S^{(m)}}\rangle_A \equiv F_1(i\xi|S^{(m)})_A = A_AH_1^{(m)}(i\xi)_A, \tag{7.18a}$$

$$\langle e^{i\xi S^{(m)}} - 1\rangle_B = A_BH_1^{(m)}(i\xi)_B. \tag{7.18b}$$

Here $\sigma_G^2(=\sigma_G^2(t))$ is the mean intensity of the gaussian component (not necessarily assumed stationary for the moment).

Full details and results for (i), broad- or narrow-band Class A noise in narrow-band (or broad-band) receivers; (ii), Class B noise in narrow-band receivers; (iii), narrow-band Class B noise in narrow-band receivers (comparable to or broader than the noise), which is now an incoherent form of Class A noise, are given in [6], also in [4] and refs. For broad-band Class A noise in broad-band receivers, however, there is as yet no previous theory. Accordingly, we give a condensed outline of the approach:

I. Broad-Band Class A Noise in Broad-Band Receivers

The c.f. (7.18a) is

$$A_A H_1^{(m)}(i\xi) = A_A \langle \int_0^{z_o} e^{i\xi S^{(m)}(z-\hat{\varepsilon};\underset{\sim}{\theta},\underset{\sim}{\lambda})} \rangle_{z_o,\underset{\sim}{\lambda},\underset{\sim}{\theta}} \; ; \; t = \bar{T}_s z \; ; \; t' = \hat{\varepsilon}\bar{T}_s, \quad (7.19)$$

(cf. (7.2), etc.), where $\bar{T}_s$ is the mean duration of a typical (coherent) emission and $\hat{\varepsilon}$ is a (dimensionless) epoch representing the emission time. The basic waveform, $S^{(m)}$, is given by [Sec. 3, [1]], extended phenomenologically here to include various path spreading ($\lambda^{-\gamma}$) and fading effects, viz.:

$$S^{(m)}(z;\underset{\sim}{\theta},\underset{\sim}{\lambda}) = \mathrm{Re}\, \frac{\hat{S}_o A}{4\pi e_o^{\gamma} \lambda^{\gamma}} \int_{-\infty}^{\infty} \mathcal{Q}_R^{(m)}(\underset{\sim}{\nu}_o - \underset{\sim}{\nu}_{oR} | f)_{norm} \mathcal{Q}_T(\underset{\sim}{\nu}_o | f) \hat{S}_T^{(m)}(f|z)_a$$

$$\cdot\, e^{i\mu\bar{T}_s\omega(z-\hat{\varepsilon})}\, e^{-i\omega\lambda}\, df, \quad (7.20)$$

where $\hat{S}_T^{(m)}(f|z)_a$ is now given by

$$\hat{S}_T^{(m)}(f|z)_a \doteq \int_{-\infty}^{\infty} \left(\int_{-\infty}^{\infty} a^{(m)}(t-\tau) e^{+i\phi_a^{(m)}(t-\tau)} s_T(\tau) d\tau \right) e^{-i\omega u\left(t - [\hat{\underset{\sim}{i}}_{oR} - \hat{\underset{\sim}{i}}_o]\cdot \underset{\sim}{r}_m / c_o u\right)} dt \quad (7.20a)$$

cf. (7.8), and represents the effects of fading (a,ϕ_a) on the (real) typical source emission, s_T.

Now if the apertures $\mathcal{Q}_R^{(m)}$, $\mathcal{Q}_T$ are comparable in bandwidth to the $m^{\underline{th}}$ array element, and if the fading is taken to be rapid, so that

$$a(t-\tau)e^{i\phi_a(t-\tau)} = a e^{i\phi_a} \delta(t-\tau)$$

effectively,* we can approximate (7.20) by

---

* We can do this because of the requirement of independent temporal sampling for the noise, which, in effect, allows only the first-order pdf's of the fading to be significant, unlike the situation of the desired signal of Secs. 6.4, 6.5, and earlier, Secs. 4, 5.

$$S^{(m)}(z;\underset{\sim}{\vartheta},\lambda) = \mathrm{Re}\left[\frac{a^{(m)}\,\hat{S}_o A}{4\pi c_o^{\gamma}\lambda^{\gamma}}\,\left|Q_R^{(m)}(\underset{\sim}{\nu}_o(\underset{\sim}{\lambda})-\underset{\sim}{\nu}_{oR};f_o)\right|\right.$$

$$\left.\cdot\,\left|Q_T(\underset{\sim}{\nu}_o(\underset{\sim}{\lambda})\,|\,f_o)\right|\,e^{i\phi_a^{(m)}-i\phi_T(f_o)-i\phi_R^{(m)}(f_o)}\right]$$

$$\cdot\int_{-\infty}^{\infty} e^{i\mu\bar{T}_s\omega(z-\hat{\varepsilon}-\lambda/\mu\bar{T}_s)}\,\hat{s}_T^{(m)}(f\,|\,z-\hat{\varepsilon}-[\underset{\sim}{\hat{i}}_{oR}-\underset{\sim}{\hat{i}}_o(\underset{\sim}{\lambda})]\cdot\underset{\sim}{r}_m/\mu c_o\bar{T}_s)\,df$$

$$\doteq\left(\mathrm{Re}\left[\frac{a^{(m)}e^{+i\phi_a^{(m)}}\,G_R^{(m)}(\vartheta_o,\phi_o)G_T(\vartheta_o,\phi_o)}{\lambda^{\gamma}}\right]\right)$$

$$\cdot\,s_T^{(m)}(\mu[z-\hat{\varepsilon}]-\lambda/\bar{T}_s-[\underset{\sim}{\hat{i}}_{oR}-\underset{\sim}{\hat{i}}_o(\underset{\sim}{\lambda})]\cdot\underset{\sim}{r}_m/c_o\bar{T}_s) \qquad (7.21)$$

where we have replaced $|\bar{Q}_R^{(\bar{m})}|\,e^{-i\phi_R^{(m)}(f_o)}$ by $G_R^{(m)}(\vartheta_o,\phi_o)$, etc. Here we have replaced the frequency-dependence of the beam patterns by average values, maintained at some average or central frequency f_o. Next, carrying out the averages over the random epochs $\hat{\varepsilon}$, for long intervals and the usual situation of "local stationarity" where there are no significant changes in the average numbers of emitting sources, so that $w_1(\hat{\varepsilon})$ is effectively uniform for all allowed values of the (normalized) time, z, (according to the detailed procedure of pp. 46-51, [32]), we get finally

$$\boxed{S^{(m)}(z;\underset{\sim}{\vartheta},\lambda) \doteq \frac{a^{(m)'}G_{RT}^{(m)}(\vartheta_o,\phi_o)}{\lambda^{\gamma}}\,s_T^{(m)}(\mu z),} \qquad (a^{(m)'} \equiv a^{(m)}\cos\phi_a^{(m)}) \qquad (7.22)$$

where $\underset{\sim}{a}[=a^{(m)'}, \mu, G_{RT}$, etc.] are a set of random variables, as is the path distance, λ.

The important thing to observe about (7.22) is that it has precisely the same form as the usual expression for narrow-band Class A noise, with the narrow-band envelope, $u_o(z)$, now replaced by the (normalized) waveform, $s_T(\mu z)$. This means that we can apply the same formal results to these broad-band Class A as we have already done for narrow-band interference, cf. [6]. Accordingly, we have for [illegible]

AD-A140 620 MULTIPLE-ELEMENT THRESHOLD SIGNAL DETECTION OF UNDERWATER ACOUSTIC SIGNAL.. (U) MIDDLETON (DAVID) NEW YORK D MIDDLETON 18 MAY 83 NOSC-CR-231 2/2

UNCLASSIFIED N66001-82-C-0322 F/G 20/1 NL

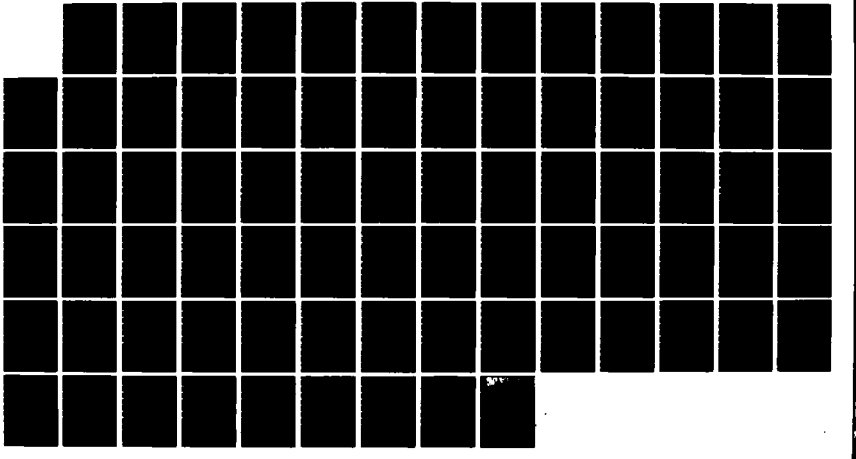

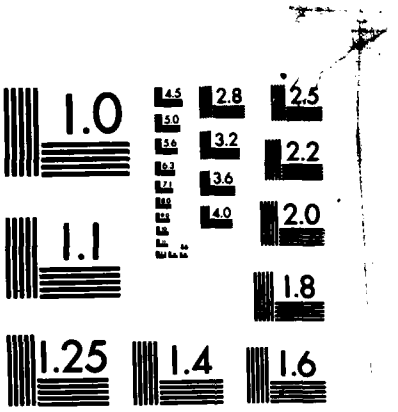

$$H_1^{(m)}(i\xi)_A = \left\langle \int_0^{z_o} \left\langle e^{i\xi a^{(m)} G_{RT}^{(m)} s_T(\mu z)/\lambda^{\gamma}} \right\rangle_{\underset{\sim}{\lambda}, a, \mu, G_{RT}} dz \right\rangle_{z_o} , \tag{7.23}$$

which is then treated according to the procedures of Secs. 3-6 of [6]. In the usual case where the odd moments of $X^{(m)}$ vanish, it can be shown* that the c.f. of $X^{(m)}$, (7.17a), for this broad-based Class A noise can be expressed as

$$\boxed{F_1(i\xi | X^{(m)})_{A+G}|_{b.b.} = e^{-\sigma_G^2 \xi^2/2 - A_A + A_A e^{-\xi^2 \Omega_{2A}^{(m)}/2}} [1 + \Psi_1^{(m)}(\xi^2)_A],}$$

$$\Omega_{2A}^{(m)} \equiv \langle X_A^{(m)2} \rangle_{\text{nongauss}} \tag{7.24}$$

where

$$\Psi_1^{(m)}(\xi^2)_A = \sum_{\ell=2}^{\infty} \frac{\xi^{2\ell} \Omega_{2A}^{(m)\ell}}{2^{\ell} \ell!} \left\langle {}_1F_1(-\ell; \tfrac{1}{2}; X^{(m)}(\underset{\sim}{\theta})_A^2 / 2\Omega_{2A}^{(m)}) \right\rangle_{\underset{\sim}{\theta}} , \tag{7.24b}$$

which the broad-band Class A analogue of (3.12), [6]; here ${}_1F_1$ is a confluent hypergeometric function.

With such methods, then, we can handle broad-based interfering signals, whose typical components are given by (6.34), for example; see Sec. 6.3, III above.

II. Narrow-Band Class A Noise in Broad- or Narrow-Band Array Elements

Our principal case in this study involves coherent narrow-band-interfering signals, of the type given by Eq. (6.32), which we use to illustrate the general approach. Thus, $X^{(m)}(t;\underset{\sim}{\theta})$, (7.11), is now n.b. Class A, for which the results are well-known [6]. Accordingly, the c.f. has the same form as (7.24). The various pdf's associated with this c.f. depend on the ACI scenario [cf. beginning of Sec. 7 above]. We have

---

* Unpublished notes of the author (June,1982).

A. Strictly Canonical Class A pdf: (Sec. 4, [6]).

Here the spatial distribution of the potentially interfering sources is such that the sources are essentially equidistant from the receiving array elements. Then $\Psi_1^{(m)}(\xi^2)_A=0$, and the associated pdf of the instantaneous amplitudes, $X^{(m)}(t_n;\underset{\sim}{\theta})$ is given by

$$\boxed{w_1(x_{mn}) = e^{-A_A} \sum_{p=0}^{\infty} \frac{A_A^p}{p!} \frac{e^{-x_{mn}^2/4\sigma_{pA}^{(m)2}}}{[4\pi\sigma_{pA}^{(m)2}]^{\frac{1}{2}}}} \quad , \tag{7.25}$$

where

$$2\sigma_{pA}^{(m)2} = \frac{p/A_A+\Gamma_A^{(m)'}}{1+\Gamma_A^{(m)'}} \quad ; \quad \Gamma_A' = \sigma_G^2/\Omega_{2A}^{(m)}; \quad x \equiv \frac{X}{\sqrt{\Omega_{2A}(1+\Gamma_A^{(m)'})}} \tag{7.25a}$$

Here, the "macro-parameters" of Class A noise are

$$\left.\begin{aligned}
A_A &= \text{"overlap index"} = (\text{av. no. of interfering sources emitting at any given instant}) \times (\text{av. duration, } \overline{T}_s, \text{ of a typical emission});\\
\Omega_{2A}^{(m)} &= A_A\langle \hat{B}_o^{(m)2}\rangle/2 = \text{mean intensity of the nongaussian component of the ACI, at the } m^{\underline{th}} \text{ element of the array, cf. (7.27) below;}\\
\Gamma_A^{(m)'} &= \sigma_G^2/\Omega_{2A}^{(m)} = \underline{\text{gaussian factor}}, \text{ a ratio of the mean intensity of the gauss to the nongauss component of the ACI;}\\
N_o^{(m)2} &= \Omega_{2A}^{(m)}+\sigma_G^2 = \text{mean total noise intensity at the (output of the) } m^{\underline{th}} \text{ array element.}
\end{aligned}\right\} \tag{7.26}$$

The envelope, $\hat{B}_o^{(m)}$, of the typical interfering (nongauss) signal (6.30) is now

$$\hat{B}_{oA}^{(m)} = a^{(m)}G_{RT}^{(m)}(\theta_o,\phi_o)/\lambda^{\gamma} \tag{7.27}$$

cf. (7.22), so that

$$\Omega_{2A}^{(m)} = \frac{\langle a^{(m)2}\rangle}{2} \langle G_{RT}^{(m)2}\rangle \left\langle \frac{1}{\lambda^{2\gamma}} \right\rangle . \tag{7.28}$$

A common source pdf is

$$\left.\begin{aligned} w_1(\underline{\lambda})_s = B_\mu \lambda^{1-\mu} d\lambda w_1(\theta_o,\phi_o); \quad B_\mu = \frac{2-\mu}{\lambda_1^{2-\mu} - \lambda_0^{2-\mu}}; \quad (0\leqslant)\ \lambda_o \leqslant \lambda_1\ (<\infty) \\ -\pi/2 \leqslant \theta_o \leqslant \pi/2; \quad 0 \leqslant \phi \leqslant 2\pi \quad (\mu\geqslant 0,\ \gamma\geqslant 0) \end{aligned}\right\} \tag{7.29}$$

cf. Fig. 3.1 of [12], or (5.1) of [6]. Consequently, from (7.29) we get

$$\langle 1/\lambda^{2\gamma}\rangle \equiv C_{\mu,\gamma}^{(2)} = \frac{2-\mu}{2\gamma+\mu-2}\left(\frac{1-\alpha_o^{2\gamma+\mu-2}}{1-\alpha_o^{2-\mu}}\right) \alpha_o^{2-2\gamma-\mu} \lambda_1^{-2\gamma}; \quad \boxed{\alpha_o \equiv \lambda_o/\lambda_1}. \tag{7.30}$$

In a similar way, we have

$$\Gamma_A^{(m)'} = 2\sigma_G^2/A_A \overline{a^{(m)2}} \langle G_{RT}^{(m)2}\rangle_{\theta_o,\phi_o} C_{\mu,\rho}^{(2)}; \quad \langle N_o^{(m)2}\rangle \equiv \psi(m)$$
$$= A_A \langle a^{(m)2}\rangle \langle G_{RT}^{(m)2}\rangle_{\theta_o,\phi_o} C_{\mu,\gamma}^{(2)}/2 + \sigma_G^2$$

(7.31)

Thus, from the ACI scenario [quantitatively embodied in the propagation law ($\lambda^{-\gamma}$), source distribution, $w_1(\lambda)\sim\lambda^{-\mu}$, and envelope structure $B_{oA}^{(m)}$, along with the overlap index, A_A, and gaussian intensity, σ_G^2], we can a priori calculate the various macro-parameters of the pdf. [Usually, these are obtained empirically, cf. [5].]

B. Approximately Canonical Class A pdf (Sec. 5, [6])

Here $\psi_1^{(m)}(\xi^2)=0$, so that we get the same structural form, (7.25), for the pdf of x_{mn} in this case. Physically, these approximately canonical Class A cases have source distributions, (7.29), where the sources are not too widely distant from the receiver: as $\alpha_o = 0.5$, cf. (7.30), is a typical upper limit.

C. Quasi-Canonical Class A pdf (Sec. 7, [6])

In this situation, source ranges from the receiver can be widely distributed, e.g., $\alpha_o = 10^{-2}$ is representative, cf. (7.30), and Sec. 7 of [6]. A suitable "correction" term in the pdf (7.25) is then required, e.g., Eqs. (3.14), [12], and Secs. 7, 8 of [6]. However, although the optimum dynamic characteristic, $\ell \equiv \frac{d}{dx} \log w_1(x|P_A)$, is thereby altered noticeably, it appears that the various parameters of the threshold algorithm's performance $L^{(2)}$, $L^{(4)}$, cf. (5.38), (5.40), as well as the necessary bias term (B^*_{coh}, etc.), cf. Sec. 3, are not noticeably changed thereby vis-a-vis the strictly or approximately canonical Class A models (1), (2) above, which is accordingly used in evaluating performance. Moreover, in practice one uses a good suboptimum approximation to the optimum dynamic characteristic, ℓ, such as a hard-limiter (cf. Secs. 10, 11ff.), so that the difficult problem of replicating the optimum does not arise. Accordingly, one can employ a canonical Class A model, (1), Eq. (7.25), and its associated statistics, $L_A^{(2)}$, $L_A^{(4)}$, etc., with a good, simple approximation to the ideal characteristic, and obtain performance results often close to the optimum, as noted in Sec. 11ff.

7.5 Remarks

The general first-order theory of these canonical nongaussian interference models is developed in [1]-[7],[32]. We emphasize their canonical nature again: the forms of the pdf's are independent of the particular noise mechanisms, acoustic or electromagnetic, for example. Particular applications require empirical [5] or a priori evaluations of the specific noise parameters ($P_{3A} = A_A$, Ω_{2A}, Γ'_A) involved. A priori evaluation can be obtained from the ACI scenario here, cf. (7.26)-(7.31), and ([6], Sec. 5.2). This relation of noise (and signal) models to real-world conditions constitutes the adaptive nature of these detection algorithms both to the noise and desired signal [cf. Sec. 4, and Figs. 4.1, 4.2]. It is this adaptive character of these algorithms, in turn, which helps produce the often very considerable improvements of these systems over those conventional systems based on second-order moment statistics (such as spectra or covariance functions) alone. [See the remarks in Section 12ff., also.]

Section 8. Specific Optimum Threshold Detection Algorithms

Although the various signal and noise fields are additive in the domain occupied by the receiving array, the required optimum processing is not: for example, the optimum coherent detector (3.2) requires the nonlinear operation of multiplying *a posteriori* noise data (in $\ell_{m,n}$) with *a priori* signal structure ($\langle\!\langle \theta_{m,n} \rangle\!\rangle$), in a generalized cross-correlation. Similarly, for incoherent (3.5) and composite detection (3.7) the nonlinearities are of a quadratic order, typical of a generalized auto-correlation. Beam-formation here is not simply adaptive because it can be directed ("steered"), but it is the most complex kind, namely weighted adaptive, signal processing beam-formation (in conventional terminology), where *a posteriori* data (in the $\ell_{m,n}$, cf. (3.1), etc.) are used as array element weighting [29], in addition to a steering capability.

Accordingly, these optimum threshold processes, which are dictated by the likelihood ratio expansion (2.6), are not the same processes one encounters in the simple sampling of signal, noise, or combined signal and noise fields, described in Secs. 6,7 preceding. The various array elements encounter the fields in the same way (because of the linearity of the medium), but the resultant beam formation and processing are much more complex than the simple adaptive beams generated in these earlier illustrative examples. However, the earlier arguments [cf. Sec. 7.3] still apply, for obtaining independent noise samples, while at the same time preserving signal waveform and wavefront coherence. How beam formation is achieved, to optimize performance, will be explicitly indicated by the examples following.

8.1 Channel Conditions

Our basic example, which we use throughout to illustrate the general approach, and to keep the presentation reasonably simple, is a somewhat specialized one. We make the following, mildly restrictive assumptions:

(i). the desired signal at the output of the m^{th}-array element is the narrow-band, fading, "dopplerized" sinusoidal signal (6.30);

(ii). beam steering is employed, cf. (6.30); beam pattern phases, $\phi_R^{(m)}$, are the same (all elements);

(iii). the fading is uniform over the array; fading amplitude and phase are independent, [26]-[28], and independent of signal waveform;

(iv). the noise field is stationary and homogeneous;

(v). the signal field is similarly stationary and homogeneous;

(vi). the doppler may have a deterministic and a gaussian random component;

(vii). in numerical cases we use narrow band, Class A interference, obeying (7.25). (8.1)

In addition, we note that beam-forming in all cases results from the summation of array outputs ($\sim\Sigma_m$) and beam-steering is achieved by the insertion of appropriate path delays $\hat{\tau}_m(=\hat{\underset{\sim}{i}}_{oR}\cdot\underset{\sim}{r}_m/c_o)$, cf. (6.30a). Our model, (8.1), is a reasonable representation of frequently desired signals.

8.2 Optimum Coherent Detection Algorithms

From (3.2) we find for the class of signals and noise described by (8.1) that here, in these coherent cases (where $\epsilon=\epsilon_o$ is known), after averaging over a purely random doppler, for example:

$$\langle s_n^{(m)}\rangle = \sqrt{2}\, e^{-(\Delta\omega_d t_n)^2/2} \langle \cos\,(\omega_o(\hat{t}_n+\Delta\tau_m) + \phi_a - \phi_T - \phi_R)\rangle_{\phi_a},\ \hat{t}_n = t_n' - \epsilon_o \tag{8.2a}$$

$$= \sqrt{2}\, e^{-(\Delta\omega_d t_n)^2/2} \langle \cos\,(\omega_o(t_n'-\epsilon_o) + \phi_a - \phi_T - \phi_R)\rangle_{\phi_a} \tag{8.2b}$$

The average signal component, $\langle s_n^{(m)}\rangle$, becomes independent of (m) here where the beam is pointed in the desired signal direction, e.g., $\Delta\tau_m=0$. However, unless ϕ_a is known <u>a priori</u>, $\langle\cos\,(\phi_a+\ldots)\rangle_{\phi_a} = 0$, and $\langle s_n^{(m)}\rangle = 0$ likewise. Frequently ϕ_a can be treated as some constant and the sampling intervals adjusted to maximize the cosine term to unity. Then only the doppler "smear" can destroy signal coherence, depending on the magnitude of the rms doppler spread:

$$\Delta\omega_d = k_o\Delta v, \quad \Delta v = \text{rms doppler (velocity)} \tag{8.3}$$

The resulting optimum threshold algorithm (3.2) is now

$$\boxed{g^*_{coh} = (\hat{B}^*_{coh} + \log \mu) - \sum_m^M \sum_n^N \ell(x_{m,n})\ \bar{a}_o\ \sqrt{2}\ e^{-(\Delta\omega_d t_n)^2/2}}, \qquad (8.4)$$

where the sampling times and phases $(\phi_o - \phi_T - \phi_R)$, $\phi_o = \omega_o \varepsilon_o$, are adjusted to make the cosine unity, all t'_n. (Note the steered, adaptive beamformation: $(\sum_m \ell_{m,n})b_n$ in (8.4), with $\Delta\tau_m = 0$.) The bias term $\hat{B}^*_{coh}$ here is

$$\hat{B}^*_{coh} = \frac{-\sigma^{*2}_{o\text{-}coh}}{2}, \qquad \text{Eq. (5.4)} \qquad (8.5)$$

which is given explicitly by (9.4) ff. in (8.5) under the above detection conditions.

8.3 Optimum Incoherent Detection Algorithms

Equation (3.5) is the appropriate algorithm here. Under the conditions (8.1) we see that the factor $\langle \theta_{m,n}\theta_{m',n'} \rangle$ reduces to

$$\langle \theta_{m,n}\theta_{m',n'} \rangle = \overline{a_o^2}\ \hat{m}_{|n-n|}\rho^{(mm')}_{|n-n'|}, \qquad (8.6)$$

where for the signal (6.30) we get the <u>effects of the doppler spreading</u> in the signal:

$$\rho^{(mm')}_{|n-n'|} = e^{-[\Delta\omega_d(n-n')\Delta t]^2/2} \langle \cos\ [\omega_o \Delta t(n-n') + \omega_o(\Delta\tau_m - \Delta\tau'_m)] \rangle_{\hat{\underline{i}}_o};$$

$$\phi_R^{(m)} = \phi_R^{(m')}, \quad t_n = n\Delta t. \qquad (8.7)$$

The average over the angles of signal arrival $(\hat{\underline{i}}_o)$ reduces to:

<u>I. Fixed signal wavefront direction</u>:

$$\rho^{(mm')}_{|n-n'|} = e^{-[\Delta\omega_d(n-n')\Delta t]^2/2} \cos\ [\omega_o(n-n')\Delta t + k_o(\hat{\underline{i}}_o - \hat{\underline{i}}_{oR})\cdot\Delta\underline{r}_{mm'}] \qquad (8.8)$$

$$\Delta\underline{r}_{mm'} \equiv \underline{r}_m - \underline{r}'_m,$$

with no degradation of the beam pattern. Clearly, $\rho^{(mm')}_{|n-n'|}$ is maximized (when summed over m,m') by setting $\hat{\underset{\sim}{i}}_{oR}=\hat{\underset{\sim}{i}}_o$, i.e., with the beam pointing in the direction of the incoming signal wavefront, cf. Fig. 6.2. (The oscillations in $\cos(\ )_{mm'}$ are then removed, $m\neq m'$.) In fact, $\rho^{(mm')}_{|n-n'|}=\rho_{|n-n'|}$, and is independent of space (m,m').

II. Random signal wavefront direction:

Here we use Sec. 6.4, II above, where a variety of possibilities can occur, depending on the angular distribution $w_1(\theta_o,\phi_o)$ of wavefront upon the array. For example, we find from (6.45a), (6.46a) that

$$\rho^{(mm')}_{|n-n'|} = e^{-[\Delta\omega_d(n-n')\Delta t]^2/2} \cos\{\omega_o(n-n')\Delta t - k_o\hat{\underset{\sim}{i}}_{oR}\cdot\underset{\sim}{\Delta r}_{mm'}\}\cdot \begin{cases} J_o(k_o|\underset{\sim}{\Delta r}_{mm'}|) \\ J_o^2(k_o|\underset{\sim}{\Delta r}_{mm''}|/2) \end{cases} \quad (8.9)$$

Dist. I, vertical array: (8.9a)

Dist. I, horizontal array: (8.9b)

The effects of fading here are exhibited in the normalized second-moment function $\hat{m}_{|n-n'|}$:

$$\hat{m}_{|n-n'|} \equiv \overline{a_{on}a_{on'}}/\overline{a_{on}^2} = \overline{a_{on}a_{on'}}/\overline{a_o^2} \quad (8.10)$$

in these uniform homogeneous and stationary cases (i.e., independent of (m,m') and dependent only on (n-n')). Here we distinguish the following physical situations:

(1) No fading: $\hat{m}_{|n-n'|} = 1$, all $(n,n'=1,\ldots,N)$; $\overline{a_o^2} = a_o^2$ (8.11a)

(2) Slow-fading (one-sided): $\hat{m}_{|n-n'|} = 1$, all n,n'; $\overline{a_o^2} = \overline{a_o^2}$ (8.11b)

(3) Rapid-fading (one-sided): $\hat{m}_{|n-n'|} = \delta_{nn'} + (1-\eta)(1-\delta_{nn'})$; $\boxed{0\leq 1-\eta\equiv\overline{a_o^2}/\overline{a_o^2}<1}$ (8.11c)

(4) General fading (two-sided): $\hat{m}_{|n-n'|} = e^{-(\Delta\omega_a(n-n')\Delta t)^2/2}$ (8.11d)

(one-sided): $\hat{m}_{|n-n'|} = e^{-(\Delta\omega_a(n-n')\Delta t)^2/2} + (1-\eta)(1-\delta_{nn'})$.

Here $y = 0$ indicates no fading, e.g., $\overline{a_o^2} = \overline{a_o^2} = a_o^2$; $w_1(\hat{a}_o) = \delta(\hat{a}_o - a_o)$, while $n \doteq 1$ denotes very heavy fading, $\overline{a_o} \sim 0$ vs. $\overline{a_o^2} > 0$. Equations (8.11), with (8.7)-(8.9), give the structure of the signal factor in the optimum incoherent threshold detection algorithm (3.5), e.g.,

$$g^*_{inc} = (\hat{B}^*_{inc} + \log \mu) + \frac{\overline{a_o^2}}{2!} \sum_{mm'}^{M} \sum_{nn'}^{N} [\ell_{m,n}\ell_{m',n'} + \ell_{m,n}\delta_{mm'}\delta_{nn'}]\hat{m}_{|n-n'|}\rho^{(mm')}_{|n-n'|}, \tag{8.12}$$

which with a steered beam ($j_{oR} = j_o$) reduces further to

$$\boxed{g^*_{inc}\Big|_{\text{coh-sig-wavefront}} = (\hat{B}^*_{inc} + \log \mu) + \frac{\overline{a_o^2}}{2} \sum_{n,n'}^{N} \hat{m}_{|n-n'|}\rho_{|n-n'|} \sum_{m,m'}^{M} (\ell_{m,n}\ell_{m',n'} + \ell_{m,n}\delta_{mm'}\delta_{nn'}),}$$

$$(\text{at } t_n,\ t_{n'}). \tag{8.13}$$

This shows the formation of the product of two steered, signal processing beams ($\sim \sum_{mm'}$), whose outputs are then subject to temporal processing [cf. Fig. 4.2, also]. The bias $\hat{B}^*_{inc}$ is again obtained according to

$$\hat{B}^*_{inc} = -\sigma^{*2}_{o\text{-}inc}/2 \tag{8.14}$$

as given explicitly in (9.13) ff. When the incident wavefront intersects randomly with the array, the beam loses its steering capability, as indicated by the fact that $\rho \to \rho^{(mm')}_{|n-n'|}$, cf. (8.9a,b) in (8.12). Thus, the wavefront incoherence of the signal, as well as the temporal effects of fading and doppler, act to degrade performance by destroying signal coherence generally.

8.4 Optimum Composite Threshold Detectors

All the above [Secs. 8.2, 8.3] apply directly to the composite threshold detector (3.7a,b), since $g^*_{comp} = g^*_{coh} + g^*_{inc} - \log \mu$, cf. (3.7).

Thus, for example, combining (8.4) and (8.13) gives ($\hat{\underset{\sim}{i}}_{oR}=\hat{\underset{\sim}{i}}_o$):

$$g^*_{comp}\,\big|\,\text{coh-sig-wavefront} = (\hat{B}^*_{coh} + \hat{B}^*_{inc} + \log\mu) - \sqrt{2\,a_o^2\,(1-\eta)}\sum_{n-1}^{N} e^{-(n\Delta\omega_d\Delta t)^2/2}\sum_{m-1}^{M}\ell(x_{mn}); + \frac{1}{2!}\,a_o^2\sum_{n,n'}^{N}\hat{m}_{|n-n'|}\rho_{|n-n'|}\sum_{m,m'}^{M}(\ell_{m,n}\ell_{m',n'}+\ell_{m,n}\delta_{mm'}\delta_{nn'}). \tag{8.15}$$

Here we see the single steered ($\hat{\underset{\sim}{i}}_{oR}=\hat{\underset{\sim}{i}}_o$), signal-processing (≡adaptive) beam-formation in the first term (after the bias), and the steered product beams in the second term. The bias here is

$$\hat{B}^*_{comp} = \hat{B}^*_{coh} + \hat{B}^*_{inc} = -(\sigma^{*2}_{o\text{-}coh} + \sigma^{*2}_{o\text{-}inc})/2 \tag{8.16}$$

given explicitly by (9.26) following.

8.5 Remarks

As expected, these optimum threshold detection algorithms have the simplest structures [cf. (8.4), (8.13), (8.15)], and as we shall see in Sec. 9 following, the best performance, when the desired signal is in every sense coherent: i.e., (1) a unique wavefront direction in space, so that there is a steerable beam formed ($\hat{\underset{\sim}{i}}_{oR}=\hat{\underset{\sim}{i}}_o$); (2), no doppler "smearing," i.e., $\Delta\omega_d=0$, cf. (8.7), or no untracked deterministic doppler ($\Delta\omega_d=\omega_{od}=v_{od}k_o$, cf. (8.3)); and (3), negligible fading ($\eta=0$). These last two are temporal effects; all three [(1)-(3)] are usually out of the control of the receiver, as they are source and medium phenomena. We stress, however, that even when signal coherence is degraded, our algorithms above are still threshold-optimum, and take into account these degradation factors explicitly.

To achieve an effective beam steering, we need either many adjacent narrow beams, or a scanning narrow beam, so that we can set $\hat{\underset{\sim}{i}}_{oR}\doteq\hat{\underset{\sim}{i}}_o$ closely.

This, in turn, requires a comparatively large number of (discrete) elements [cf. Sec. 6.2]. The steering process consists of appropriate time delays inserted in the signal's matched filter, in the manner of Figs. 4.1, 4.2. The specific structure of the matched filter for the signal is obtained here by applying (8.2) to (7.1) in the coherent cases, and (8.6), with (8.8)-(8.11), to (4.6). Figures 4.1, 4.2 constitute both the general and (with the results of Secs. 8.2, 8.3 above) the specific operational structures of these adaptive beam processing algorithms.

Section 9. Optimum Threshold Performance

Optimum threshold performance is described canonically in Section 5, where the governing probabilities of detection are given by (5.3) and (5.3a). The critical quantity here is the variance, $\text{var}_o\, g^* = \sigma_o^{*2}$, which we determine here for our general example of Secs. 7, 8 preceding, where the noise fields are homogeneous and stationary and the fading is likewise uniform over the receiving array. In addition, the desired signal wavefront is spatially coherent, arriving at a specified direction, to which the receiving beam is steered ($\hat{\underset{\sim}{i}}_{oR}=\hat{\underset{\sim}{i}}_o$). Thus, the results of Secs. 5.2, II, and 8.3 apply specifically.

9.1 Canonical (Optimum) Performance Measures

From (5.3) and the fact that the bias is related to σ_o^{*2} by (5.4), we may write for the (conditional) probability of correctly detecting the presence of a signal (in these threshold optimum cases where sample size J=MN is large)

$$p_D^* \simeq \frac{1}{2}\left\{1 + \Theta\left[\sigma_o^*/\sqrt{2} - \Theta^{-1}(1-2\alpha_F^*)\right]\right\}, \tag{9.1}$$

where now, since $\langle g^* \rangle_o = \hat{B}_J^* + \log \mu$, the false alarm probability α_F^* is alternatively expressed as

$$\alpha_F^* \simeq \frac{1}{2}\left\{1 - \Theta\left[\frac{\hat{B}_J^* - \log(K/\mu)}{\sqrt{2}\,\sigma_o^*}\right]\right\}, \text{ with } \quad \hat{B}_J^* = -\sigma_o^{*2}/2, \text{ cf. (5.4)} \tag{9.2a}$$

(Similarly, since $\langle g^* \rangle_1 = -\hat{B}_J^* + \log \mu$, the false signal detection probability, cf. (5.3a), becomes

$$\beta^* \simeq \frac{1}{2}\left\{1 - \Theta\left[\frac{-\hat{B}_J^* - \log(K/\mu)}{\sqrt{2}\ \sigma_o^*}\right]\right\}. \qquad (9.2b)$$

These relations (9.2a,b) show explicitly how α_F^* and β^* depend on the bias. This, in turn, emphasizes the critical importance of using the correct bias for the threshold algorithm g* in question. We have shown (Appendix A3 of [12]) that this bias is obtained by terminating the expansion (2.6) of the likelihood ratio correctly (here for independent samples), and that the result is such that $\hat{B}_J^* = -\sigma_o^{*2}/2$, which extablishes the AO character of g*, needed for these large samples and weak input signals. (Figure 7.4 of [12] shows p_D^* vs. $10 \log_{10}(\sigma_o^*)^2$, for various values of α_F^*.)

A more convenient procedure is to express σ_o^{*2} in terms of the probability controls p_D^*, α_F^* by means of (5.36), since these latter are usually prechosen; (see Fig. 7.5 of [12] for $C_{NP} \equiv \sqrt{B_{NP}^*}$ vs p_D^*, given α_F^*). In any case, the larger σ_o^{*2}, the better is detector performance, so that any physical factors, such as fading and doppler, which act to destroy, or at least weaken, signal (temporal) coherence, in turn worsen performance by decreasing σ_o^{*2}, cf. (9.1), (9.2), above.

9.2 Optimum Threshold Variances σ_o^{*2}

For our particular class of problem--which we are using here to illustrate the general procedure [cf. remarks, Sec. 9.1 --we need to apply our results of Sec. 8 to the expressions for σ_o^{*2} given above in Sec. 5.2, II (A). The results are directly:

I. Coherent Reception

$$\boxed{\sigma_{o\text{-coh}}^{*2} = 2\,\overline{a_o^2}\,(1-n)\,MNL^{(2)}H_1(N\Delta t\Delta\omega_d)} = 2\,\overline{a_o^2}\,\hat{\pi}_{coh}^*\ ; \qquad (9.3)$$

$$[\hat{\pi}_{coh}^* = \hat{\pi}_{coh}^*(1-n)]\ ,$$

with

$$H(x) \equiv \frac{\sqrt{\pi}}{2}\,\Theta(x)/x; \qquad \therefore H(0) = 1; \quad H(\infty) \to O(\tfrac{1}{x}) \to 0 \tag{9.3a}$$

where $T=N\Delta t$, $(N>>1)$, is the observation period (cf. (8.4) and procedures like (9.7).)

Clearly, the doppler spread ($\sim\Delta\omega_d$) acts, as expected, to reduce the temporal coherence of the desired signal's waveform. If $T\Delta\omega_d \tilde{<} x_o = 0.20$, $H(x_o=0.2) \geqslant 0.99$, and little coherence is lost. But if x_o is at all large, say $x_o \geqslant 3$, then $H = 0.295$, or a 5.3 db reduction in σ_o^{*2}. For $x \geqslant 3$, $H(x_o) = 0.886/x_o$, so that the reduction in the level of σ_o^{*2} is inversely proportional to x_o, or equivalently, to $T\Delta\omega_d = N\Delta t\Delta\omega_d$: the longer the observation period ($\sim N$), the greater the decoherence of the signal produced by the doppler uncertainty ($\Delta\omega_d$), until for very long intervals ($\sim$ time-bandwidth product N), the coherent receiver is essentially inoperable ($\sigma^{*2}_{o\text{-coh}} \to 0$) even though phase coherence ($\varepsilon=\varepsilon_o$) is maintained. The associated incoherent detector must then be used.

From (5.4), or (9.2a), we have explicitly for the proper bias in 8.4,

$$\boxed{B^*_{n\text{-coh}} = \hat{B}^*_{n\text{-coh}} + \log\mu = \log\mu - \overline{a_o^2}\,(1-n)\,MNL^{(2)}\,H_1(N\Delta t\Delta\omega_d)}. \tag{9.4}$$

In (9.3) we also observe the deleterious effects of fading [$\sim(1-n)$]: whether or not the fading is slow, rapid, or in between [cf. (8.4)] is immaterial, since in this coherent case it is always possible to select the maximum of the (sinusoidal) waveform because the epoch is known. However, fading reduces σ_o^{*2} ($\sim(1-n)\leqslant 1$), and deep fading [$(n\doteq 1)$, or $1-n\doteq 0$], by considerable amounts: if $1-n = 10^{-2}$, then σ_o^{*2} is reduced by 20 db, for example.

II. Incoherent Reception

From (5.40), with (8.6), (8.7), we readily reduce the expression for $\sigma^{*2}_{o\text{-inc}}$ to

$$\boxed{\sigma^{*2}_{o\text{-inc}} = 2\,\overline{a_o^2}^2\,\{\tfrac{MN}{8}\,(L^{(4)} + 2L^{(2)^2}[MQ_N - 1])\} \equiv 2\,\overline{a_o^2}^2\,\Pi^*_{inc}}. \tag{9.5}$$

Specifically, now we have from (8.6) the signal structure factor in these homogeneous, stationary cases

$$Q_N \equiv \frac{1}{N} \sum_{nn'}{}' \hat{m}^2_{|n-n'|} \rho^2_{|n-n'|} = 1 + \frac{1}{N} \sum_{nn'}{}' \hat{m}^2_{|n-n'|} \rho^2_{|n-n'|} \tag{9.6}$$

Using the two-sided (or symmetrical) fading model (8.11d) and the doppler model (8.8) for our basically sinusoidal signals here (viz. (8.2)), we can write (9.6) as

$$Q_N^{(2)} - 1 = \frac{1}{N} \sum_{nn'}{}' e^{-[\Delta\omega_a \Delta t(n-n')]^2} \; e^{-[\Delta\omega_d \Delta t(n-n')]^2} \cos^2 \omega_o \Delta t(n-n'). \tag{9.7a}$$

This is now readily approximated (since $\Delta\omega_a \Delta t << 1$) by

$$Q_N^{(2)} - 1 = \frac{N}{u_o^2} \iint_0^{u_o} e^{-(u-v)^2} \cos^2 b(u-v) du dv,$$

$$b \equiv \omega_o/(\Delta\omega_d + \Delta\omega_a) \; (>>1); \tag{9.7b}$$

$$u_o \equiv T(\Delta\omega_d + \Delta\omega_a) = N\Delta t(\Delta\omega_d + \Delta\omega_a).$$

If we employ

$$\iint_0^A F(|x-y|) dx dy = \iint_{-A/2}^{A/2} F(|x-y|) dx dy = 2\int_0^A (A-z) F(z) dz \tag{9.8}$$

(from Rice, [33], p. 227, or (p. 95) of article), and note that $b>>1$ so that

$$2\int_0^{u_o} (u_o - z) e^{-z^2} \cos^2 bz dz \doteq u_o \int_0^{u_o} e^{-z^2} (1+\cos 2bz)(1-z/u_o) dz$$

$$\doteq u_o \int_0^{u_o} e^{-z^2} (1-z/u_o) dz = \frac{u_o \sqrt{\pi}}{2} \Theta(u_o) + \frac{e^{-u_o^2} - 1}{2}. \tag{9.9}$$

Thus we can write $Q_N^{(2)}$, (9.7), finally as

$$\boxed{Q_N^{(2)} \equiv 1 + N\Phi_2(u_o) = 1 + N\Phi_2[N\Delta t(\Delta\omega_D+\Delta\omega_a)]} \tag{9.10}$$

with

$$\boxed{\Phi_2(u_o) \equiv \frac{\sqrt{\pi}}{2}\,\Theta(u_o)/u_o + \frac{e^{-u_o^2}-1}{2u_o^2} = H_1(u_o) + \frac{e^{-u_o^2}-1}{2u_o^2}\ .} \tag{9.10a}$$

Note that for a completely coherent signal, including no and slow fading, $(\Delta\omega_D+\Delta\omega_a=0)$, $\Phi_2(0) = 1/2$, and

$$\therefore\ Q_N^{(2)}\Big|_{\substack{\text{no, slow}\\ \text{coh}}} \doteq 1 + N/2 = N/2 \quad (N>>1), \tag{9.11}$$

which agrees with Eq. A.2-42e of [12]; see also p. 83, [12]. For a completely incoherent signal, i.e., one whose temporal structure has been totally destroyed by doppler spread $(\Delta\omega_d\to\infty)$ and/or rapid fading $(\Delta\omega_F\to\infty)$, e.g., $u_o\to\infty$, $\Phi_2(\infty)\to 0$, we have at once in these two-sided fading cases

$$Q_N^{(2)}\Big|_{\text{inc}} = 1\ , \tag{9.12}$$

(which is equivalent to setting $\hat{m}_{|n-n'|} = \delta_{nn'}$, or $\rho_{|n-n'|} = \delta_{nn'}$, or both, in (9.6)). As u_o becomes large ($\tilde{>}3$), the governing factor in the decrease of Φ_2 is H_1, e.g. $\Phi_2 = H_1(u_o)$, $u_o>10$, say, so that for large degradations ($u_o>10$) the destruction of signal coherence here due to doppler only occurs in essentially the same quantitative fashion as for coherent reception. Fading, however, appears differently, cf. (9.5) or (9.3), as we note below.

In this case the bias term is from (5.4) and (9.5)

$$\boxed{B^*_{\text{inc}} = \hat{B}^*_{\text{inc}} + \log\mu = \log\mu - \frac{\overline{a_o^2}^2}{8}\,MN\{L^{(4)} + 2L^{(2)^2}\,(MQ_N-1)\}}\ . \tag{9.13}$$

(We observe in both (9.5) and (9.13) when M = 1 that these relations reduce, as expected, to our earlier results, cf. Sec. 5.2.)

The effects of fading here combine with doppler "smear" to reduce signal coherence, unlike the coherent cases, cf. (9.3). For slow or no fading, $N\Delta t\Delta\omega_a \doteq 0$ in Φ_2, (equivalent to $\hat{m}_{|n-n'|} = 1$), regardless of the depth of fading [~(1-η)], while for rapid fading ($N\Delta t\Delta\omega_a >> 1$), $\Phi_2 \doteq 0$, and $\therefore Q_N^{(2)} = 1$ once more, cf. (9.12): the signal is completely incoherent. In this latter case our model has $\hat{m}_{|n-n'|} = \delta_{nn'}$, which corresponds to rapid, two-sided fading, cf. 8.11d), as we would expect from our original choice (9.7a). On the other hand, we can easily construct one-sided fading models corresponding to (9.7a), by writing now

$$\hat{m}_{|n-n'|}\Big|_{\text{rapid}} = e^{-[\Delta\omega_a\Delta t(n-n')]^2/2} + \frac{\overline{a_o^2}}{\overline{a_o^2}}(1-\delta_{nn'}); \quad 1-\eta \equiv \frac{\overline{a_o^2}}{\overline{a_o^2}} \tag{9.14}$$

for "rapid" fading cases, where there is fading ($\Delta\omega_a > 0$) during the observation interval T, and

$$\hat{m}_{n-n'}\Big|_{\text{slow,no}} = 1 \tag{9.15}$$

for slow or no fading, which is characterized by no changes of amplitude (i.e., $\Delta\omega_F = 0$) during the interval T.

Applying (9.14) to (9.6), with the results of (9.7)-(9.10), allow us to write for the signal structure factor $Q_N(=Q_N^{(1)})$ in these one-sided fading situations with sinusoidal signals and large N:

$$Q_N^{(1)}\Big|_{\text{rapid}} = 1 + \frac{1}{N}\sum_{nn'}{}' \{e^{-[\Delta\omega_a\Delta t(n-n')]^2/2} + \overline{a_o^2}/\overline{a_o^2}\}^2 \cdot e^{-[\Delta\omega_d\Delta t(n-n')]^2} \cos^2\omega_o\Delta t(n-n') \tag{9.16a}$$

$$\therefore \boxed{Q^{(1)}\Big|_{\text{rapid}} \doteq 1 + N\{\Phi_2[N\Delta t(\Delta\omega_d+\Delta\omega_a)] + 2(1-\eta)\Phi_2[N\Delta t(\Delta\omega_d+\Delta\omega_a/\sqrt{2})] + (1-\eta)^2\Phi_2[N\Delta t\Delta\omega_d]\}, \quad N \gg 1.} \tag{9.16b}$$

Similarly, with (9.15) in (9.6) we get directly

$$Q_N^{(1)}\Big|_{\text{slow,no}} = 1 + \frac{1}{N}\sum_{nn'}{}' e^{-[\Delta\omega_d\Delta t(n-n')]^2}\cos^2\omega_o\Delta t(n-n') \tag{9.17a}$$

$$\therefore \boxed{Q_N^{(1)}\Big|_{\text{slow,no}} = 1 + N\Phi_2[N\Delta t\Delta\omega_d]} \tag{9.17b}$$

from (9.10) for slow or no fading.

Consequently, for very rapid fading ($N\Delta\omega_a\Delta t \gg 1$) and a coherent signal structure ($N\Delta t\Delta\omega_d \ll 1$), since then $\Phi_2(0) = \frac{1}{2}$, $\Phi_2(\infty) = 0$, we have from (9.16b)

$$Q_N^{(1)}\Big|_{\substack{\text{very rapid,}\\ \text{coh}}} \doteq 1 + \frac{N}{2}(1-\eta)^2 + \frac{N}{2}(1-\eta)^2, \quad \frac{N}{2}(1-\eta)^2 \gg 1, \quad N \gg 1. \tag{9.18}$$

Alternatively, with any kind of fading (no, slow, rapid) and an incoherent signal structure ($N\Delta\omega_d\Delta t \gg 1$), we get from (9.16b) and (9.17b)

$$Q_N^{(1)}\Big|_{\text{inc}} \doteq 1, \quad N \gg 1. \tag{9.19}$$

Incoherent signal structures (usually produced by doppler "smear" ($\Delta\omega_d > 0$)), always lead to the smallest values of the signal structure factor $Q_N^{(1)}$ and $Q_N^{(2)}$, cf. (9.12). In the case of slow or no fading, cf. (9.17b), with coherent signals ($N\Delta t\Delta\omega_d \ll 1$), we have

$$Q_N^{(1)}\Big|_{\substack{\text{no, slow}\\ \text{coh}}} \doteq \frac{N}{2}, \quad N \gg 1. \tag{9.20}$$

like (9.11) for two-sided fading.

We can now apply (9.10)-(9.12) for $Q_N^{(2)}$, and (9.16b)-(9.20) for $Q_N^{(1)}$, to express limiting forms of the variance σ_o^{*2}, (9.5), in more detail by

$$(1)\quad \sigma^{*2}_{o\text{-inc}}\,\Big|_{\substack{\text{2-sided,slow}\\ \text{coh. sig.}}} \doteq 2\overline{a_o^2}^2 \left\{\frac{MN}{8}\left(L^{(4)} + 2L^{(2)^2}[MN/2 - 1]\right)\right\}$$

$$\doteq \overline{a_o^2}^2 \left\{MNL^{(2)}/2\right\}^2, \tag{9.21}$$

since $N>>1$ and $L^{(4)} \sim 2L^{(2)^2}$ (see Figs. 7.7, 7.8, 7.11, 7.22 of [12]).

For <u>rapid two-sided fading</u> (9.12) applies and the result is the same as for the incoherent signal, for which we have similarly

$$(2)\quad \sigma^{*2}_{o\text{-inc}}\,\Big|_{\substack{\text{1-sided}\\ \text{2-sided}\\ \text{inc. sig.}}} \doteq 2\overline{a_o^2}^2 \left\{\frac{MN}{8}\left(L^{(4)} + 2L^{(2)^2}(M-1)\right)\right\} \tag{9.22}$$

$$\doteq \frac{\overline{a_o^2}^2}{2} M^2 NL^{(2)^2}, \quad M >> 1, \quad N >> 1. \tag{9.22a}$$

Also, we have for the one-sided fading cases

$$(3)\quad \sigma^{*2}_{o\text{-inc}}\,\Big|_{\substack{\text{1-sided}\\ \text{no,slow}\\ \text{coh. sig.}}} \doteq (9.21) = \overline{a_o^2}^2 \left\{MNL^{(2)}/2\right\}^2, \tag{9.23}$$

and for very rapid fading,

$$(4)\quad \sigma^{*2}_{o\text{-inc}}\,\Big|_{\substack{\text{1-sided}\\ \text{very rapid}\\ \text{coh. sig.}}} \doteq 2\overline{a_o^2}^2 \left\{\frac{MN}{8}\left(L^{(4)} + 2L^{(2)^2}\left\{\frac{MN}{2}(1-n)^2 - 1\right\}\right)\right\}$$

$$\doteq \overline{a_o^2}^2 \left\{\frac{MN(1-n)L^{(2)}}{2}\right\}^2. \tag{9.24}$$

Although the fading may be rapid here, there is enough signal coherence in $\overline{a_o}$ to maintain the same dependence on sample size MN as in the no or slow fading cases, (9.23).

Finally, for incoherent signals and fading of intermediate extent, we must, of course, use (9.10), (9.16b), or (9.17b). The result is a reduction in the magnitude of $Q_N^{(1),(2)}$ from the maximum values O(N), cf. (9.11), (9.18), (9.20) to something larger than $Q_{N\text{-inc}} = 1$, as we would expect. The bias, (9.13), is described in the same way.

III. Composite Detection

From (5.41), and the fact that $\sigma^{*2}_{o\text{-comp}} = \sigma^{*2}_{o\text{-coh}} + \sigma^{*2}_{o\text{-inc}}$, (5.29), we may use (9.3) and (9.5) to write

$$\sigma^{*2}_{o\text{-comp}} = 2\overline{a_o^2}\,(1-n)\,MNL^{(2)}H_1(N\Delta t\Delta\omega_d) + 2\overline{a_o^2}\left\{\frac{MN}{8}\left(L^{(4)} + 2L^{(2)^2}\{MQ_N - 1\}\right)\right\}$$

$$\equiv 2(\overline{a_o^2})_{min\text{-}comp}\,\Pi^*_{comp}\,. \tag{9.25}$$

This shows at once that the (optimum) composite (threshold) detector is always equal to or better than the individual coherent or incoherent threshold detectors themselves, e.g., $\sigma^{*2}_{o\text{-comp}} \geq \sigma^{*2}_{o\text{-coh}}, \sigma^{*2}_{o\text{-inc}}$ in (9.1). The proper bias term here is simply

$$B^*_{comp} = \hat{B}^*_{comp} + \log\mu = \log\mu - \sigma^{*2}_{o\text{-comp}}/2\,. \tag{9.26}$$

Using (9.3a) for H_1 and the various Q_N, cf. (9.10), (9.16b), (9.17b), and their limiting cases allows us to evaluate $\sigma^{*2}_{o\text{-comp}}$ quantitatively. For our subsequent numerical examples (Sec. 11.2), however, it is more convenient to consider minimum detectable signals and their associated processing gains.

9.3 Processing Gains and Minimum Detectable Signals

From (5.6), (5.10), and (5.30d), (5.32), and (5.33) in the composite cases, we obtain at once the processing gains Π^*. These are the coefficients

of $2\overline{a_o^2}$ and $2\overline{a_o^2}^2$, respectively, in (9.3), (9.5) above for the coherent and incoherent (optimum threshold) detectors, with these results applied to (5.33) to give Π^*_{comp}.

Our main interest, however, is the minimum detectable signals $\langle a_o^2\rangle^*_{min}$. With the help of (5.36) to replace σ_o^* in (5.6), (5.10) we have the following results:

I. Coherent Detection

$$\boxed{\langle a_o^2\rangle^*_{min\text{-}coh} = B^*_{NP}/(1-\eta)\, MNL^{(2)}H_1(N\Delta t\Delta\omega_d)}, \tag{9.27}$$

with an upper bound $x^*_{o\text{-}max}$ on $\langle a_o^2\rangle^*_{min}$ determined from (5.43), as discussed in Section 5.3 preceding, according to

$$\check{x}^*_{o\text{-}max} = \check{x}^*_o - (10 \text{ to } 15 \text{ db}) \tag{9.28}$$

[Here $(\check{})$ denotes decibels, e.g., $10\log_{10}x^*_{o\text{-}max}$, etc., and we shall take 10 db in (9.28) for the amount by which $x^*_{o\text{-}max}$ is to be less than x^*_o, (5.44).] Specifically, we have from (8.11) in (5.44), N>>1:

$$x^*_o\Big|^{(1,2)}_{no,slow} \doteq L^{(2)}\Big/\left|\frac{L^{(2,2)}}{2} - L^{(2)^2}\right|, \tag{9.28a}$$

$$x^*_o\Big|^{(1,2)}_{rapid} = L^{(2)}\Big/\left|\frac{L^{(2,2)}}{2} - (1-\eta)L^{(2)^2}\right|, \tag{9.28b}$$

for the various fading extremes, when, however, the signal is still coherently observed. The quantity B^*_{NP}, (5.3b), embodies the probability controls on the detection process.

II. Incoherent Detection

$$\boxed{\langle a_o^2\rangle^*_{min\text{-}inc} = \left\{8B^*_{NP}/MN\{L^{(4)} + 2L^{(2)^2}(MQ_N-1)\}\right\}^{\frac{1}{2}}.} \tag{9.29}$$

Here the upper bound $y^*_{o\text{-max}}$ on minimum detectable signal is given by

$$\check{y}^*_{o\text{-max}} = \check{y}^*_o - (10 \text{ to } 15 \text{ db}) \tag{9.30}$$

where y^*_o is obtained from (5.46). For the type of (sinusoidal) signals chosen here [cf. (8.2) and remarks at the beginning of Section 9], signal structure factors Q_N and R_N are independent of the array structure (m,m') for steered beams, so that (5.46) becomes

$$\boxed{y^*_o = \frac{L^{(4)} + 2L^{(2)^2}(MQ_N - 1)}{\left|\frac{L^{(6)}}{2} + 6L^{(2)}L^{(2,2)}MQ_N + L^{(2)^3}M^2R_N\right|}\,.} \tag{9.31}$$

The signal structure factor R_N, cf. (5.45b), reduces to various simpler forms when the signal is coherent or incoherent. [We consider here only these limiting cases (reserving to a later study evaluation of the intermediate forms based on the more general fading and doppler models (8.8), (8.11).] We therefore have (for the sinusoidal signals, (8.2), used here and large N):

1. Coherent Signal ($\Delta\omega_d = 0$)

$$R_N^{(1,2)}\Big|\begin{matrix}\text{(1,2-sided)}\\ \text{no, slow coh}\end{matrix} \doteq 4N/\pi \quad , \text{ cf. } \{\text{(A.2-42d), [12]}\}\ 2\omega_o\Delta t = \pi/2;\ \therefore \Delta t = 1/8f_o; \tag{9.32a}$$

$$R_N^{(2)}\Big|\begin{matrix}\text{2-sided}\\ \text{very rapid coh}\end{matrix} = 0, \qquad (\hat{m}_{|n-n'|}) = \delta_{nn'}; \tag{9.3ab}$$

$$\left.\begin{aligned} R_N^{(1)}\Big|\begin{matrix}\text{1-sided}\\ \text{very rapid coh}\end{matrix} &\doteq \frac{4N(1-\eta)^2}{\pi} - \eta(1-\eta)^2N^2\,; \\ &\doteq 0, \quad \text{very deep fading } (\eta = 1) \end{aligned}\right\} \tag{9.32c}$$

2. Incoherent Signal ($N\Delta\omega_d >> 0$)

$$R_N\Big|_{inc} = 0 \; ; \qquad \rho_{|n-n'|} = \delta_{nn'}, \text{ etc.} \tag{9.32d}$$

Accordingly, for incoherent signals ($\Delta\omega_d = 0$) R_N always vanishes and $Q_N = 1$, cf. (9.12), (9.19). Also, R_N can be negative for very rapid, one-sided fading ($\eta \neq 0$, $N >> 1$), cf. (9.32c), that is not too deep, i.e., $1-\eta > 0$. Usually, we expect very rapid fading to involve a large angle ($\phi_a > \pi/2$), so that (Re or Im $ae^{i\phi_a}$) is equally likely to be positive or negative, with the result that two-sided fading then occurs, so that $R_N = 0$, (9.32b). In other words, two-sided rapid fading is the much more probable physical model when fading is rapid.

Consequently we have for y_o^* the following relations:

1. Coherent Signal (no, slow, 1- and 2-sided fading)

$$y_o^*\Big|_{\substack{(1,2)\\ \underline{no,slow}\\ coh}} = \frac{L^{(4)} + L^{(2)^2} MN}{|L_2^{(6)} + 3L^{(2,2)}L^{(2)}MN + L^{(2)^3}M^2N\ 4/\pi|}, \quad \Delta\omega_d \doteq 0, \tag{9.33}$$

from (9.11), (9.20), and (9.32a), $N >> 1$.

2. Coherent Signal (rapid, 2-sided fading)

$$y_o^*\Big|_{\substack{(2)\\ \underline{rapid}\\ coh}} = \frac{L^{(4)} + 2L^{(2)^2}(M-1)}{|\frac{L^{(6)}}{2} + 6L^{(2)}L^{(2,2)}M|} \tag{9.34}$$

from (9.12), (9.32b). At the other extreme of incoherent signals, produced either by, or jointly by, very rapid fading and doppler "smear":

3. Incoherent Signal

$$y_o^*\Big|_{inc} = \frac{L^{(4)} + 2L^{(2)^2}(M-1)}{\left|\frac{L^{(6)}}{2} + 6ML^{(2)}L^{(2,2)}\right|} \tag{9.35}$$

cf. (9.12), (9.19), (9.32d), which is identical with (9.34): rapid, 2-sided fading, and/or doppler "smear," always destroys signal coherence. In fact, doppler "smear" by itself always insures that signal coherence is destroyed, not surprisingly. These results (9.33)-(9.35) are analogous to (9.28a,b) for the coherent signal cases.

A. $\langle a_o^2\rangle^*_{min\text{-}inc}$: Limiting Cases

We have the following specific results for the minimum detectable signals here (since $2L^{(2)^2} \sim L^{(4)}$, usually).

1. Coherent Signal (no, slow fading)

$$\boxed{\langle a_o^2\rangle^*_{min\text{-}inc}\Big|^{(1,2)}_{\substack{coh\\slow,no}} \doteq \frac{\sqrt{8B^*_{NP}}}{MNL^{(2)}}}, \qquad (N \gg 1);\ \Delta\omega_d \doteq 0 \tag{9.36}$$

from both one- and two-sided fading, from (9.11), (9.20) in (9.29).

2. Coherent Signal (rapid, one-sided fading)

$$\boxed{\langle a_o^2\rangle^*_{min\text{-}inc}\Big|^{(1)}_{\substack{coh\\rapid}} \doteq \frac{\sqrt{8B^*_{NP}}}{(1-\eta)MNL^{(2)}}}, \qquad (MN(1-\eta)^2 \gg 1),\ \Delta\omega_d \doteq 0 \tag{9.37}$$

from (9.18) in (9.29).

3. Coherent Signal (rapid, two-sided fading)

$$\boxed{\langle a_o^2 \rangle^*_{\text{min-inc}} \Big|^{(2)}_{\underline{\text{coh}}\ \underline{\text{rapid}}} \doteq \left\{ \frac{8B^*_{NP}}{MN[L^{(4)} + 2L^{(2)^2}(M-1)]} \right\}^{\frac{1}{2}}}, \qquad \Delta\omega_d \doteq 0 \tag{9.38}$$

from (9.12) in (9.29). As expected, this rapid, two-sided fading destroys signal coherence, cf. (9.34), (9.35), and (9.39)ff.

Similarly, from (9.12), (9.19) in (9.29), we get for incoherent signals (any fading):

4. Incoherent Signals [$(N\Delta\omega_d >> 0)$, any fading]

$$\langle a_o^2 \rangle^*_{\text{min-inc}} \Big|^{(1,2),\text{no}}_{\underline{\text{inc}}\ \underline{\text{any}}} \doteq \left[\frac{8B^*_{NP}}{MN\{L^{(4)} + 2L^{(2)^2}(M-1)\}} \right]^{\frac{1}{2}}$$

$$\left(\doteq \frac{2\sqrt{B^*_{NP}}}{L^{(2)}M\sqrt{N}}, \; M > 1 \right) \tag{9.39}$$

(when we use the approximation $L^{(4)} \sim 2L^{(2)^2}$). Equation (9.39), with doppler "smear," is the same as Case (3), (9.38) although the mechanism of destruction of the temporal signal coherence as manifest by the factor $N^{-\frac{1}{2}}$ in (9.39) is not the same. (This is not the case for one-sided rapid fading, since some signal coherence resides in $\overline{a_o^2}$ (>0), or $1 \geq 1-n > 0$.)

The expected dependence of $\langle a_o^2 \rangle^*_{\text{min-inc}}$ on $(MN)^{-1}$ is observed from (9.36), (9.37) when the signal waveform coherence in time (as well as in space here) is maintained. When temporal signal coherence is destroyed, cf. (9.38), (9.39), even though spatial coherence remains, $\langle a_o^2 \rangle^*_{\text{min-inc}}$ varies as $(MN)^{-\frac{1}{2}}$. In all cases, however, the reduction in $\langle a_o^2 \rangle^*_{\text{min}}$ is affected by the factor $(L^{(2)})^{-1}$ (with $2L^{(2)^2} \sim L^{(4)}$), cf. (9.36)-(9.39) [as well as (9.27)]: the larger the departure from gauss

noise ($L^{(2)}=1$, $L^{(4)}=2$, cf. Eq. A.1-22, [12]), the greater the decrease in this optimum minimum detectable signal. [This, incidentally, shows the well-known result that gauss interference is the worst type, i.e., requires the largest $\langle a_o^2\rangle^*_{min}$, against which the threshold detector--always properly optimized to the noise in question--must operate.] Finally, the bounds on $\langle a_o^2\rangle^*_{min\text{-}inc}$, cf. (9.30), are given by (9.31), as specialized by (9.33)-(9.35).

III. Composite Detection

From (5.32) and the processing gain for the coherent and incoherent detectors, obtained according to the first paragraph of Sec. 9.3 above, we find finally that now

$$\boxed{\langle a_o^2\rangle^*_{min\text{-}comp} = \frac{4(1-n)L^{(2)}H_1(N\Delta t\Delta\omega_d)}{(L^{(4)} + 2L^{(2)2}\{MQ_N-1\})}\left\{\sqrt{1 + \frac{B^*_{NP}\{L^{(4)} + 2L^{(2)2}(MQ_N-1)\}}{2(1-n)^2MNL^{(2)2}H_1^2(N\Delta t\Delta\omega_d)}} - 1\right\},} \tag{9.40}$$

where specifically

$$\pi^*_{coh}\,\hat{b}_{coh} = (1-n)MNL^{(2)}H_1(N\Delta t\Delta\omega_d)\ ; \qquad \hat{b}_{coh} = 1-n \tag{9.40a}$$

$$\pi^*_{inc}\,\hat{b}^2_{inc} = \frac{MN}{8}\,[L^{(4)} + 2L^{(2)2}\,(MQ_N-1)]; \quad \hat{b}_{inc} = 1 \tag{9.40b}$$

Applying (9.3a), (9.11), (9.12), (9.18)-(9.20) now to the general relation (9.40), for the specific special cases (1)-(4) above (II,A), we get directly the following results for the desired minimum detectable signals:

1. Coherent Signal (no, slow fading)

$$\boxed{\langle a_o^2\rangle^*_{min\text{-}comp}\Big|^{(1,2)}_{\substack{no,slow\\coh}} \doteq \frac{1}{MNL^{(2)}}\left\{\sqrt{8B^*_{NP} + 16(1-n)^2} - 4(1-n)\right\}} \tag{9.41a}$$

$$\doteq \{\sqrt{8B^*_{NP}} - 4(1-n)\}/MNL^{(2)}\ ;\quad N\gg1,\ B^*_{NP}\gg2(1-n)^2;\quad \Delta\omega_d \doteq 0 \tag{9.41b}$$

2. Coherent Signal (rapid, one-sided fading)

$$\langle a_o^2 \rangle^*_{\text{min-comp}} \Big|^{(1)}_{\underline{\text{rapid}}\ \text{coh}} \doteq \frac{1}{MNL^{(2)}(1-\eta)} \{\sqrt{8B^*_{NP} + 16} - 4\}$$

$$\doteq \{\sqrt{8B^*_{NP}} - 4\}/MNL^{(2)}(1-\eta), \quad N>>1, \quad B^*_{NP}>>2, \quad \Delta\omega_d \doteq 0 \ , \tag{9.42}$$

which shows the deleterious effects of fading $[\sim(1-\eta)^{-1}]$: deep(rapid) fading $(1-\eta \doteq 0)$ raises the minimum detectable signal by a consequently large factor $(1-\eta)^{-1}$, although the signal structure remains coherent since $\overline{a_o} > 0$ here in these one-sided cases.

3. Coherent Signal (rapid, two-sided fading)

$$\langle a_o^2 \rangle^*_{\text{min-comp}} \Big|^{(2)}_{\underline{\text{rapid}}\ \text{coh}} \doteq \frac{L^{(2)}}{L^{(4)} + 2L^{(2)^2}(M-1)} \cdot \left(\sqrt{\frac{8B^*_{NP}\{L^{(4)} + 2L^{(2)^2}(M-1)\}}{MNL^{(2)^2}} + 16(1-\eta)^2} - 4(1-\eta) \right) \tag{9.43a}$$

$$\doteq \frac{2}{ML^{(2)}} \left\{ \sqrt{\frac{B^*_{NP}}{N} + (1-\eta)^2} - (1-\eta) \right\}; \quad 2L^{(2)^2} \underset{M>1}{\approx} L^{(4)} \tag{9.43b}$$

$$\doteq B^*_{NP}/MNL^{(2)}(1-\eta), \quad M>1 \ . \tag{9.43c}$$

4. Incoherent Signal ($N\Delta\omega_d >> 0$); any fading

$$\langle a_o^2 \rangle^*_{\text{min-comp}} \Big|^{(1),(2)}_{\text{no slow}\ \underline{\text{rapid}}\ \text{inc}} \doteq \text{Eqs. (9.43a,b)}. \tag{9.44}$$

We note the contrasting behavior of (9.38), (9.39) for incoherent detection vis-à-vis that for composite detection (9.43), (9.44): if the fading is not too deep (i.e., 1-η not too small), the composite detector can be superior to the purely incoherent detector according to N^{-1} vs. $N^{-\frac{1}{2}}$, where N>>1, even though $B^*_{NP}>4$ for usual applications, cf. (5.3b). Similarly, (9.41) vs. (9.36), and (9.42) vs. (9.37), show the expected superiority (i.e., smaller $\langle a_o^2 \rangle^*_{min}$) of the composite detector over the incoherent detector. From (9.27) the coherent detector is seen to be sensitive to fading, whereas in the slow-fading situations both the incoherent and composite detectors, (9.36), (9.41), are not.

9.4 Remarks on Optimum Threshold Detectors in Gauss Noise

When the noise is entirely gaussian in time and space we can explicitly obtain the optimum threshold detector (2.6b) and usually evaluate its performance when the number of effectively independent samples J(=MN) is large. In general, the expansion in powers of the signal level θ , (2.66), of the log-likelihood ratio (2.6a) does not terminate, because of the statistical distributions of the signal parameters (amplitude, phase, etc.), vide (2.1). The likelihood ratio is only conditionally gaussian.*

The practical importance of the general gaussian situation, which can now include the effects of samples correlated in space and time (because we know the required pdf's of the noise), lies in the following:

1. There are occasions when the nongaussian component of the external interference is negligible, so that only the gaussian component of the ambient noise field is significant (in addition to receiver noise);
2. It may be possible to resolve, by sufficiently narrow beams [cf. Fig. 7.1], the individual interfering sources producing the nongaussian component, and thereby isolate them from the

---

* An exception, of course, is the academic special case of an entirely known signal, which can then be treated exactly for all signal levels.

desired signal emission. Then, it is this gaussian background which is the principal limiting noise.

In addition, by comparing the correlated and uncorrelated sampling in the gaussian situation, we can

3. Estimate the possible theoretical improvement in performance to be obtained by employing "dense" sampling (in the limit, continuous sampling) over the present "sparse," or independent, sampling used throughout the present general nongaussian treatment.

[However, from previous experience we may expect only small [$o(\leqslant$ db)] gains using dense sampling vs. "sparse" (i.e., independent) sampling, in the same data interval (in space and time). These gains are overwhelmed by the operational complexity of the associated "dense" algorithms vis-à-vis the (present) "sparse" ones. See remarks VII, Sec. 12.3 ff.]

Here we shall be content to outline the gaussian case. for later study. Thus, we begin with the general, normalized $J(=MN)^{\underline{th}}$-order pdf of noise alone

$$w_J(\underset{\sim}{x}) = \frac{e^{-\underset{\sim}{x}\underset{\sim}{k}_o^{-1}\underset{\sim}{x}}}{\sqrt{(2\pi)^n \det \underset{\sim}{k}_o}}; \quad \langle \underset{\sim}{x} \rangle = 0; \quad \underset{\sim}{k}_o \equiv \langle \underset{\sim}{x}\tilde{\underset{\sim}{x}} \rangle = \tilde{\underset{\sim}{k}}_o; \quad \langle \underset{\sim}{x}^2 \rangle = [1], \tag{9.45}$$

with $(\underset{\sim}{x},\underset{\sim}{k}_o)$ real, etc. From (9.45) in (2.8a) we readily obtain

$$\underset{\sim}{y} = -\underset{\sim}{k}_o^{-1}\underset{\sim}{x}; \quad \underset{\sim}{z} = -\underset{\sim}{k}_o^{-1}, \tag{9.46}$$

so that the general (optimum) threshold detector structure (2.6b) becomes explicitly

$$\boxed{g_J^* \Big|_{\text{gauss}} = (\log u + \hat{B}_J^*) + \theta_J \tilde{\underset{\sim}{x}}\underset{\sim}{k}_o^{-1}\bar{\underset{\sim}{s}}' + \frac{\theta_J^2}{2}\{\tilde{\underset{\sim}{x}}\underset{\sim}{k}_o^{-1}\underset{\sim}{k}_s'\underset{\sim}{k}_o^{-1}\underset{\sim}{x} - \text{trace } \underset{\sim}{\rho}_s'\underset{\sim}{k}_o^{-1}\}}, \tag{9.47}$$

where

$$\underset{\sim}{k}_s' \equiv \underset{\sim}{\rho}_s' - \bar{\underset{\sim}{s}}\tilde{\bar{\underset{\sim}{s}}}' = \langle \underset{\sim}{s}'\tilde{\underset{\sim}{s}}' \rangle - \bar{\underset{\sim}{s}}\tilde{\bar{\underset{\sim}{s}}}'. \tag{9.47a}$$

The bias, $\hat{B}_J^*$, as before, is found from

$$\hat{B}_J^*\Big|_{inc} = \langle\theta_4\rangle_0 = H_0\text{-average over } (\underset{\sim}{x}) \text{ in terms } o(\theta_J^4) \text{ in the expansion of (2.6) of } \log \Lambda_J; \tag{9.48a}$$

$$\hat{B}_J^*\Big|_{coh} = \langle\theta_2\rangle_0 = \frac{\theta_J^2}{2}\ \langle\tilde{\underset{\sim}{x}}\underset{\sim}{k}_0^{-1}\underset{\sim}{k}'_s\underset{\sim}{k}_0^{-1}\underset{\sim}{x} - \text{trace } \underset{\sim}{\rho}'_s\underset{\sim}{k}_0^{-1}\rangle_0\,, \tag{9.48b}$$

respectively for incoherent and coherent detection. Since

$$\langle\tilde{\underset{\sim}{x}}\underset{\sim}{k}_0^{-1}\underset{\sim}{k}'_s\underset{\sim}{k}_0^{-1}\underset{\sim}{x}\rangle_0 = \text{trace } \underset{\sim}{k}'_s\underset{\sim}{k}_0^{-1} = \text{trace } \underset{\sim}{\rho}'_s\underset{\sim}{k}_0^{-1} - \text{trace } (\bar{\underset{\sim}{s}}'\bar{\underset{\sim}{s}}'\underset{\sim}{k}_0^{-1})$$

by (9.7a), we find for the general optimum coherent (threshold) detector here

$$\boxed{g_J^*\Big|_{gauss\text{-}coh} = [\log \mu - \frac{\theta_J^2}{2}\ \text{trace } (\bar{\underset{\sim}{s}}'\bar{\underset{\sim}{s}}'\underset{\sim}{k}_0^{-1})] + \theta_J\ \tilde{\underset{\sim}{x}}\underset{\sim}{k}_0^{-1}\bar{\underset{\sim}{s}}'} \tag{9.49}$$

For the optimum incoherent threshold detector, $\bar{s}' = 0$, and (9.47) reduces to

$$\boxed{g_J^*\Big|_{gauss\text{-}inc} = \{\log \mu + \hat{B}_{inc}^*\} + \frac{\theta_J^2}{2}\ \{\tilde{\underset{\sim}{x}}\underset{\sim}{k}_0^{-1}\underset{\sim}{\rho}'_s\underset{\sim}{k}_0^{-1}\underset{\sim}{x} - \text{trace } \underset{\sim}{\rho}'_s\underset{\sim}{k}_0^{-1}\}} \tag{9.50}$$

(We reserve the explicit derivation of the bias for $g_J^*\big|_{gauss\text{-}inc}$ to a later study.) The associated composite detector is the sum of (9.49), (9.50), less $\log \mu$.

Equations (9.47) and (9.49) can be formally simplified if we use the "whitening" transformation

$$\underset{\sim}{s}_0 \equiv \underset{\sim}{k}_0^{-1}\underset{\sim}{s}' \tag{9.51}$$

e.g., $\underset{\sim}{k}_0$ onto $\underset{\sim}{k}_0^{-1} = \underset{\sim}{I}$ for the noise. Thus, (9.47) becomes

$$g_J^*\Big|_{gauss} = (\log \mu + \hat{B}_J^*) + \theta_J\ \tilde{\underset{\sim}{x}}\bar{\underset{\sim}{s}}_0 + \frac{\theta_J^2}{2}\ \{\tilde{\underset{\sim}{x}}\underset{\sim}{k}_{s_0}\underset{\sim}{x} - \text{trace } \underset{\sim}{k}_0\underset{\sim}{\rho}_0\},\ \underset{\sim}{\rho}_0 \equiv \langle\underset{\sim}{s}_0\tilde{\underset{\sim}{s}}_0\rangle, \tag{9.52}$$

and (9.49) reduces to the equivalent form

$$g_j^*\Big|_{\text{gauss-coh}} = \left[\log \mu - \frac{\theta_j^2}{2} \text{ trace } (\underset{\sim}{k}_o \bar{\underset{\sim}{s}}_o \bar{\underset{\sim}{s}}_o)\right] + \theta_j \tilde{\underset{\sim}{x}} \bar{\underset{\sim}{s}}_o \tag{9.53}$$

When the data samples are independent in space and (correlated) gaussian in time, we see that

$$\underset{\sim}{k}_o = \begin{bmatrix} \underset{\sim}{k}_o^{(1)} & & 0 \\ & \underset{\sim}{k}_o^{(2)} & \\ & & \ddots \\ 0 & & \underset{\sim}{k}_o^{(M)} \end{bmatrix}; \quad \therefore \underset{\sim}{k}_o^{-1} = \begin{bmatrix} \underset{\sim}{k}_o^{(1)^{-1}} & & 0 \\ & \ddots & \\ & & \\ 0 & & \underset{\sim}{k}_o^{(M)^{-1}} \end{bmatrix}. \tag{9.54}$$

When all (noise) samples are independent, $\underset{\sim}{k}_o = \delta_{jj'}$, $\underset{\sim}{k}_o^{-1} = \delta_{jj'}$, $\underset{\sim}{k}_o^{(m)} = \delta_{nn'}$, $m = 1, \ldots, M$, etc., and (9.47) [(9.49), (9.52)] all reduce, as expected, to our earlier results (cf. Sec. 6.2, [12]), e.g.,

$$g_j^*\Big|_{\text{gauss-coh-indep}} = (\log \mu - \frac{\theta_j^2}{2} \sum_j \bar{s}_j'^2) + \theta_j \tilde{\underset{\sim}{x}} \bar{\underset{\sim}{s}}' \ , \tag{9.55}$$

with corresponding relations for the incoherent and composite cases. The important point here is that we can use (9.49) (and (9.47)), and their appropriate statistics, in comparison with (9.55), etc., to obtain measures of the improvement in performance to be gained by employing "dense" or correlated samples, vis-à-vis "sparse" (independent) sampling. (This is reserved for a subsequent study.)

Section 10. Suboptimum Detectors

In practice we cannot readily construct the indicated optimum (threshold) algorithms [cf. Sec. 8]. Instead, we may employ a variety of suboptimum detectors. Among these are (1), the simple correlator, or familiar "matched-filter" detector, which is optimum in gauss noise, cf. Sec. 9.4, and with the proper bias; (2), the clipper-correlator, which employs a

hard-limiter (i.e., "super-clipper") before the correlation operation. This latter is known to be (threshold) optimum against Laplace noise, e.g.,

$$\text{(i)}\quad \underline{\text{Laplace Noise}}: \quad w_1(x)_{\text{clip-corr}} = \frac{1}{\sqrt{2}}\, e^{-|x|\sqrt{2}};\ \ \overline{x^2}=1;\ \ \bar{x}=0\ ; \tag{10.1a}$$

$$\text{(ii)}\quad \underline{\text{Gauss Noise}}: \quad w_1(x)_{\text{simple-corr}} = \frac{1}{\sqrt{2\pi}}\, e^{-x^2/2};\ \overline{x^2}=1;\ \bar{x}=0\ , \tag{10.1b}$$

cf. Sec. A.4-1, D, [12], for independent sampling. An important practical task is to compare the performance of such generally suboptimum algorithms against the theoretical optimum for the actual (usually nongauss or nonLaplacian) noise. This permits us to estimate the degradation in performance vis-à-vis the optimum and to assess whether or not we should strive for a closer approximation of our algorithm to the theoretical limit.

Let us apply the pertinent results of [12] to the specific signal cases of Sec. 8 earlier, regarding the above two types of suboptimum algorithm. The conditions of Sec. 8.1 apply throughout. Thus, in Section 11, for a typical signal and noise example, we shall compare performances with the corresponding, limiting optimum cases.

10.1 The Simple Correlator

The algorithm in question is obtained from (8.4) with $\ell(x_{mn}) \to -x_{mn}$, with a bias where $L^{(2)}=1$, cf. (9.4) (cf. Sec. A.4-1, D, [12]). The result here is

1. Coherent Detection (Cross-Correlator)

$$g_{\text{coh}}\Big|_{\text{corr}} = \{\log \mu - \overline{a_o^2}\,(1-\eta)MNH_1(N\Delta t\Delta\omega_d)\} + \sqrt{2}\,\overline{a_o}\ \sum_m \sum_n x_{mn} e^{-(n\Delta\omega_d\Delta t)^2/2}\ . \tag{10.2}$$

This algorithm is threshold optimum in gauss noise, for the particular

class of signals obeying (8.1), (8.2), which are pertinent to our study here.

For performance, the corresponding minimum detectable signal is

$$\langle a_o^2 \rangle_{\text{min-coh}}\Big|_{\text{correl}} = B_{NP}^* \,/\, (1-\eta)MNH_1(N\Delta t \Delta\omega_d)\,, \tag{10.3}$$

cf. (9.27), so that the degradation factor, Φ_d^*, is defined by, and is specifically

$$\boxed{\langle a_o^2 \rangle_{\text{min-coh}} \equiv \Phi_d^*\Big|_{\text{coh-corr}} \cdot \langle a_o^2 \rangle_{\text{min-coh}}\Big|_{\text{corr}}\,, \text{ or}} \tag{10.4a}$$

$$\boxed{(1\geqslant)\ \Phi_d^*\Big|_{\text{coh-corr}} = 1/L^{(2)} \quad (>0),\ (=\pi_{\text{coh-corr}}/\pi^*_{\text{coh}}),} \tag{10.4b}$$

cf. Sec. 7.4 of [12]. This degradation factor measures the amount by which the minimum detectable signal of the simple correlator is increased over that of the corresponding, optimum (threshold) detector, when the noise is nongaussian and everything else in the detection process remains unaltered, i.e., same probability controls, sample sizes, etc. [In the gauss case, of course, $L^{(2)} = 1.$ and $\Phi_d^* = 1$: the simple correlator is now (threshold) optimum.] Note that Φ_d is independent of sample size here and depends only on the statistics of the noise ($\sim L^{(2)}$).

Similarly, we have from (8.13) [now with $\ell_{m,n} \to -x_{mn}$, $\ell'_{m,n} = -1$], and $L^{(2)} \to 1$, $L^{(4)} \to 2$, cf. (9.13):

2. Incoherent Detection (Auto-Correlator)

$$g_{\text{inc-corr}} = \{\log \mu - \frac{\overline{a_o^2}^2 M^2 N}{4} Q_N\} + \frac{\overline{a_o^2}}{2} \sum_{mm'} \sum_{nn'} (x_{mn}x_{m'n'} - \delta_{mm'}\delta_{nn'}) \cdot \hat{m}_{|n-n'|}\rho_{|n-n'|} \tag{10.5}$$

for these coherent wavefronts, desired signal waveforms (8.2), and steered

beams, subject to (8.8)-(8.11) for $\hat{m}$, ρ. Again, this algorithm is threshold optimum in gauss noise. The degradation factor here is defined once more by

$$\langle a_o^2 \rangle^*_{\text{min-inc}} \equiv \Phi_d^* \Big|_{\text{inc-corr}} \cdot \langle a_o^2 \rangle_{\text{min-inc}} \Big|_{\text{corr}} \tag{10.6a}$$

cf. (10.4a), where now specifically (as the extension of (6.38), [12], to $M \geq 1$ independent spatial samples):

$$\boxed{\begin{aligned} \Phi_d^* \Big|_{\text{inc-corr}} &= 4M^2 Q_N^2 \Big/ \left[(\overline{x^4} - 1) + 2(MQ_N - 1) \mathrm{I\!I} L^{(4)} + 2L^{(2)^2} (MQ_N - 1) \right] \\ &= \mathrm{I\!I}_{\text{inc,corr}} \; / \; \mathrm{I\!I}^*_{\text{inc}} \end{aligned}} \tag{10.6b}$$

with an evident dependence on sample size (M,N). (Again, we note that for gauss noise, $\overline{x^4} = 3$ and $L^{(2)} = 1$, $L^{(4)} = 2$, so that $\Phi_d^* \Big|_{\text{inc-corr}} = 1$, as required: the <u>autocorrelator</u> represented by (10.5) is threshold optimum in gauss noise, and, of course, suboptimum in any other.)

As an example, we have for a <u>coherent (sinusoidal) signal</u> ($N\Delta\omega_d \doteq 0$), <u>with no or slow fading</u> [(1), (2)-sided], so that $Q_N \doteq N/2$, cf. (9.11), (9.20),

$$\Phi_d^* \Big|_{\text{inc-corr}} \doteq (1/L^{(2)})^2 , \tag{10.6c}$$

where we have used the fact that $L^{(4)} \approx 2L^{(2)^2}$. Again, in this important limiting case, Φ_d^* is independent of sample size, cf. (10.4b). Note also that Φ_d^* (10.6b), is canonical in the signal waveform, like (10.4b).

<u>3. The Composite Detector</u> (Correlator Sums)

Since here we have generally, in terms of the processing gains (cf. Sec. 5.2),

$$\Phi_d^* \equiv \mathrm{I\!I}/\mathrm{I\!I}^* , \tag{10.7a}$$

we can obtain the degradation factor for the composite detector from

$$\Phi^*_{comp} \equiv \Pi_{comp}/\Pi^*_{comp} = \left[\langle a_o^2\rangle^*_{min\text{-}comp} \Big/ \langle a_o^2\rangle_{min\text{-}comp}\right] \tag{10.7b}$$

where Π_{comp}, Π^*_{comp} are obtained from (5.33), on replacing Π^*_{coh} by Π_{coh}, etc. therein, for the suboptimum cases. Here Π^*_{coh}, Π^*_{inc} are given by (9.3), (9.5), so that Π_{coh}, Π_{inc} are found here from (10.4b), (10.6b) in (10.7a) to be

$$\Pi_{coh\text{-}corr} = MNH_1; \qquad \Pi_{inc\text{-}corr} = \frac{M^3NQ_N^2/2}{(\overline{x^4}-1) + 2(MQ_N-1)} . \tag{10.8}$$

From (5.33) and (10.7b) we have finally the composite degradation factor, relating the minimum detectable signals according to (10.7b):

$$\boxed{\Phi^*_{d\text{-}comp}\Big|_{corr} = \left(\frac{\Phi^*_{d\text{-}inc}\ _{corr}}{\Phi^*_{d\text{-}coh}\ _{corr}}\right)^2 \left(\frac{\sqrt{1 + \dfrac{4B^*_{NP}\Pi^*_{inc}}{[\Pi^*_{coh}(1-\eta)]^2}} - 1}{\sqrt{1 + \dfrac{4B^*_{NP}\Pi_{inc}}{\Pi^2_{coh}(1-\eta)^2}} - 1}\right)^2_{corr}} , \tag{10.9}$$

with

$$\Pi^*_{inc} \Big/ \Pi^{*2}_{coh} = \frac{L^{(4)} + 2L^{(2)^2}(MQ_N-1)}{8MNH_1^2L^{(2)^2}} \tag{10.9a}$$

$$\Pi_{inc} \Big/ \Pi^2_{coh}\Big|_{corr} = \frac{M}{2NH_1^2} \frac{Q_N^2}{[(\overline{x^4}-1) + 2(MQ_N-1)]} \tag{10.9b}$$

from (9.3), (9.5), (10.8), exhibiting, in general, dependence on sample size (M,N). (When the noise is gaussian, both (10.9a,b) reduce to $Q_N/4NH_1^2$, and, of course, $\Phi^*_{d\text{-}comp}\big|_{corr} = 1$, as required.) Like (10.6b), Φ^*_d here is also canonical in the signal waveform.

In the previous example [of a coherent sinusoidal signal with no or slow (1,2)-sided fading] we find that (10.9a,b) reduces to $1/8H_1^2$ ($\overline{x^4} << MN$), and so (10.9), with the help of (10.4b), (10.6c), becomes the particularly simple result

$$\Phi^*_{\text{d-comp}}\Big|_{\text{corr}} \doteq (1/L^{(2)})^2, \qquad N >> 1 \tag{10.10}$$

here, cf. (10.6c). Once more, in this limiting situation, the degradation factor is independent of sample size (~MN).

Finally, we note again that the (suboptimum) composite correlation algorithm here is simply the sum of (10.2) and (10.5), less log μ.

10.2 The Clipper-Correlator

Here a hard limiter is used, preceding the correlation operation. From Sec, A.4-31, [12], we find for the signal class (8.2) that (8.4) now is modified by setting $\ell_{m,n} = -\sqrt{2}\ \text{sgn}\ x_{mn}$, and $L^{(2)}$ is replaced by $\sqrt{2}\ w_1(0)$, where $w_1(0)$ is the (1st-order) pdf of the interference. The result is now the suboptimum algorithm:

1. Coherent Detection

$$g_{\text{coh}}\Big|_{\text{clip}} = \log \mu - \sqrt{2}\ \overline{a_o^2}\ (1-\eta)MNH_1(N\Delta t\Delta\omega_d)w_1(0) + \sqrt{2}\ [\overline{a_o^2}(1-\eta)]^{1/2} \sum_m \sum_n \text{sgn}\ x_{mn}\ e^{-(n\Delta\omega_d\Delta t)^2/2}, \tag{10.11}$$

cf. (10.2) for the simple correlator above. [It has been shown (Sec. A.4-1, II, D, [12]) that $g_{\text{coh}}|_{\text{clip}}$, (10.11), is threshold optimum when the noise is Laplacian, e.g., $w_1(x)$ obeys (10.1a).] The degradation factor here is found to be (cf. Table 6.2, VI, [12])

$$\boxed{\Phi^*_{\text{d}}\Big|_{\text{coh-clip}} = 4w_1(0)^2/L^{(2)}, \quad (>0) \quad (\equiv \Pi_{\text{coh}}/\Pi^*_{\text{coh}})} \tag{10.12a}$$

where

$$\langle a_o^2 \rangle^*_{\text{min-coh}} = [\Phi^*_{\text{d-coh}} \langle a_o^2 \rangle_{\text{coh}}]_{\text{clip}}. \tag{10.12b}$$

[In Laplace noise (10.1a) we have $L^{(2)} \to 4w_1(0)^2$, $w_1(0) = 1/\sqrt{2}$, so that $\Phi^*_{\text{d-coh}|\text{clip}} \to 1$, as required, since then the algorithm (10.11) is threshold optimum in this noise.] Note once more that the degradation factor here is independent of sample size, cf. (10.4b), and is canonical in the signal waveform.

Similarly, we have from (8.13) (now with $\ell_{m,n} \to -\sqrt{2}\ \text{sgn}\ x_{m,n}$, {and the term $\ell'_{m,n}$ omitted because it is not physically realizable [vide pp. A100, A101, [12]}]), and (A.4-66b), [12], for the bias, the algorithm for the following incoherent clipper correlator.

2. Incoherent Detection

$$g_{\text{inc-clip}} = \log \mu + \hat{B}'_{\text{inc}}\Big|_{\text{clip}} + \overline{a_o^2} \sum_{mm'}^{M} \sum_{nn'}^{N} \hat{m}_{|n-n'|} \rho_{|n-n'|} \text{sgn}\ x_{mn}\ \text{sgn}\ x_{m'n'}, \tag{10.13}$$

again for these coherent wavefronts, selected signal waveforms (8.2), and steered beams, where now (8.8)-(8.11) apply specifically for $\hat{m}_{|n-n'|}$, $\rho_{|n-n'|}$. The bias here is

$$\hat{B}'_{\text{inc}}\Big|_{\text{clip}} = -\{(1-\sqrt{2}\ w_1(0)\ \overline{a_o^2}\ MN + \frac{1}{4} \sum_{mm'} \sum_{nn'} \{8w_1(0)^2$$

$$-[\sqrt{2}\ w_1''(0) + 8w_1(0)^2]\delta_{mm'}\delta_{nn'}\} \cdot \hat{m}^2_{|n-n'|}\ \rho^2_{|n-n'|}\}. \tag{10.14}$$

From Table 6.2, VI, [12] extended to include the M independent spatial samples, we can write finally the desired degradation factor here as

$$\boxed{\Phi^*_{\text{d-inc}}\Big|_{\text{clip}} = \frac{\{-\sqrt{2}w_1''(0) + 8w_1(0)^2(MQ_N-1)\}^2}{\{1 + 2(MQ_N-1)\}\{L^{(4)} + 2L^{(2)2}(MQ_N-1)\}}\ (=\Pi_{\text{inc-clip}}/\Pi^*_{\text{inc}}).} \tag{10.15}$$

Unlike the coherent cases (10.4b), (10.12a) the degradation factor now depends on sample size, generally, but remains canonical in the signal waveform. [When the noise is Laplacian, we use $w_1(0) = 1/\sqrt{2}$, $w_1''(0) = -\sqrt{2}$, $L^{(2)} = 2$, $L^{(4)} = 4$, cf. A.4-65a,b, dropping the δ-function factors as physically unrealizable, cf. pp. A100, A101, [12]. Thus, the degradation factor (10.15) reduces to unity, as it should.] The incoherent clipper-correlator (10.13) is generally suboptimum, of course, unless the noise is Laplacian, cf. (10.1a).

As an example, we take again the coherent sinusoidal signal ($N\Delta\omega_d \doteq 0$), with no or (1,2-sided) slow fading, where again $Q_N \doteq N/2$, and find that (10.15) reduces to

$$\Phi^*_{d\text{-inc}}\Big|_{clip} \doteq [4w_1(0)^2/L^{(2)}]^2, \qquad N >> 1, \tag{10.16}$$

cf. (10.6c), where we again used the fact that $L^{(4)} = 2L^{(2)^2}$.

3. The Composite Detector

Here we use the general form (10.9), observing that $\Phi^*_d \to \Phi^*_{d\text{-}(\ )}\big|_{clip}$ and that

$$\Pi_{coh\text{-}clip} = 4w_1(0)^2 MNH_1; \quad \Pi_{inc\text{-}clip} = \frac{MN[-\sqrt{2}w_1''(0) + 8w_1(0)^2(MQ_N-1)]^2}{8\{1 + 2(MQ_N-1)\}}. \tag{10.17a}$$

We also have from (9.3) and (9.5)

$$\Pi^*_{coh} = MNL^{(2)}H_1; \quad \Pi^*_{inc} = \frac{MN}{8}\{L^{(4)} + 2L^{(2)^2}(MQ_N-1)\} \tag{10.17b}$$

so that

$$\Pi^*_{inc}/\Pi^{*2}_{coh} = \frac{L^{(4)} + 2L^{(2)^2}(MQ_N-1)}{8MNL^{(2)^2}H_1^2}, \quad \text{cf. (10.9a)} \tag{10.18a}$$

$$\Pi_{inc}/\Pi^2_{coh}\Big|_{clip} = \frac{[-\sqrt{2}w_1''(0) + 8w_1(0)^2(MQ_N-1)]^2}{\{1 + 2(MQ_N-1)\}MNH_1^2 \cdot 128w_1(0)^4}, \tag{10.18b}$$

to be used in (10.9), in conjunction with (10.12a), (10.15). Again, the degradation factor here generally depends on sample size, but is once more canonical in signal waveform.

For the preceding example of the coherent sinusoidal signal, subject to no, or (1,2)-sided slow fading, we find that

$$\Phi^{*}_{\text{d-comp}}\Big|_{\text{clip}} \doteq \left\{\frac{4w_1(0)^2}{L^{(2)}}\right\}^2, \qquad N >> 1, \tag{10.19}$$

cf. (10.16) above. In this limiting situation the degradation factor for composite detection is again invariant of sample-size (as long as N>>1), but does depend (weakly) on signal waveform.

Finally, we can use the results of Secs. 10.1, 10.2 directly to compare the generally suboptimum systems embodied in the simple- and clipper-correlators above. We have

$$\Phi_{\text{d-}(\quad)}\Big|_{\frac{\text{corr}}{\text{clip}}} \equiv \frac{\Phi^{*}_{\text{d-}(\quad)}\big|_{\text{corr}}}{\Phi^{*}_{\text{d-}(\quad)}\big|_{\text{clip}}} = \left\{\Phi_{\text{d-}(\quad)}\Big|_{\frac{\text{clip}}{\text{corr}}}\right\}^{-1}, \tag{10.20}$$

where specifically we use (10.4b), (10.6b), (10.9), in the simple correlator cases, and (10.12a), (10.15), and (10.19) adapted to these above clipper-correlators, through (10.17a)-(10.18b). For our common, limiting example of the coherent sinusoid (N>>1), we readily find that

$$\Phi_{\text{d-coh}}\Big|_{\frac{\text{corr}}{\text{clip}}} \doteq [4w_1(0)^2]^{-1}; \quad \Phi_{\text{d-inc}}\Big|_{\frac{\text{corr}}{\text{clip}}} \doteq [4w_1(0)^2]^{-2} = \Phi_{\text{d-comp}}\Big|_{\frac{\text{corr}}{\text{clip}}}. \tag{10.21}$$

These relations show by how much the minimum detectable signal for the simple correlators is increased vis-à-vis that of the clipper-correlators, for the various detection modes (coherent, incoherent, and composite).

Section 11. Numerical Examples

In this Section we use the results of Secs. 9, 10 to evaluate (threshold) detector performance for a variety of typical (or possible) operating conditions.

The signal in question is the sinusoidal waveform (6.30), obeying the conditions (8.1), cf. Sec. 8.1, with the various fading and doppler-spread effects described in Secs. 8.2-8.4 earlier. A typical time waveform with interfering signal(s) (= Class A noise) and (gaussian) ambient noise (as it is received and emitted by the $m^{\underline{th}}$-element in the receiving array [cf. Fig. 6.2]) is sketched in Fig. 11.1 below:

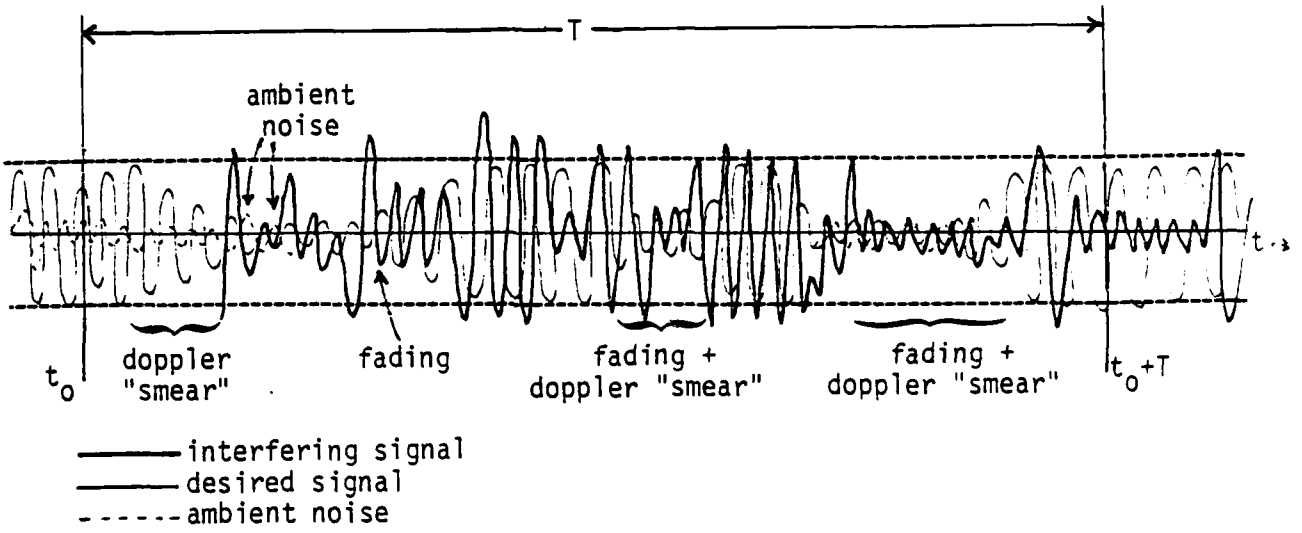

Figure 11.1 A typical received waveform (at array-element $\underline{m}$) over the period (t_o, t_o+T), showing desired, interfering (Class A) signal(s), and ambient background noise.

The ambient gaussian background is usually much less intense than the structured, nongaussian signal interference, which in turn can be much stronger than the desired signal. The structural interference is Class A noise.

11.1 Numerical Operating Conditions

Our numerical examples are obtained for the following operating conditions:

(i). $p_D^{(*)} = 0.90$: 90% probability of correctly detecting the desired signal, if it is present;
$= 0.50$: 50% probability of correctly detecting the desired signal, if it is present; (11.1a)

(ii). $\alpha_F^{(*)} = 10^{-2}$: false-alarm probability (not so small as to lose desired signals, nor so large as to create excessive false alarms); (11.1b)

(iii). $N = 10^2, 10^3$: "time-bandwidth products" or numbers of temporally independent noise samples; (11.1c)

(iv.) $M = 1, 10, 100$: number of (independent) array elements: (spatial independence); (11.1d)

(v.) Class A Interference (I) :

$A_A = 0.3$: (typical, highly structured, cw interference, mainly from ships, some biological sources, etc.);

$\Gamma_A' = 10^{-3}$: gauss background 30 db below maximum average interfering signal level; (11.1e)

Class A Interference (II) :

$A_A = 5.0$: (dense, nearly gaussian interference caused by many overlapping signals);

$\Gamma_A' = 10^{-3}$: (same relative level of ambient gaussian background noise). (11.1f)

With these choices of interference parameters we find from the figures and calculations† of [12] the following associated statistical parameters needed for the evaluation of the performance measures developed in Secs. 9, 10 preceding:

Fig. 7.5, [12]: $B^*_{NP|0.9} = 8.2$ db $(=6.61)$; $B^*_{NP|0.5} = 4.4$ db $(=2.75)$; $\alpha_F^{(*)} = 10^{-2}$. (11.2)

---

† The statistics $L^{(2)}$, $L^{(4)}$, etc., given in (11.3) are computed from strictly or approximately canonical Class A distributions (pdf's), which preliminary calculations indicate are not appreciably different when quasi-canonical Class A models are employed ($\alpha_o << 1$). See footnote, p. 134, [12]; also [6].

	Case I: (11.1e)	Case II: (11.1f)	
Fig. 7.7, [12]:	$L_A^{(2)} = 28.0$ db	= 1.9 db	
Fig. 7.8, [12]:	$L_A^{(4)} = 60.0$ db	= 26.8 db	(11.3)
Fig. 7.9, [12]:	$L_A^{(2,2)} = 63.0$ db	= 11.7 db	
Fig. 7.10, [12]:	$L_A^{(6)} = 94.0$ db	=-43.0 db	
Fig. 7.25, [12]:	$w_1(0)_{A+G} = 8.6$	= 0.58 .	(11.4)

Next, we assume the following fading conditions:

(i). "rapid, two-sided fading": "rapid," in the sense of fading one or more times in the observation period (t_o, t_o+T), as sketched in Fig. 11.1. [If the fading is "rapid," it is usually two-sided $0 \leq \phi_a \leq \pi$ at least.] This effectively destroys the temporal coherence of the signal waveform when reception is coherent, cf. remarks leading to (9.12) et seq., but does not do so if signal epoch is known or tracked at the receiver, so that coherent reception is possible, cf. (9.4) et seq. (11.5)

(ii). "slow fading": signal level does not change during (t_o, t_o+T), whether the fading is one- or two-sided. What can be important is the depth of fading, embodied in the factor $(1-\eta)$, cf. (9.3), (9.4), (9.18), (9.24), (9.25), and (9.27), (9.37), (9.40)-(9.44) above. The signal, however, retains its coherent structure (vis-à-vis fading) under incoherent reception. (11.6)

Here we shall consider the following fading levels:

$1 - \eta = 1$ (0 db, no fading);
$= 10^{-1}$ (-10 db, some fading);
$= 10^{-3}$ (-30 db, strong fading ≈ gauss background noise). (11.7)

There remain the effects of "doppler-smear." These can be quite serious, if the signal frequency is at all high and the (rms) doppler spread is not

negligible, as the sample calculations below indicate. For example, let us suppose, typically, that

$$f_o = 10^2 \text{ Hz: signal frequency;} \quad T_o = 10^2\text{-}10^3 \text{ seconds,} \tag{11.8}$$

so that (since 1 knot = 0.51 m/sec) we have (cf. (8.3)) for the "doppler-spread"

$$\Delta\omega_d = \Delta v \frac{\omega_o}{c_o} = (\Delta v)\ 4.19 \cdot 10^{-1}\ (\text{Hz}); \quad c_o = 1.5 \cdot 10^3 \text{ m/sec}. \tag{11.9}$$

Accordingly, [cf. (9.3), (9.10), (9.17b)], we find that the doppler-spread parameter here is

$$\boxed{T_o\Delta\omega_d = (T_o\Delta v)\ 4.19 \cdot 10^{-1}}, \quad \text{for } f_o = 10^2 \text{ Hz}. \tag{11.10}$$

Representative values range from:

(1). $\Delta v = 0$: <u>no doppler spread</u>, either because of no medium effects and/or no doppler smearing due to irregular source motion; (here the signal source is assumed to be tracked, so that any deterministic doppler component is removed); (11.11a)

(2). $\Delta v = 0.1$ kt $= 0.051$ m/sec; (11.11b)

(3). $\Delta v > 0.1$ kt. (11.11c)

In case (1), (11.11a), $T_o\Delta\omega_d = 0$ and $H_1 = 1$, (9.3a), $\Phi_2(0) = 1/2$, (9.17b): there is, as expected, no degradation in performance attribution to "doppler-smear." On the other hand, with (11.11b), we get here

$$\left.\begin{aligned} T_o\Delta\omega_d &= (10^2 \text{ sec})\ (4.19 \cdot 10^{-2}) = 4.19: \quad H_1(4.19) = 0.21\ (= -7 \text{ db}) \\ T_o\Delta\omega_d &= (10^3 \text{ sec})\ (4.19 \cdot 10^{-2}) = 41.9: \quad H_1(41.9) = 0.021\ (= -17 \text{ db}) \end{aligned}\right\} \tag{11.12}$$

Thus, for this frequency (f_o) and these observation times (T_o), there is noticeable to large degradation [$H_1 << 1$] caused by the random doppler component (Δv), which though small, exerts a cumulative effect as the observation period is increased. Basically, the doppler-smear destroys

waveform coherence. Some typical values of $H_1(x)$, $x = T_o\Delta\omega_d$, are

$$H_1(1) = 0.75; \quad H_1(2) = 0.44; \quad H_1(3) = 0.30; \quad \text{etc.} \tag{11.13}$$

cf. (9.3a). In fact, $H_1(x) \sim 1/x$, $x \to \infty$.

Finally, we shall need the performance "bounds" (x_o^*, y_o^*), (9.28a, b); (9.31), (9.34), (9.35), in the optimum threshold cases, particularly. For the values of M, N, n, and the Class A noise chosen here, (11.1)-(11.4), etc., we have [cf. (9.28a, b)]

$$(x_o^*)^{(1,2)}_{\text{no,slow}} = -29.8 \text{ db}: \quad (n = 0), \text{ all } M,N > 1 \qquad \underline{\text{Case I}}; \tag{11.14a}$$

$$(x_o^*)^{(1,2)}_{\text{no,rapid}} = \begin{matrix} -29.8 \text{ db}: & (n = 0), \text{ all } M,N = 10^2\text{-}10^5 \\ -32 \text{ db}: & (n = 10^{-3}), \text{ all } MN = 10^2\text{-}10^5 \end{matrix} \quad \underline{\text{Case I}}; \tag{11.14b}$$

$$(x_o^*)^{(1,2)}_{\text{no,slow}} = -3.1 \text{ db}: \quad (n = 0), \text{ all } MN > 1 \qquad \underline{\text{Case II}}; \tag{11.14c}$$

$$(x_o^*)^{(1,2)}_{\text{no,rapid}} = \begin{matrix} -3.1 \text{ db}: & (n = 0), \\ -6.8 \text{ db}: & (n = 10^{-3}), \text{ all } MN = 10^2 \end{matrix} \quad \underline{\text{Case II}}. \tag{11.14d}$$

In a similar way, we obtain y_o^* for the various incoherent cases, from (9.33)-(9.35):

$$(y_o^*)^{(1,2)}\Big|_{\substack{\text{no,slow} \\ \text{coh}}} \begin{matrix} = -20.0, -40.0 \text{ db}; & M = 1; \\ & N = 10^2, 10^3 \\ = -41 \text{ db}; & M = 10 \\ & N = 10^2, 10^3 \\ = -48.0 \text{ db}; & M = 10^2 \\ & N = 10^2, 10^3 \end{matrix} \Bigg\} \underline{\text{Case I}}; \tag{11.15a}$$

$$(y_o^*)^{(1,2)}\Big|_{\substack{\text{rapid} \\ \text{and/or} \\ \text{incoh-sig}}} \begin{matrix} = -39.0 \text{ db}; & M = 1, \text{ all } N \\ = -40.0 \text{ db}; & M = 10, 10^2 \\ & \text{all } N \end{matrix} \Bigg\} \underline{\text{Case I}}; \tag{11.15b}$$

$$(y_o^*)^{(1,2)}\Big|_{\substack{\text{no,slow}\\ \text{coh.}}} \left.\begin{array}{ll} = 4.9 \text{ db}; & M = 1 \\ & N = 10^2\text{-}10^3 \\ = -5.0 \text{ to } -3.0 \text{ db}; & M = 10\text{-}10^2 \\ & N = 10^2\text{-}10^3 \end{array}\right\} \underline{\text{Case II}}. \qquad (11.15c)$$

With these numerical results above, we are ready to obtain the desired minimum detectable signals, derived analytically in Sec. 9.3 preceding.

11.2 Minimum Detectable Signals: Examples†

From I, Sec. 9.3, Eq. (9.27), we obtain the following numerical results, for the situations of Sec. 11.1 above. We have (with negligible "doppler-smear," e.g., $H_1(0) = 1$, cf. (11.11) et seq.) for coherent reception (Case I):

A. Coherent Detection, Case I

$$\langle a_o^2 \rangle^*_{\text{min-coh}}\Big|_{\substack{p_D^* = 0.95\\ \Delta v = 0}} \text{db} = -19.8 - (1\check{-}\eta) - (\check{M}\check{N}):$$

	$(1\check{-}\eta)$	$\check{M}$	$\check{N}$	$\check{N}$	$N=10^2$	$N=10^3$	
(1),	$= -19.8 -$ 0	0	-20	-30	$= \begin{Bmatrix}-39.8\\ -29.8\\ -9.8\end{Bmatrix}$	$\begin{Bmatrix}-49.8\\ -39.8\\ -29.8\end{Bmatrix}$	
(2),	$= -19.8 - \left\{\begin{matrix}\\ +10\\ \\ \end{matrix}\right\}$	-10	-20	-30	$= \begin{Bmatrix}-49.8\\ -39.8\\ -19.8\end{Bmatrix}$	$\begin{Bmatrix}-59.8\\ -49.8\\ -29.8\end{Bmatrix}$	(11.16)
(3),	$= -19.8 -$ +30	-20	-20	-30	$= \begin{Bmatrix}-59.8\\ -49.8\\ -39.8\end{Bmatrix}$	$\begin{Bmatrix}-69.8\\ -59.8\\ -39.8\end{Bmatrix}$	

---

† We use the symbol ($\check{}$) to denote decibels, i.e., $\check{A} = 10 \log_{10} A$ (db).

This includes all fading types, as long as waveform coherence is maintained. If there is noticeable "doppler-smear," cf. (11.12), we add $-\check{H}_1(db)$: for example, in the case of $T_o = 10^2$ seconds observation time, $-\check{H}_1 = +7.0$ db, and (1) in (11.16) becomes -32.8 db ($N=10^2$), -42.8 db ($N=10^3$). (With $p_D^* = 0.50$, we replace -19.8 db in (11.16) by -23.6, thus subtracting 3.2 db from these results.)

Using (9.28) and the 10 db increment therein between $x^*_{o\text{-}max}$ and x^*_o, we see from (11.14a, b) that in all cases of no fading, slow, and rapid fading (except for deep fading: $n=10^{-3}$) and negligible doppler, the bound $\langle a_o^2 \rangle^*_{min} \leq x^*_{o\text{-}min}$ is satisfied. For the deep fading conditions in (11.14a, b), $x^*_{o\text{-}max}$ is exceeded, by small amounts. With a small excess the equal variance condition $[(\sigma^*_o)^2 \doteq (\sigma^*_1)^2]$ is not too seriously violated, so that we can still regard the algorithms as effectively (asymptotically) threshold optimum, and the evaluation of performance according to Secs. 9.1, 9.2 (where $(\sigma^*_1)^2 \doteq (\sigma^*_o)^2$) as essentially correct. [On the other hand, when the bound $x^*_{o\text{-}max}$ is noticeably exceeded, these performance measures can be correspondingly distorted from the true relations for which $(\sigma^*_1)^2 > (\sigma^*_o)^2$, etc., so that the former are no longer reliable and can be noticeably incorrect. This does not destroy the utility of the algorithm itself, which although no longer threshold optimum, gives useable results.]

B. Coherent Detection, Case II

Similar calculations may be made for the noise of Case II, cf. (11.1f), (11.3), (11.14c, d) and (11.15c). We have

$$\langle a_o^2 \rangle^*_{min\text{-}coh} \Big|_{\substack{p_D^*=0.95 \\ \Delta v \doteq 0}}^{db} = 6.3 - (\check{1-n}) - (\check{MN}): \text{ add 26.1 db to (11.16), etc.} \qquad (11.17)$$

(With $p_D^* = 0.5$, these figures are reduced by 3.8 db (= 8.2 - 4.4), cf. (11.2).) Typically, the minimum detectable signal here is much larger (by O(26 db), to be O(-3 to -23 db). This is because now the noise is considerably more gaussian than Case I, (11.1e), and consequently is more difficult to work against (since gauss noise, for the same mean intensity, is the most "random" interference). The equal-variance condition is roughly

satisfied here [cf. (11.14c), (11.14d)], even when the fading is deep (and slow), when the algorithm is approximately threshold optimum, as noted above for Case I, A.

C. Incoherent Detection, Case I

The minimum detectable signals for the incoherent cases of Sec. 9.3 are now obtained from (9.36)-(9.39). We have (again for negligible "doppler-smear," $\Delta v \doteq 0$):

Eq. (9.36):

$$\langle a_o^2 \rangle^*_{\text{min-inc}} \Big|_{\substack{p_D^*=0.9 \\ \Delta v \doteq 0 \\ \text{no,slow (1,2)}}} = \left(\frac{9.0+8.2}{2}\right) - 28.0 - (\check{M}\check{N})$$

	$\check{M}$	$\check{N}$	$\check{N}$		$N=10^2$	$N=10^3$
$=-19.4 +$	0	-20	-30	=	-39.4	-49.4
-19.4	-10	-20	-30	=	-49.4	-59.4
-19.4	-20	-20	-30	=	-59.4	-69.4

(11.18)

for no or slow (one- and two-sided) fading, as long as a coherent signal waveform is maintained.

With rapid one-sided fading (where some signal waveform coherence is preserved, because of the one-sided character of the fading, e.g., $|\overline{a_o}| > 0$), Eq. (9.37) applies, and we therefore increase the results of (11.17) by $-(1-\check{n}) = 0$, 10, 30 db, cf. (11.7), according to these particular degrees of fading, as long as $MN(1-n)^2 \gg 1$. (With $p_D^* = 0.5$, we reduce (11.18) by 3.8 db.) We also note that the incoherent detector has the advantage over the coherent detector of being insensitive to slow fading, cf. (11.18) vs. (11.16).

However, when the signal waveform is made incoherent, either by rapid two-sided fading, and/or "doppler-smear," so that (9.38), (9.39) apply, we have (since $L^{(4)} \doteq 2L^{(2)2}$, $M > 1$):

D. Incoherent Detection, Case I

Eqs. (9.38), (9.39):

$$\langle a_o^2 \rangle^*_{\text{min-inc}} \Big|_{\substack{p_D^*=0.9\ (N>1) \\ \text{rapid (2)} \\ \text{and/or (1,2)} \\ \text{and } \Delta v>0}} = \{3 + 8.2/2 - 28.0 - \check{M} - \frac{\check{N}}{2}\}$$

$$= -20.9 \quad \begin{array}{cc|c|c|c} \check{M} & \check{N} & \check{N} & N=10^2 & N=10^3 \\ \hline -10 & -10 & -15 & = -40.9 & -45.9 \\ -20 & -10 & -15 & = -50.9 & -55.9\ . \end{array} \qquad (11.19)$$

When M = 1, (9.38), (9.39) reduce to

$$\langle a_o^2 \rangle^*_{\text{min-inc}} \Big|_{\text{inc-sig}} \doteq (8\, B^*_{NP}/MNL^{(4)})^{\frac{1}{2}} = \frac{1}{2}(9.0 + 8.2 - 60.0 - \check{N})$$

$$= -21.4 - \frac{\check{N}}{2}$$

$$= -31.4 \text{ db } (N=10^2);\ -36.4 \text{ db } (N=10^3). \qquad (11.19a)$$

From (11.19a) vs. (11.19), we see that having more than one independent sensor can, as expected, considerably improve performance [O(9-19 db)] i.e., lower the minimum detectable signal. Moreover, being able to maintain a coherent signal waveform (C) likewise greatly improves performance, cf. (11.19) vs. (11.18).

Comparing (11.18) with the bounds y_o^* (11.15a, b), we see that the 10 db difference in (9.30) is satisfied, and often by more than 10 db. The same is true for (11.19), (11.19a) vs (11.15b), although not by so much. For practical purposes, then (as long as the fading is not too deep), these threshold detection algorithms remain AO and the corresponding performance measures are acceptably accurate, particularly for J = MN>>1, i.e., large "space-time-bandwidth products."

E. Incoherent Detection, Case II

From (11.3) we see that $L^{(2)}$ now becomes $L_{II}^{(2)} = 1.9$ db, and $L_{II}^{(4)} = 26.8$ db, so that we must increase the results of (11.17) by 26.8 - 2.9 = 24.9 db:

$$\text{Eq. (9.36):}\quad \langle a_o^2 \rangle^*_{\text{min-inc}} \Big|_{\substack{p_D^*=0.9 \\ \Delta v \doteq 0 \\ \text{no,slow (1,2)}}} = \begin{array}{c|cc} \check{M} & N=10^2 & N=10^3 \\ \hline 0 & -14.5 & -24.5 \\ -10 & -24.5 & -34.5 \\ -20 & -34.5 & -44.5 \end{array}, \qquad (11.20)$$

which amply satisfy the condition (9.30) vis-à-vis (11.15c), so that these algorithms are AO. Again, because the noise is "semi-gaussian" (A_A=5.0), optimum threshold performance is decreased (absolutely), i.e., the minimum detectable signal is raised.

In the situation of incoherent signal waveform, (9.38), (9.39), it is no longer true that $L^{(4)} \simeq 2L^{(2)2}$, so that the basic form (9.38) must be used. We have

$$\text{Eq. (9.38,9):}\quad \langle a_o^2 \rangle^*_{\text{min-inc}} \Big|_{\substack{p_D^*=0.9 \\ \text{inc.sig.}}} = \frac{9.0+8.2}{2} - \frac{(\check{M}N)}{2} = \begin{array}{c|ccc} & \check{M} & N=10^2 & N=10^3 \\ \hline -13.4 & 0 & -14.4 & -19.4 \\ -13.4 & -10 & -19.8 & -24.8 \\ -14.9 & -20 & -26.3 & -31.3 \end{array}, \qquad (11.21)$$

which, also as expected, is both greater than (11.20) and (11.19a) (i.e., performance is worse), for these more nearly gaussian noises. Again, comparison with (11.15c) shows that (9.30) is well-obeyed here, so that these algorithms are threshold optimum and AO, as required.

F. "Anomalous Performance"

A comparison of the results (11.18) with (11.16) for coherent signal waveforms for the noise conditions of Case I; and of (11.20) with (11.17) for the noise of Case II above, shows a characteristic "anomalous" behavior: incoherent (threshold) detection appears better (i.e., smaller minimum detectable signals) than coherent (threshold) detection, under otherwise the same conditions of reception.

The explanation of this phenomenon is given in detail in [12], Sec. 6.4, III (pp. 112-113). In essence, it lies in the fact that more relevant information regarding the noise is used [(ℓ,ℓ') vs. ℓ and how these quantities are structured in the threshold algorithm] vis-à-vis what is lost (in the signal) for having to use the signal correlation function ($\sim\rho_s^{(m)}$) in place of the signal waveform directly <u>in these discrete, independent sampling cases</u>. Of course, if continuous sampling were employed <u>and</u> the corresponding threshold-optimum algorithms were available, then we would expect that coherent detection would never be less favorable than incoherent detection under the same noise and signal conditions, sample size, probability controls, etc., since thus having ℓ' (and its continuous extensions) adds no additional information to the noise statistics available for coherent detection.

From (11.18) vs. (11.16), Case I, we see that here the superiority of the incoherent algorithm is about O(0.5 db) over the coherent case, for these particular noise conditions and discrete, independent sampling. Similarly, for Case II ((11.20) vs. (11.19)), the difference is O(1.0 db). Thus, the precise amount depends, as we might expect, on the actual degree of nongaussianness, as described by the relevant noise statistics ($\sim L^{(2)}$, $L^{(4)}$, etc., cf. (11.3)).

G. The Composite Detector, Cases I and II

There remains the composite detector, which is never worse than either the coherent or incoherent detector, cf. Sec. 9.3, III. For the conditions of these examples, we have now

<u>Eq. (9.41):</u>

$$\langle a_0^2\rangle^*_{\text{min-comp}}\Big|_{\substack{\text{no,slow (1,2)}\\ \text{coh.sig.}}} = \text{Numerator of (9.4)} - 28.0 - (\check{M}\check{N}) \quad \longleftarrow \check{A} \longrightarrow \qquad (11.22a)$$

	$(1-\check{\eta})$	$\check{A}$	$\check{M}$	$\check{N}$	$\check{N} =$	10^2	10^3
Eq. (9.41a)	= 0 db	-21.5db	0	-20	-30 =	-41.5	-51.5
Eq. (9.41b)	-10	-19.6				-39.6	-49.6
	-30	-19.4			($\check{M}$=0)	-39.4	-49.4
			-10	-20	-30 =	-51.5	-61.5
						-49.6	-59.6
					($\check{M}$=10)	-49.4	-59.4
			-20	-20	-30 =	-61.5	-71.5
						-59.6	-69.6
					($\check{M}$=20)	-59.4	-69.4

(11.22b)

Comparison with Eq. (11.16) shows at once the expected superiority of the composite detector over both the coherent and incoherent detectors, particularly over the former when there is fading (as long as coherent signal waveform is maintained). The maximum superiority here is O(1.1 db), vs. the incoherent detector, and can be much larger vs. the coherent detector O(50 db), cf. (11.22b) vs. (11.16), for $1-\check{\eta} = -30$ db. [For Case II noise, cf. (11.3), we add 26.1 (=28.0 - 1.9) db to Ⓐ, and the results, in (11.22a, b).]

With rapid one-sided fading (and a still-coherent signal waveform) (9.42) applies. Now the performance can be considerably degraded by the fading [$\sim -(1-\check{\eta})$], as noted earlier. Other possibilities are contained in Eqs. (9.43-9.43c) and Eq. (9.44): with incoherent signal waveforms we can do better than D, Case I, (11.19), according to (9.43), (9.44), depending on sample size and the amount of fading.

Finally, the bounds on $\langle a_o^2 \rangle^*_{min}$ here are the stricter of x_o^*, y_o^*, according to (9.28), or (9.30). This usually requires that we use y_o^* in (9.30), cf. (11.15). The composite detector here obeys this AO ("equal-variance") condition quite readily.

11.3 Comparison with Suboptimum Detectors: Numerical Examples

Here we use the results of Secs. 10.1, 10.2 to determine by how much the performance of various suboptimum detectors, e.g., simple correlators and "super-clipper" correlators, is degraded, i.e., by how much the minimum detectable signal, $\langle a_o^2 \rangle^*_{min}$, is <u>increased</u> vis-a-vis that for the appropriate optimum (threshold) detector, specifically for the particular noise environments embodied in Cases I and II above [cf. (11.1), (11.3)].

In the following numerical examples we again postulate a received coherent sinusoidal signal, of the type specified in Sec. 8.1 preceding. We postulate also large (independent) sample sizes (space-time-bandwidth products). We consider accordingly:

Example 1: Cross-Correlator (Coherent Detection)

From (10.4) we get the desired degradation factor† $\Phi_d^{(*)}$:

$$\Phi_d^* \Big|_{\text{coh-corr}} = 1/L_A^{(2)} = \begin{matrix} -28.0 \text{ db (Class I)} \\ -\ 1.9 \text{ db (Class II)}, \end{matrix} \Bigg\} \tag{11.23}$$

e.g.,

$$\langle \check{a}_o^2 \rangle_{\text{min-coh}} \Big|_{\text{corr}} = \langle \check{a}_o^2 \rangle^*_{\text{min-coh}} + \check{\Phi}^*_{d\ \text{coh-corr}} \quad \text{(db)}, \tag{11.23a}$$

so that for Class I noise the cross-correlator (10.2) is (for these threshold signals for which (11.16) etc. apply specifically) 28 db worse than the optimum threshold algorithm (8.4) for Class I noise, and is only 1.9 db worse for Class II noise, which is much more nearly gaussian. This is entirely to be expected: the (cross)-correlator is threshold optimum in gaussian noise, and is heavily degraded vis-à-vis the proper threshold optimum detector (8.4) where the noise is heavily nongaussian ($A_A \leqslant 1$ or 2).

Example 2: Auto-Correlators (Incoherent Detection)

Here (2) of Sec. 10.1 applies, and for these coherent signal waveforms we have from (10.6c) for the suboptimum detector (10.5)

$$\Phi_d^* \Big|_{\text{inc-correl}} = (1/L_A^{(2)})^2 = \begin{matrix} -56.0 \text{ db (Class I)} \\ -\ 3.8 \text{ db (Class II)} \end{matrix} \Bigg\} \doteq \Phi_d^* \Big|_{\substack{\text{comp-correl,} \\ (10.10)}} \tag{11.24}$$

which shows from (10.6a) directly that now $\langle a_o^2 \rangle_{\text{min-inc}}$ is respectively

---

† The degradation factor Φ_d^* here (for large space-time bandwidth products, $J \gg 1$) is also equal to the Asymptotic Relative Efficiency $(\text{ARE})^2$, which is sometimes used as a performance measure {Sec. 6.3.3 and pp. 168-170 of [12]}. Because the ARE's are not always unique, Φ_d^* in conjunction with $\langle a_o^2 \rangle^*_{\text{min}}$ provides the proper way (cf. 10.4a, etc.) to obtain the performance of suboptimum systems.

-56 db and 3.8 db worse (i.e., larger) than $<a_0^2>_{min\text{-}inc}$ of the optimum threshold detector (8.13). Again, the "mismatch" can be sizeable [α(56 db) here] when the noise is highly nongaussian, and much less so than the noise is nearly gaussian (Case II). For the large samples here ($N>>1$), the degradation is the same when the optimum composite threshold detector is used, cf. (10.10).

Example 3: Clipper-Correlator (Coherent Detection)

The (suboptimum) algorithm (10.11) has the degradation factor (10.12a) here:

$$\Phi_d^*\Big|_{coh\text{-}clip} = 4w_1(0)_A^2/L_A^{(2)} = 6.0 + 18.6 - 28.0 \text{ db} = -3.4 \text{ db (Class I)}$$
$$= 6.0 - 2.4 - 1.9 \text{ db} = -1.7 \text{ db (Class II)}. \quad (11.25)$$

Even for the highly nongaussian noise (Case I) the clipper-correlator comes rather close to the optimum threshold algorithm (i.e., 3.4 db less effective), as compared to the cross-correlator above, which is 28 db worse, cf. (11.23). The degradation is about half that of Case I when Case II noise is in effect, cf. (11.25). Since the clipper-correlator is optimum in Laplace noise, cf. (10.1a), which is "closer" (with respect to the pdf $w_1(x)$) than is w_1 for gauss, (10.1b), to these Class A interferences (cf. Sec. 7.4 above), in the sense of having much more pronounced "tails" (as $|x| \to \infty$) than gauss, we may expect the clipper-correlator to be much better matched to these (Class A) interferences than correlators without clipping.

Example 4: Clipper-Correlator (Incoherent Detection)

Here the suboptimum algorithm is given by (10.13), while the corresponding optimum threshold detector is described by (8.13). Now the degradation factor is found from (10.16):

$$\Phi_{d\text{-}inc}^*\Big|_{clip} = \{4w_1(0)^2/L_A^{(2)}\}^2 = -6.8 \text{ db (Class I)}$$
$$= -3.4 \text{ db (Class II)}$$
$$= \Phi_{d\text{-}comp}^*\Big|_{clip} \quad (10.19), \quad (11.26)$$

Again, introducing the hard limiter ("super-clipper") greatly reduces the degradation vis-à-vis the simple auto-correlator, although the factor (6.8 db) here, while small compared to the 56 db of Example 2, (11.24), can be significant in applications, as can even the 3.4 bd above (Class II noise).

Example 5. Auto- vs. Clipper-Correlators

It is instructive also to compare the performance of the various correlation detectors. This is readily done for these coherent (sinusoidal) signal waveforms with the help of (10.20), and specifically from (10.21). We obtain here, from (11.23), (11.25) and (11.24), (11.26):

$$\left.\Phi_{\text{d-coh}}\right|_{\frac{\text{corr}}{\text{clip}}} = [4w_1(0)A^2]^{-1} \begin{cases} = -24.6 \text{ (Class I)} \\ = -0.2 \text{ (Class II)} \end{cases} \text{db} \qquad (11.27)$$

$$\left.\Phi_{\text{d-inc}}\right|_{\frac{\text{corr}}{\text{clip}}} = [4w_1(0)A^2]^{-2} \begin{cases} = -49.2 \text{ (Class I)} \\ = -0.4 \text{ (Class II)} \end{cases} \text{db} = \left.\Phi_{\text{d-comp}}\right|_{\frac{\text{corr}}{\text{clip}}}.$$

These results show much more degraded are the correlators vis-à-vis the clipper-correlators, as we expect from the preceding examples: employing a hard-limiter is an essential factor in overcoming the degradation experienced by conventional matched-filter detectors. [This, of course, is not a new result practically, but is quantitatively new here, for these explicit classes of canonical noise models (Class A, etc.). The DIMUS receiver is an earlier practical example of this technique.]

11.4 Remarks

The major conclusions reached here from our numerical examples are:

I. Always employ a composite (threshold) detector, particularly in the optimum cases. This provides robustness with respect to slow fading, and rapid fading (to a lesser extent) when signal waveform coherence can be maintained (as in one-sided rapid fading).

II. Use a hard-limiter as one practical approximation to the actual transfer characteristic, $\ell(x_i)$, whenever conventional matched-filter detectors are employed. [Further approximations to the optimum characteristic ($\sim\ell(x)$) may be needed to overcome the residual degradation O(5-7 db or more)), cf. (11.26), depending on the application.]

III. Use as large space-time-bandwidth products, e.g., J = MN, as possible, consistent with the spatial and temporal stability of the medium.

Doppler spread, or "smear," can be a seriously degrading factor on performance, cf. Eqs. (11.8)-(11.13), as can fading, particularly rapid 2-sided fading, both of which work to destroy the (temporal) waveform coherence of the desired signal. When the signal structure is no longer coherent, we must use the more general results developed in Sec. 10. (For further remarks, see Sec. 12.3 ff.)

Finally, we note that although the optimum threshold algorithms cease to be optimum when the input signal level rises (to the point where var $g_1^* \neq$ var g_0^*), these algorithms are still absolutely better as signal level rises, and can, of course, be used at all signal levels. Other, simpler algorithms may then be better, but usually then the signal is sufficiently strong that questions of optimality are practically irrelevant.†

Section 12. Conclusions and Recommendations

In the preceding sections we have developed a canonical "top-down," or global approach to our basic general problem of weak signal detection in nongaussian interference environments, when M elements (or sensors) are employed in arbitrary spatial configurations to form beams suitable for steering and appropriate to the requirements of optimum threshold signal processing.

The main general new results here are:

1. Optimum threshold detection algorithms for any type of interference (combined with the usual gaussian noise backgrounds) and

---

† This is not necessarily true in the case of "quality" performance.

general signals, which include adaptive, data processing steerable beams;

2. Performance measures, i.e., minimum detectable signals, probabilities of correct signal detection, etc., corresponding to these space-time processing algorithms; and
3. Quantitative comparisons with typical suboptimum detectors, such as simple correlators (i.e., "matched-filter" detectors) and clipper-correlators, which are respectively optimum in gauss noise alone, and so-called Laplace noise, cf. (10.7a).

Specific classes of signals have been considered, which are typically encountered in practice, and which also constitute the nongaussian component of the overall interfering noise (Secs. 6, 7). A variety of particular results is described in Sec. 12.1 following, the details of whose derivations are contained in Sections 2-11 above, along with typical numerical values.

12.1 General Results (Part I)

Here we briefly summarize the principal general results of this study, referring the reader to the appropriate text above, and noting that these items are not necessarily ordered by degree of importance:

1. Canonical optimum threshold detection algorithms, involving M spatial elements to sample the combined signal and noise fields, are obtained for the basic binary detection problem: H_1: S+N vs. H_0: N, e.g., "signal plus noise" vs. the alternative "noise alone." [The global formulation of Sec. 2 includes non-independent space-time samples, possible nonstationarity and inhomogeneity of the input signal and noise, and any signal waveforms as well as arbitrary noise statistics.]
2. A sufficient condition that these algorithms are Locally Optimum Bayes (LOB) and asymptotically optimum (AO) for large space-time bandwidth products ($J' = M'N' >> 1$) is given in Section 2.3. [Here ($M' \leq M$, $N' \leq N$) are the effective number of independent samples, cf. discussions in below, Sec. 12.3.]
3. When sampling of the received data is statistically independent with respect to the noise or interference, spatial and temporal

sampling are interchangeable--so-called "separability," cf. Sec. 2.4. [In all subsequent Sections of this Report we postulate independent (noise) samples; again, see VIII below, Sec. 12.3. This, of course, does not impinge upon the stationarity or nonstationarity of the received data, or upon its homogeneity, etc.]

4. Canonical optimum threshold detection algorithms, specifically for independent (noise) sampling, are obtained in Sec. 3 for the three principal modes of reception:
   i. coherent detection ($\underset{\sim}{\bar{s}} \neq 0$);
   ii. incoherent detection ($\underset{\sim}{\bar{s}} = 0$);
   iii. composite detection, which is the sum of (i) and (ii).
   These algorithms are LOB and AO.
5. To achieve tractable algorithms g_j^* (one or two terms of data processing) for the expansion of the general (likelihood ratio) result, it is essential to truncate the expansion with an appropriate bias term [cf. Secs. 2.2, 2.3]. This bias term is $(-\frac{1}{2})\mathrm{var}_{H_0}\, g_j^*$, as shown elsewhere (Appendix A-3 of [12]). Without the correct bias the threshold algorithms are no longer AO and can be very suboptimum in performance.
6. Canonical diagrams of the optimum threshold detection algorithms are provided in Section 4. Fundamentally, the detection process here consists of first "matching to the noise," via the transformation $x_{m,n} \rightarrow \ell(x_{m,n}) \equiv y_{m,n}$, which is usually a highly nonlinear operation, determined by the first-order pdf of the total noise, e.g., $\ell = \frac{d}{dx} \log w_1(x|\mathcal{P})$. The resultant, $y_{m,n}$, is then passed through a linear filter matched in the usual way to the signal (cf. Sec. 4.3), and as shown in Figs. 4.1, 4.2. Beamforming and steering are simply introduced at appropriate stages of the processing.
7. These threshold algorithms are basically adaptive processors, since they require a current calibration of the noise data field, by measurement of the appropriate (few) noise parameters, $\mathcal{P}$, to be used in the analytic form, $w_1(x|\mathcal{P})$. [The analytic first-order pdf $w_1(x|\mathcal{P})$ of the noise is obtained from basic statistical-physical

considerations [1]-[7], which permit the practical description of nongaussian noise sources by two main classes of model: Class A and Class B, cf. Sec. 7 here, and refs.]

8. Because of the large space-time-bandwidth products (i.e., large numbers of effectively independent samples) required, the probabilities of error and correct signal detection can be determined by the Central Limit Theorem, since the statistics (under H_0, H_1) of the algoritms (g_J^*, g_J) are asymptotically normal. The key quantity here is $\text{var}_{H_0}(g_J^*, g_J) \equiv \sigma_o^{(*)2}$, from which we define the associated <u>minimum detectable signals</u> $\langle a_o^2 \rangle_{\text{min}}^{(*)}$, and <u>processing gains</u>, $\Pi^{(*)}$. These are developed in Secs. 5.1, 5.2, where from the general nonstationary, inhomogeneous formulations for $\sigma_o^{(*)2}$ are obtained the stationary, homogeneous results used throughout the rest of the study [Sections 6-11]. These latter are comparatively simple analytic structures from which various other important results may be observed;
9. With coherent and incoherent reception (and coherent signal waveforms) $(\sigma_o^*)^2$ is ~J=MN: performance can be greatly improved by increasing the number of (independent) spatial samples, as well as time samples. [See 19. following for more details.]
10. The earlier conditions for asymptotic optionality (AO) for temporal sampling alone are extended to include spatial sampling as well (Sec. 5.3).

We stress again that the general theory described above in Part I is a canonical theory, in that the formal structures of the algorithm and performance measures are independent of specific signal waveforms and specific noise distributions, and hence even of particular physical applications. However, to apply these general procedures and results to our particular class of underwater acoustic problems, we must obtain specific analytical models of the appropriate underwater acoustic signals, and, similarly, develop the statistical-physical models of the related nongaussian interference. This is done in Part II (Sections 6, 7).

12.2 Particular Results (Part II)

Here we devote our main attention to special signal types, basically sinusoidal signals representing various kinds of man-made and natural

emissions. These are subject to possible fading and "doppler-smear," attributable to the long- or short-range channel effects, and source movements, as well. We have obtained:

11. A detailed, physical model of a general deterministic signal, subsequently specialized to a narrow-band structure, as seen at the output of the $m^{\underline{th}}$-sensor in a general (three-dimensional) array of elements, cf. Fig. 6.1, and Sec. 6.
12. Formation of (receiving) beams, and their steering (Sec. 6.1), with illustrative examples (for signal alone) in Sec. 6.2; also Fig. 6.2.
13. Various analytic signal models: narrow-band and broad-band (i.e., signals involving harmonics).
14. The space-time covariance function of the signal <u>field</u>. This is important in determining the extent of the desired signal wavefront (i.e., spatial) coherence across the array. With good spatial coherence of the desired (single) signal source, it is then possible to form an effective (receiving) beam and steer it in the direction of the incoming signal wavefront (cf. Figs. 6.2 and 7.1), with an appropriate beam gain in the main-lobe direction. However, when the multi-path structure is not resolvable (in direction), so that many wavefronts impinge on the array elements from different angles, spatial coherence is destroyed and directional beam-forming is not possible (Sec. 6.4);

Also,

15. From the results of Section 6, acoustic interference scenarios are developed (Sec. 7.1), and the resulting nongaussian noise field statistics are outlined (Sec. 7.2). In particular, the second-order space-time moments of the nongaussian interference field are obtained (Sec. 7.3), for both narrow- and broad-band noise sources, including the interaction of the general M-element receiving beam with the noise field, where it may or may not be possible to locate array elements such that the resulting spatial samples of the noise field are (at least second-order) independent. In Section 7.4 the needed first-order pdf, $w_1(x|\mathcal{P}_A)$, is

obtained, now for broad-band sources, with fading, which is a new result, also, in addition to a summary of earlier results for $w_1(x|\mathcal{P}_A)$ in the narrow-band cases.

16. It is noted (again) in Section 8 that although the signal and noise fields are additive (the medium is assumed to be linear), the required optimum processing is not linear. Beam-forming is not simply adaptive, but requires in addition to steering delays, appropriate data weighting by the a posteriori data samples. For coherent reception one has a single generalized beam (a "signal-processing" beam), but for incoherent and composite detection product-beams of this type are required, which are much more complex than conventional, simple adaptive beam-forming. (See Sec. 8 for comments.)
17. Specific optimum threshold detection algorithms are obtained in Secs. 8.2-8.4, for coherent, incoherent, and composite detection, based on the often reasonable physical conditions summarized in Sec. 8.1. These specific algorithms provide the required explicit data-processing "instructions," including beam-forming, by which the detection process is implemented. (See also Sec. 4 for the general flow-diagrams).
18. Canonical measures of optimum performance in these threshold cases are presented in Sec. 9.1, along with their specific arguments (σ_o^{*2}) for the three main modes of reception in Sec. 9.2. New features are the inclusion of doppler and fading effects, both one- and two-sided in the latter instance.
19. Of particular importance are the minimum detectable signals $\langle a_o^2 \rangle^*_{min}$ (Sec. 9.3). For coherent waveforms (regardless of the mode of reception), $\langle a_o^2 \rangle^*_{min} \sim (MN)^{-1}$: this shows the effect of having more than one independent spatial sample (when a steerable beam can be formed). Moreover, $\langle a_o^2 \rangle^*_{min} \sim 1/L^{(2)}$, where $L^{(2)} >> 1$ for strongly nongaussian noise (Sec. 9.3).
20. The composite detector [II, Sec. 9.3] is always better than, or at least no worse than, the coherent or incoherent detector, as measured by $\langle a_o^2 \rangle^*_{min\text{-}comp}$ for otherwise the same operating conditions and probability controls ($\sim \beta^*_{NP}$) on the detection process.

21. Specific results for the optimum threshold algorithms are given when the noise is solely gaussian are reviewed, including correlated sampling. These are important in the study of the effects of correlation on performance vis-à-vis the uncorrelated (noise) samples postulated here.

22. The structure and performance of two important classes of suboptimum detectors are analytically obtained in Section 10. These are: (1) the simple correlator (i.e., "matched filter" detector), which operates as a cross-correlator in the coherent mode of reception, as an autocorrelator in the incoherent mode, and as a combination of these devices when composite detection is employed (cf. Sec. 10.1); (2) a second class of suboptimum detector is provided by the clipper-correlator, where a hard-limiter is employed before the matched (signal) filter (Sec. 10.2). Performance is obtained by relating a degradation factor, Φ_d^*, to $\langle a_o^2 \rangle_{min}^*$, to get the corresponding $\langle a_o^2 \rangle_{min}$ in the suboptimum situations, cf. Sections 10.1, 10.2. The importance of the simple correlator is that it is optimum in gauss noise, and is thus the conventional optimum (or "matched-filter," cf. [17], Sec. 16.3) receiver in common use over the last three or more decades. On the other hand, the significance of the clipper-correlator lies in the addition of the hard-limiter to mitigate the effects of impulsive or otherwise highly structured (Class A) nongaussian noise. Practically, the hard-limiter is found to give a considerable improvement (cf. Sec. 11), vis-à-vis conventional unclipped systems, but may still be a significant degree away from the optimum for various applications [cf. Sec. 11.3, Example 4].

23. The performance of optimum and suboptimum threshold detectors in the three modes of reception are numerically illustrated by the Examples of Secs. 11.2, 11.3, for two typical operating conditions: Case I, with highly nongauss (Class A) noise, and Case II, where the noise is rather close to gauss statistically (Sec. 11.1). Included are various fading effects. Simple correlation detectors can be badly degraded vis-à-vis the optimum in the strongly

nongaussian cases, while clipper-correlators are considerably less sensitive to noise "mismatch."

24. The apparent "anomaly" of better performance of incoherent vs. coherent detection with discrete sampling [cf. F, Sec. 11.2] is explained by the greater amount of relevant noise information vis-à-vis loss in signal information (e.g., "epoch") for the former mode of reception. The magnitude of the "anomaly," however, is usually rather small.

12.3 General Observations

We make a few general observations here, based on both the analytic and numerical results of the preceding Sections 2-11:

I. To the extent possible, always try to obtain the largest number of independent space and time (noise) data samples, consistent with the stability of the medium and signal source. This means, in effect, "sparse" sampling in time and possibly in space. [For the theory to be applicable, a large effective space-time-bandwidth product $J'(=M'N')>>1$ is needed, O(40 or more, for example).]

II. Again, to the extent possible, it is most desirable to have coherent signal waveforms (in space and time) at the receiving array elements. This permits us to use the coherent structure of the signal vis-à-vis the incoherent structure (independent samples) of the accompanying noise.

III. A composite detector should always be employed. Not only is such a device robust with respect to slow fading, but it always is as good as, or better than, a purely coherent or incoherent algorithm [cf. Sec. 9.3].

IV. Fading is generally deleterious, unless it is slow (i.e., not noticeable during the particular observation period). Rapid two-sided fading generally destroys signal coherence, but leads only to a $(1-\eta)^{-1}$ dependence on the minimum detectable signal,

cf. (9.43b), in the case of the composite detector, with a $(MN)^{-\frac{1}{2}}$-dependence for incoherent detection otherwise.

V. A useful, simple approximation to the actual optimum dynamic transfer characteristic, $\ell(x)$, here is provided by the hard limiter (i.e., "super-clipper"). This is much better than conventional matched-filter detectors (simple correlators) when the noise is noticeably nongaussian, but it can be O(6-10 db) inferior (in Class A noise) to the optimum algorithm [Sec. 11.3, Example 4]. This may encourage an effort toward a closer approximation to the optimum characteristic. [The clipper-correlator works somewhat closer to the optimum when the noise is Class B, of the same intensity, gaussian content ($\Gamma_B' = \Gamma_A'$) and overlap index ($A_B = A_A$).]

VI. Random doppler ("doppler-smear") always degrades performance because it works to destroy the waveform coherence of the signal. Thus, $H_1(N\Delta t\Delta\omega_d) \to 0$, cf. (9.3a), and $\therefore Q_N \to 1$ [(9.12), (9.13)], so that both the incoherent and composite detectors, cf. (9.44a), give the expected dependence $\langle a_o^2 \rangle^*_{min} \sim (MN)^{-\frac{1}{2}}$ as opposed to $(MN)^{-1}$ for coherent waveforms. This effect can be serious, so that strong efforts to minimize or counter the (random) doppler of the source and medium are often needed. [Deterministic doppler can be compensated.]

VII. Independent sampling (of the noise) in both space and time has been postulated [cf. Sec. 5.4 above]. Even if this cannot be achieved for each data sample, with "sparse" sampling [$\sim\Delta f_B^{-1}$, $\sim(\Delta\nu_B)^{-1}$] and moderately large values of J(=MN>>1) there remains still a large number of effectively independent (noise) samples J'(=M'N'>>1), J'$\leq$ J. The original threshold algorithms, based on J independent samples, while no longer strictly optimum, are close to being threshold optimum for J' independent samples.

Even if we knew how to construct the associated optimum (threshold) algorithms for "dense" sampling [which requires the $n^{\underline{th}}$-order pdf's, $w_n(\underline{x}^{(m)}|\mathcal{P})$, which in turn are unknown (for

$n>2$) and are extremely complex (even for $n=2$)], initial calculations strongly suggest that the corresponding decrease in $\langle a_o^2 \rangle^*_{min}$ would not be more than O(2-3 db) for highly nongaussian noise. (It is well-known that for gaussian noise and large time-bandwidth products the gain in performance is negligible for "dense" (i.e., continuous) sampling vs. sampling at intervals $\Delta t = \Delta f_B^{-1} = (\text{bandwidth})^{-1}$.) For example, let us consider an observation period $T_o = N\Delta t$, where N is the number of samples taken and Δt the interval between them. Thus, we can write

$$T_o = N\Delta t = (N/k)(k\Delta t) = N'\Delta t', \qquad N' = N_{eff}. \tag{12.1}$$

Here k (≥ 1) is determined from an examination of the hierarchy ($n>2$) of (normalized) covariance functions $\rho_n = \rho_n(t_1, \ldots t_n)$ of the (nongaussian) noise in question, such that these correlation functions fall at least to 10^{-2}, say, in $\tau = \Delta t$. Then, $N' = N_{eff}$ ($<N$) is the effective number of "independent samples" (at 99% level) now, with $\Delta t'$ ($=k\Delta t$) the new sampling interval. For highly nongaussian Class A noise ($A_A = O(0.3)$, $\Gamma'_A < 10^{-3}$ typically) it has been found by the author that $k = 1.4 = O(3/2)$, cf. [9], 1975 Report OT-75-67. But $k = 3/2 \rightarrow 5$ db - 3 db = 2 db. Thus, N is reduced to N' be the factor k, and consequently $\langle a_o^2 \rangle^*_{min}$ ($\sim N'$) is increased by 2 db: even if we used all the (noise) information in the higher-order correlation functions (i.e., contained in the pdf, w_n, $n \rightarrow \infty$) we could expect no more than O(2 db) improvement in performance here.

The great advantage of models and algorithms based on statistically independent samples is, of course, the vast reduction in analytic (i.e., equivalently operational) complexity, cf. Figs. 4.1, 4.2) as compared to those based on $n^{\underline{th}}$-order joint probability densities, as is amply evident from the results of Sec. 3-11 vs. Sec. 2 above. Moreover, we do not yet know the $w_n(\underset{\sim}{x})$, $n \geq 3$ explicitly, except that they are very complex, i.e., involving n-fold infinite summations,

so that the question of explicit algorithms based on w_n is entirely moot.

VIII. Our present approach, using the complete first-order pdf $w_1(x|\mathcal{P})$, contains all first-order moment information [$\langle x^k \rangle < \infty$, k = 0, 1, 2, ... here]. Moreover (cf. VII), since we estimate that the correlation statistics of the noise can reduce $\langle a_o^2 \rangle_{min}^{(*)}$ at best O(2-3 db) [i.e., if we could use the optimum algorithms (Sec. 2.2) associated with the J^{th}-order (>> 1) pdf's, the minimum detectable signal would only be lowered by an amount O(2 db)], we expect our present algorithms to be superior to any based on second-order second moments (e.g., correlation functions or spectra), even finite higher-order correlation functions.

In addition, unlike methods which depend on our practical ability to obtain these second- (or higher-) order moments when only noise is present (it being difficult to ensure that the desired signal is not present in our measurements), the possible occurrence of the desired signal produces an ignorable perturbation of the noise parameters, $\mathcal{P}$, in $w_1(x|\mathcal{P})$, because the signal is weak vis-à-vis the noise, and because w_1 is robust in $\mathcal{P}$. On the other hand, the presence of even a weak signal can seriously distort the measured "tails" of the noise correlation function, which are important for detection (and estimation) methods based on these second-order second moment techniques.

12.4 Next Steps (General Recommendations)

A broad variety of next steps awaits subsequent study and implementation. Some are specific natural follows-on of the present study; others are more general and may be pursued elsewhere. Our purpose here is to recommend these topics generally. They may be divided conveniently into five principal categories (with no particular interior prioritization):

A. Noise and Signal Models

(i). Applications of more detailed analysis of real-world data (starting with the large body of available data), to establish the specifics of Class A (and Class B) scenarios and parametric values. This includes the frequency of such models, their environmental duration, and the extent of their departures from gaussian backgrounds, which need documentation and evaluation.

(ii). The empirical rôles of fading and "doppler-smear" in signal modification needs quantitative attention;

(iii). Identification and extension of signal models (multiple sources, multipath, harmonic mechanisms, etc.);

(iv). Extend and develop in detail the broad-band noise theory outlined in Sec. 7.4, along the lines of [6];

(v). Develop the first-order spatial pdf of the noise field; combine with the first-order temporal pdf's.

(vi). Extend (v) to the joint second-order pdf, both spatially and temporally.

(vii). Examine the robustness (i.e., sensitivity) of these non-gaussian noise models to modifications of their parameters.

B. Arrays and Sampling

(i). Establish the conditions (in terms of relevant parameters of the noise models) for effectively independent temporal and spatial sampling [cf. VII, Sec. 12.2 and Sec. 5.4];

(ii). Obtain the field covariances for desired signal fields and determine their associated "spatial matched filters" for the threshold cases;

(iii). Employ combined horizontal and vertical arrays for the required beam-forming and obtain their structures, gains, in noise-alone, signal-alone, and threshold (optimum) signal detection [cf. Secs. 6-8];

(iv). Examine high-resolution arrays which can isolate individual strong interference sources, so that one has to deal solely with gaussian ambient fields (Sec. 9.4). Compare "dense"

with "sparse" sampling.

(v). Examine the robustness of array performance (in conjunction with the temporal processing algorithms) with regard to the effects of (measurement/calculation) errors in the values of the array parameters.

C. Signal Detection

(i). Explain the physical significance of the elements of the general coherent, incoherent, and composite detection algorithms involving general M-sensor arrays, from the point of view of practical implementation, including questions of medium and target stability, nonstationarities, space-time-bandwidth products, sample-sizes, etc.;

(ii). From (available) empirical data establish reasonable limits on the operating parameters (sample-size, etc.) [35];

(iii). Provide practical procedures for the "adaptive" portion of the detection process (i.e., determining the class and parameters of the noise; this should parallel the results of [5], for example); determine the principal problems here;

(iv). Examine the effects of nonuniform fading over the array, on structure and performance [Sec. 5.1];

(v). Obtain explicit performance measures for the often more complex, realistic signals of Sec. 6.

(vi). Develop more explicit numerical comparisons [different Class A (and Class B = biologic noise) case parameters, cf. data of (i), A above] for both optimum and suboptimum cases here;

(vii). Establish more precise bounds on the (limited) gain in performance to be achieved by using "dense" sampling vs. "sparse" or independent sampling.

(viii.) Establish the strong conjecture (stated here, cf. VII, Sec. 12.3) that threshold detection algorithms based on the first-order noise pdf are always considerably better than

detection algorithms based solely on noise and signal spectra and covariances;

(ix). Extend the general M-element binary threshold detection theory of the present study (1983) to an L-alternative signal detection theory ($L \geq 2$) employing M sensors, as before (cf. [14], now with the proper biases, composite detectors, etc.);

(x). Develop results (analytic and numerical) for other sub-optimum algorithms (i.e., "hole-punchers," "soft-limiters," etc.) and compare with the results of (vi) here, and this Report (Sec. 1));

(xi). Determine the size and content of the relevant data bases required under (i);

(xii). Examine the robustness (insensitivity to parameter error) of these various (threshold) detection algorithms;

D. Signal Extraction (Estimation)

(i). Extend the results of [22] to M-element arrays;

(ii). Extend the results of [22] to the estimation of implicit parameters (range, phase, frequency, etc.), and develop them explicitly for M-element arrays;

(iii). Develop an "implementation" analysis along the lines of (i), C above, here for signal waveform and parameter extraction, cf. [22];

(iv). Extend C and D here to optimum signal waveform design in time and space, cf. [34];

(v). Determine the size and content of the relevant data bases required to implement (i), (ii);

(vi). As in the detection problems above, examine the robustness of the various signal extraction algorithms.

E. Computational Implementation and Testing

(i). Simulate typical detection algorithms using real noise and interference data, with their associated "ground truths,"

and computer-simulated signals (which permits local control of level, waveforms, etc.). Compare performances of optimal and suboptimal algorithms for appropriate ranges of operational parameters, cf. C (i);

(ii). Compare the results of (i) with other detection methods, e.g., those based on spectrum/covariance algorithms;

(iii). Extend the procedures and approaches of (i) to selected problems in signal extraction (cf. D);

(iv). Compare the results of (iii) with other signal extraction methods (such as spectrum or covariance algorithms);

(v). Determine various practical bounds on the magnitudes of the elements in the data bases required for (i)-(iv);

(vi). As in A (vii), B (v), C (xii), and D (vi), examine the robustness of the implemented algorithms to errors in both the noise and signal parameters, and the constraints on the observation process (i.e., sample size, coherence, stationarity, etc.). [We note from this that another major study area could equally well be designated F: "Robustness Studies."]

It is clear from the above that much remains to be done in the further development of the theory and its implementation. Our list of problems and next steps is extensive but not necessarily complete, nor are all the topics cited of equal importance or priority. However, the next immediate effort should be directed to a combination of the following:

1. Evaluation of real-world data to obtain specific values (and their associated "ground truth") of the parameters of the noise model;
2. Theoretical evaluation of the performance of threshold algorithms based on (1), using the results of the present study. This will include further relevant work on the noise and signal field statistics, sampling, etc.;
3. Comparisons with the performance of matched-filter and clipper-correlation detectors for the above (real-world) data;
4. Physical descriptions of the factors affecting the threshold algorithms, from the viewpoint of practical implementation;
5. Preliminary implementation of the threshold algorithms by simulation.

Glossary of Principal Symbols and Abbreviations

A. A_A = overlap index
ACI = acoustic interference
AAI = ambient acoustic interference
AO = Asymptotically Optimum
A_o, $A_o^{(m)}$ = signal amplitudes, modulations
a_o, a_o^* = (amplitude) signal-to-noise ratios
$\langle a_o^2 \rangle_{min}^{(*)}$ = minimum detectable signal
$Q_{R.T}$, Q_{RT} = complex beam patterns
α, α^* = Type I error probabilities
α_s = delay per unit distance

B. $\hat{B}_{OA}^{(m)}$ = signal envelopes
B_J^*, $\hat{B}_J^*$, $\hat{B}_C^*$ = biases, etc.
B_{NP}^* = probability control (5.3b)
β, β^* = Type II error probabilities; (β = doppler factor (6.3a))

C. c_o = speed of wavefront
c.f. = characteristic function

D. $\delta_{mm'}$, $\delta_{nn'}$ = Kronecker deltas

E. η = var $a_o/\overline{a_o^2}$, (5.44)
ε_1, ε_o = signal epochs

F. $F_J(\underline{x}|\ )$ = $J^{\underline{th}}$-order probability density
$F_1(i\xi)$ = 1st-order c.f.
$F_J(i\underline{\xi},\underline{t})$ = $J^{\underline{th}}$-order characteristic function, (7.5)
f_o = carrier or central frequency

G. g, g^*, g_J^* = threshold detection algorithms
Γ_A' = gaussian factor (7.26)
γ = propagation law

H. $H_1(x)$ = fading factor
H_0, H_1 = hypothesis states;
H_o = Strüve function (6.46c)
h_M, $\hat{h}_M$ = filter response functions

I. $\hat{i}_o$, $\hat{i}_x$, $\hat{i}_y$, $\hat{i}_z$ = unit vectors

J. J = MN = discrete space-time-bandwidth product
J_o, J_1 = Bessel functions

K. K, $\mathcal{K}$ = fixed detection thresholds
K_{N_o}, K_I, K_G = field covariance functions
$\underline{k}_o$ = normalized noise correlation matrix

L. $\mathcal{L}$ = field solution to wave equations
LOB = Locally Optimum Bayes
LOBD = Locally Optimum Bayes Detector
$L^{(2)}_{m,n}$, $L^{(2)}$, $L^{(4)}$, etc. = statistics of $\ell_{m,n}$; ℓ.
ℓ^*_J = log-likelihood ratio
ℓ, $\ell_{m,n}$ = input-output detector characteristic, (3.2)
Λ_J = generalized likelihood ratio
λ, λ_m = distances (in units of seconds)

M. M, M' = number of independent spatial samples
M_{2s} = second-order second-moment function
m = spatial index
$\hat{m}$ = amplitude index
μ = p/q; also a doppler scale factor (6.3a); distribution law exponent (7.29)

N. N_I = nongauss noise process
N, N' = number of independent temporal samples
dN = counting functional
n = temporal index
$\underline{\nu}$, $\underline{\nu}_o$, $\underline{\nu}_{oR}$, $\underline{\nu}_{oT}$ = spatial frequencies

$\underset{\sim}{Q}$. $\Omega_{2A}^{(m)}$ = intensity of nongauss component

ω, ω_o = angular frequencies

$\Delta\omega_a$, $\Delta\omega_d$ = fading, and doppler variances (frequencies)

$\underset{\sim}{P}$. $P_D^{(*)}$, $p_D^{(*)}$ = signal detection probabilities

pdf = probability density function

p = <u>a priori</u> probability of a signal

p_s = signal pressure field

Φ_d = degradation factor

ϕ, ϕ_T, ϕ_R = phases

ψ ψ_n = mean total background noise

$\underset{\sim}{\pi}^{(*)}$, π, π^* = processing gains

$\underset{\sim}{Q}$. Q_N, $Q_N^{(m,m')}$ = signal structure factors, (5.37c)

q = <u>a priori</u> probability of noise only

$\underset{\sim}{R}$. R_N, $R_N^{(m,m')}$ = signal structure factors, (5.45b)

$\underset{\sim}{R}_o$, $\underset{\sim}{r}_m$ = vector distances

$\underset{\sim}{\rho}_s'$, $\underset{\sim}{\rho}$, $\underset{\sim}{\rho}^{(mm')}$ = signal covariance matrixes; also a distance difference, cf. (6.36)

$\hat{\rho}$ = process density

$\underset{\sim}{S}$. $\underset{\sim}{S}$ = signal vector

$\underset{\sim}{S}$, $\underset{\sim}{S}^{(m)}$ = normalized signal vectors

$\hat{S}_o$ = signal waveforms

$(\sigma_o^*, \sigma_{oJ}^*, \sigma_\upsilon)^2$ = variances of g*, g

σ_S = spatial distribution of interference sources

σ_G = intensity of gauss noise component

$\underset{\sim}{I}$. t = time

t_m^* = remainder in expansion of log Λ_J

Δt = (time) sampling interval

Θ = error function, cf. (5.1a)

Θ^{-1} = inverse error function

θ = signal-to-noise ratio

$\underset{\sim}{\theta}$ = parameter set, normalized signal vector

τ, τ_m, $\Delta\tau_m$ = path delays

$\underset{\sim}{U},\underset{\sim}{V}.$	Δv	= doppler velocity variance (11.9)
$\underset{\sim}{W}.$	w_1	= a first-order pdf
	w_J	= J^{th}-order pdf of noise
$\underset{\sim}{X},\underset{\sim}{Y},\underset{\sim}{Z}.$	$x^{(m)}$	= received waveform at m^{th}-sensor
	$\underset{\sim}{x}$	= sampled data set (vector)
	$\underset{\sim}{y}$	= vector of y_i's; Eq. (2.8a)
	x_o^*, y_o^*	= bounds on $\langle a_o^2 \rangle^*_{min}$
	$\underset{\sim}{z}$	= matrix of z_{ij}'s; Eq. (2.8a).
	z, z_o	= normalized time, (7.19)

REFERENCES AND BIBLIOGRAPHY

[1]. D. Middleton, "Statistical-Physical Models of Urban Radio-Noise Environments, Part I: Formulations," IEEE Trans. Electromagnetic Compatability, Vol. EMC-14, pp. 38-56, May, 1972.

[2]. _____, "Probability Models of Received, Scattered, and Ambient Fields," Proc. IEEE--1972 Int'l. Conf. on Engineering in the Ocean Environment, Newport, R.I., Sept. 13-16, 1972, IEEE Pub. 72-CHO-666-1-OCC, pp. 8-14, "Ocean '72."

[3]. _____, "Statistical-Physical Models of Man-Made Radio Noise, Part I: First-Order Probability Models of the Instantaneous Amplitude," Report OT-74-36, April, 1974, Office of Telecommunications, U.S. Dept. of Commerce.

[4]. _____, "Statistical-Physical Models of Electromagnetic Interference," IEEE Trans. on Electromagnetic Compatability, EMC-19, No. 3, pp. 106-127, Aug., 1977.

[5]. _____, "Procedures for Determining the Parameters of the First-Order Canonical Models of Class A and Class B Electromagnetic Interference," IEEE Trans. on Electromagnetic Compat., EMC-21, No. 3, pp. 190-208, Aug., 1979.

[6]. _____, "Performance of Telecommunication Systems in the Spectral Use Environment; VII. Interference Scenarios and the Canonical and Quasi-Canonical (First-Order) Probability Models of Class A Interference," Contractor Report NTIA-CR-2-18, March, 1982, NTIA/FSSM, U.S. Dept. of Commerce. [A shortened version is scheduled to appear in the IEEE Trans. on Electromagnetic Compat., Vol. 25, No. 2, May 1983.]

[7]. _____, "Canonical Non-Gaussian Noise Models: Their Implications for Measurement for Prediction of Receiver Performance," IEEE Trans. on Electromag. Compat. EMC-21, No. 3, August, 1979, pp. 209-220.

[8]. _____, "Canonically Optimum Threshold Detection," IEEE Trans. on Information Theory, Vol. IT-12, No. 2, April, 1966, pp. 230-243. [For the original threshold development about the null-signal, see "The Statistical Theory of Detection, I," M.I.T. Lincoln Lab. Rpt. No. 35, Nov., 1953, and highlights, in "Statistical Theory of Detection," Symp. on Statistical Methods in Communication Engineering, IRE Trans. in Info. Theory, PGIT-3, p. 26, March, 1954.]

[9]. A. D. Spaulding and D. Middleton, "Optimum Reception in an Impulsive Interference Environment: Part I, Coherent Detection; Part II, Incoherent Reception," IEEE Trans. on Communications, Vol. COM-25, Sept., 1977, pp. 910-934. [For a more extended version, see OT-Rpt. 75-67, June, 1975, Office of Telecommunications (now NTIA), U.S. Govt. Printing Office, Wash., D.C. 20402.]

[10]. D. Middleton, "Threshold Signal Reception in Electromagnetic Interference Environments: Part II. Receiver Structures and Performance for Class A EMI Environments and Scenarios," Report NTIA-CR-81-17, March, 1982, for NTIA/ITS Boulder, Colorado 80303; (U.S. Govt. Printing Office, Wash., D.C. 20402).

[11]. _____, "Threshold Detection in Non-Gaussian Interference Environments: Exposition and Interpretation of New Results for EMC Applications," Paper B1, Proceedings, 5th Int'l. Symposium on Electromagnetic Compatability, March 8-10, 1983, Zurich, Switzerland.

[12]. D. Middleton and A. D. Spaulding, "Optimum Reception in Nongaussian Interference Environments: II. Optimum and Suboptimum Threshold Signal Detection in Class A and Class B Noise," NTIA Tech Rpt., pp. 83-120, May, 1983, (Boulder, Colo. 80303) and U.S. Govt. Printing Office, Wash., D.C. (20402).

[13]. A. D. Spaulding, "Optimum Threshold Signal Detection in Broad-Band Impulsive Noise Employing both Time and Spatial Sampling," IEEE Trans. on Communications, Vol. COM-29, No. 2, February, 1981, pp. 147-152.

[14]. L. M. Nirenberg, "Low SNR Digital Communication over Certain Additive Non-Gaussian Channels," IEEE Trans. on Communications, Vol. COM-23, No. 3, 332-341, 1975. [See, also, Letter to Editor, ibid., Vol. COM-23, No. 5, p. 1002, Sept., 1975.]

[15]. J. J. Sheehy, "Optimum Detection of Signals in Non-Gaussian Noise," J. Acous. Soc. Amer. 63 (1), Jan., 1978, pp. 81-90.

[16]. D. Middleton and A. D. Spaulding, Correspondence, IEEE Trans. on Information Theory, 1983.

[17]. D. Middleton, An Introduction to Statistical Communication Theory, McGraw-Hill (New York), 1960, Chapters 18, 19, esp.

[18]. D. Middleton and D. Van Meter, "On Optimum Multiple-Alternative Detection of Signals in Noise," IRE Trans. on Information Theory, Vol. IT-1, 1-, 1955. See in particular [17], Section 23.1.

[19]. D. Middleton and H. L. Groginsky, "Detection of Random Acoustic Signals by Receivers with Distributed Elements: Optimum Receiver Structures for Normal Signal and Noise Fields," JASA, Vol. 38, No. 5, pp. 727-737, November, 1965.

[20]. D. Middleton, Topics in Communication Theory, McGraw-Hill (New York), 1965.

[21]. J. H. Van Vleck and D. Middleton, "A Theoretical Comparison of the Visual, Aural, and Meter Reception of Pulsed Signals in the Presence of Noise," J. Appl. Phys. 17, 940, 1946. See Sec. 16.3 of [17].

[22]. D. Middleton, "Threshold Signal Reception in Electromagnetic Interference Environments: Part III. An Introduction to Canonical Threshold Signal and Parameter Estimation," NTIA Rpt. CR-83-21, January, 1983, U.S. Dept. of Commerce, Boulder, Colorado 80303.

[23]. J. T. Evans and A. S. Griffiths, "Design of a Sanguine Noise Processor Based on World-Wide Extremely Low Frequency (ELF) Recordings," IEEE Trans. Comm. Vol. COM-22, pp. 528-539, April, 1974.

[24]. N. W. McLachlan, "Bessel Functions for Engineers," Oxford (1934).

[25]. D. Middleton, "Doppler Effects for Randomly Moving Scatterers and Platforms," J. Acous. Soc. Amer., 61, 1262-1267, No. 5, May, 1977.

[26]. H. A. De Ferrari et al., "Measurements of Transmission Fluctuations at Three Ranges for Refracted Paths through the Deep Ocean," JASA, (Spring '83), Vol. 68. See also for references to earlier work.

[27]. I. Dyer, "Statistics of Sound Propagation in the Ocean," JASA, 48, 337-345 (1970). (This is primarily a theoretical paper.)

[28]. S. M. Flatté et al., Sound Transmission through a Fluctuating Ocean, Camb. Univ. Press (N.Y., 1979); see Chapter 9 for multipath and fading.

[29]. B. D. Steinberg, Principles of Aperture and Array System Design, John Wiley, N.Y. (1976), Chapter 11.

[30]. I. S. Gradshteyn and I. M. Ryzhik, Tables of Integrals, Series, and Products, Academic Press (N.Y., 1965).

[31]. D. Middleton, "New Approaches to Scattering in Linear Random Media: I, Canonical Formulations, Operators, and Innovations; II, Statistical-Physical Structures and Radiation Statistics; III, Examples from Underwater Acoustics," papers submitted to JASA in late 1983 (work supported under ONR Contracts N00014-76-C-0543; N00014-81-C-0258).

[32]. D. Middleton, "Statistical-Physical Models of Man-Made and Natural Radio Noise: Part II. First-Order Probability Models of the Envelope and Phase," OT Rpt. 76-86, April, 1976, Office of Telecommunications, U.S. Dept. of Commerce, U.S. Govt. Printing Office, Wash., D.C.

[33]. S. O. Rice, "Mathematical Analysis of Random Noise," (p. 95 of article; p. 25 of book), in Noise and Stochastic Processes, Ed. Nelson, W., Dover Pub. (New York), 1954.

[34]. D. Middleton, "Threshold Signal Reception in Electromagnetic Signal Environments: Part IV. An Initial Conceptual Study of Signal Design Against Nongaussian Interference," Report NTIA-CR-83-22, Jan. 1983, ITS/NTIA, U.S. Dept. of Commerce, U.S. Govt. Printing Office, Wash., D.C.

[35]. J. Caruthers, "A Preliminary Assessment of Soviet Development of Optimum Signal Discrimination Techniques: Optimum Space-Time Processing," NORDA Tech. Note 168, Oct., 1982, Naval Ocean Research and Development Activity (NSTL Station, Mississippi 39529). See also the many available references therein.

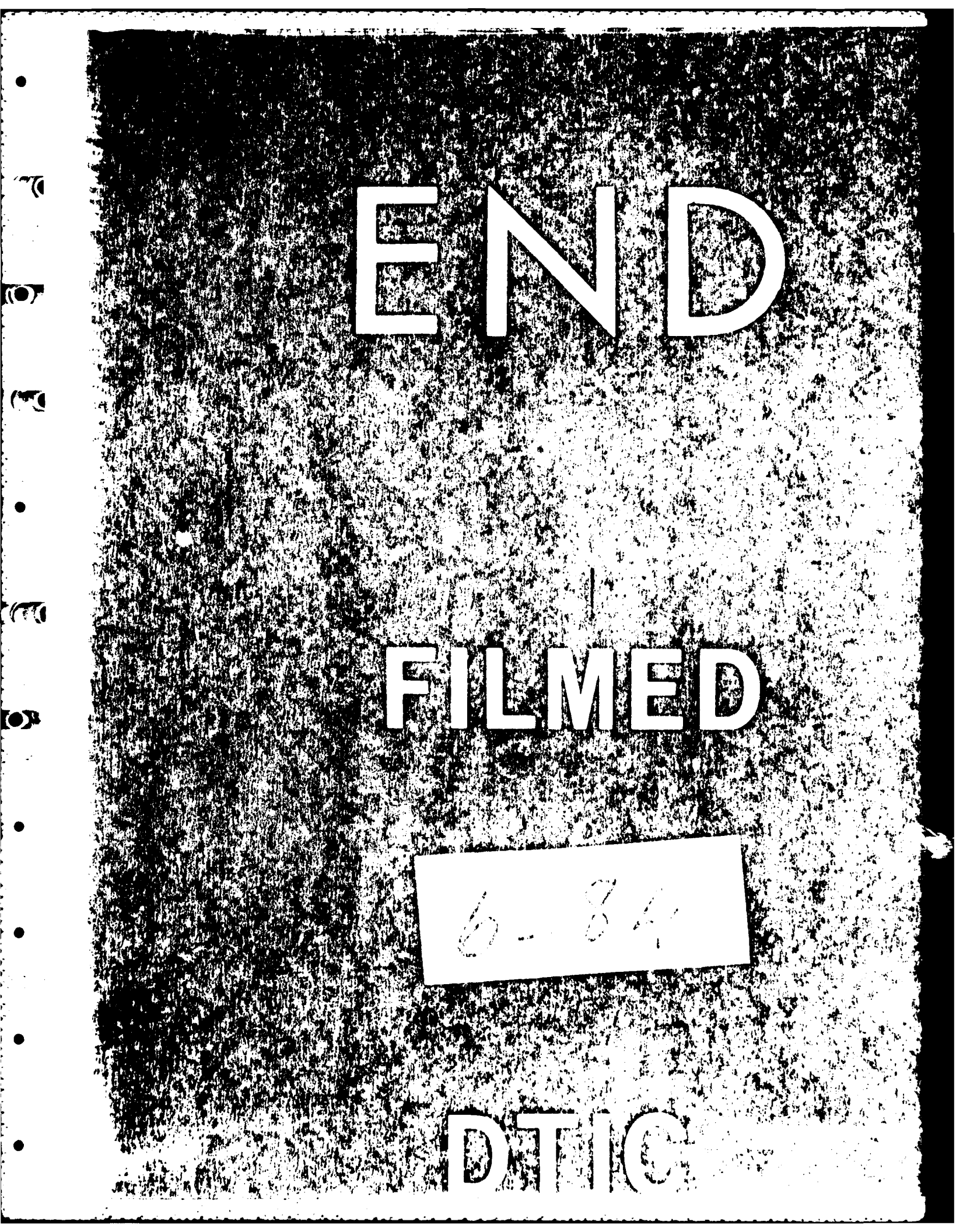
END
FILMED
6-84
DTIC